1-1-1995

Salt complex formation in atactic poly(propylene oxide) :: chain conformation and structure effects on ionic conduction/

Sunghoe, Yoon
University of Massachusetts Amherst

SALT COMPLEX FORMATION IN ATACTIC POLY(PROPYLENE OXIDE) : CHAIN CONFORMATION AND STRUCTURE EFFECTS ON IONIC CONDUCTION

A Dissertation Presented

by

SUNGHOE YOON

Submitted to the Graduate School of the

University of Massachusetts Amherst in partial fulfillment

of the requirements for the degree of

DOCTOR OF PHILOSOPHY

September 1995

Department of Polymer Science and Engineering

SALT COMPLEX FORMATION IN ATACTIC POLY(PROPYLENE OXIDE) : CHAIN CONFORMATION AND STRUCTURE EFFECTS ON IONIC CONDUCTION

A Dissertation Presented

by

SUNGHOE YOON

Approved as to style and content by :

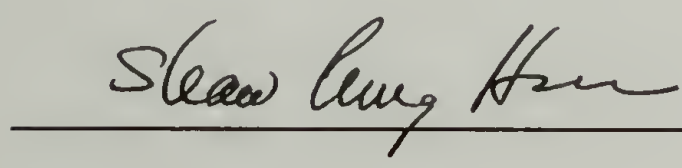

Shaw L. Hsu, Co-Chairman

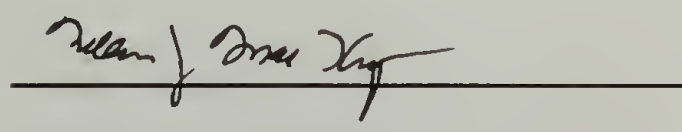

William J. MacKnight, Co-Chairman

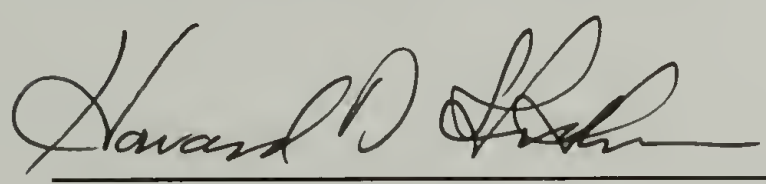

Howard D. Stidham, Member

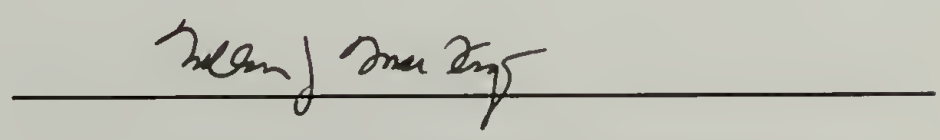

William J. MacKnight, Department Head

Polymer Science and Engineering

ACKNOWLEDGMENTS

I would like to acknowledge the guidance, support and encouragement given to me by my advisors, Professor Shaw Ling Hsu and Professor William John MacKnight, through the course of this research. I would also like to thank Professor Howard D. Stidham for his helpful comments.

I am deeply grateful to Dr. Douglas A. Cates and Yang-Gul Lee for their cooperation in helping me in the use of computer program for normal coordinate analysis and their helpful suggestions. I would like to express my special appreciation to Dr. Curtis W. Meuse for his experimental assistance, many thoughtful discussions and, more importantly, for his friendship and sincere encouragement. Dr. Hun-Jan Tao, Dr. Michael Connolly and Professor L. Charles Dickinson also are acknowledged for their useful advice and discussion on a wide variety of subjects.

I wish to thank my classmates and all the members of my research groups for their companionship and discussions over four years. My special thanks go to Susane Ferlin, Brian Price, C-W Alice Ng, Chao Cheng Chen, and Yuan Ren for their friendship and useful discussions on the scientific and more often nonscientific subjects. I would also like to thank all of faculties and staffs in the Department who gave me this unexpected opportunity to learn advanced polymer science.

Finally, I am deeply indebted to my mother, father, aunt, uncles, sisters, brother and cousins for their love, patience and encouragement in the completion of this work. Specially, I thank my niece, Ho-jung who always makes me laugh. I would also like to thank all of my Korean friends in Amherst who have taken care of my health and given me a sincere love.

ABSTRACT

SALT COMPLEX FORMATION IN ATACTIC POLY(PROPYLENE OXIDE) :

CHAIN CONFORMATION AND STRUCTURE EFFECTS ON IONIC CONDUCTION

SEPTEMBER 1995

SUNGHOE YOON, B.S., EWHA WOMANS UNIVERSITY

M.S., EWHA WOMANS UNIVERSITY

Ph.D., UNIVERSITY OF MASSACHUSETTS AMHERST

Directed by : Professor Shaw Ling Hsu and Professor William John MacKnight

Atactic poly(propylene oxide) in both linear and network form has been studied as a matrix for polymer electrolytes to characterize chain conformational changes in salt-polymer complexes and to estimate the polymer structure effect to the ionic conduction mechanism at the molecular level.

The chain conformational changes of amorphous poly(propylene oxide) in the presence of $LiClO_4$ have been analyzed by utilizing Fourier transform Raman(FT-Raman) spectroscopy in combination with normal coordinate analysis to characterize the structure of the salt-polymer complexes. Our spectral analysis indicated that interaction between the lithium cation and ether oxygen was achieved by formation of trans-gauche α-trans($TG_{\alpha}T$) conformations of the propylene oxide backbone.

End group effects on the chain flexibility of poly(propylene oxide) in the oligomeric molecular weight range has been studied without salt and in the presence of salt. Differential scanning calorimetry(DSC) together with Raman spectroscopic study in the D-LAM region showed greater chain flexibility in methoxy terminated poly(propylene oxide)(MPPO) than hydroxy terminated poly(propylene oxide)(HPPO). Decreased chain

segmental mobility in HPPO has been attributed to the hydrogen bonding interaction between hydroxy group and ether oxygen. This interaction caused steric hindrance to the segmental mobility by the -CH_3 side group.

In the presence of $LiClO_4$, macroscopic phase separation was observed in MPPO complexes while no such behavior existed in HPPO complexes. It has been attributed to the higher binding interaction of the lithium cation with the hydroxy group than with the ether oxygen. MPPO-$LiClO_4$ complexes showed about one order of magnitude higher ionic conductivity than HPPO based complexes. This is attributed to the improved chain mobility of the MPPO matrix compared to HPPO matrix in spite of the reduced number of free ions in MPPO-$LiClO_4$ complexes. Therefore this result indicates that chain segmental mobility is the predominant factor to determine the ionic conductivity of the poly(propylene oxide) based polymer electrolytes.

Finally, the model network derived from poly(propylene oxide) with tris(4-isocyanatophenyl) thiophosphate(triisocyanate) in the presence of $LiClO_4$ was studied by FT-Raman spectroscopy. Preferential interaction of the lithium cation with the crosslink points, urethane groups in this system, was observed. Therefore ionic conductivity in this particular network based polymer electrolyte is determined by the combination of two mechanisms, one coupled to the poly(propylene oxide) chains and the other to the urethane groups present at the crosslink points.

TABLE OF CONTENTS

LIST OF TABLES

LIST OF FIGURES

CHAPTER 1

INTRODUCTION

For more than 20 years, polyethers have received attention as media capable of dissolving salts to form a new class of ionic conductor. This new category of ionic conductor is named a polymer electrolyte after the components constituting of the system.[1-5] The development of polymer electrolytes has been stimulated because of their superior chemical and dimensional stability compared with conventional inorganic and liquid electrolytes and most importantly for the realization of high energy density batteries.

Poly(ethylene oxide) was the first polymer to receive attention for use as a polymer electrolyte because of the electron donating ability of the ether oxygens and the optimal spacing of the solvating units. Later on, new salt complexed polymers have been developed for improved ionic conductivity at working temperature. For all cases, the effort was concentrated on the search for the proper polymers because the polymer structure turned out to be the most important factor to determine salt solubility and ion transport properties in polymer electrolytes. In this chapter, we would like to briefly summarize the characteristics of polymer-salt complexes.

1.1 Formation of Polymer-Salt Complexes

A polymer electrolyte is simply a system in which macromolecules are used as a solvent for salts. In this system, salt solubility is determined by a balance of forces between the solvating power of the polymer and the lattice energy of salts just as in liquid

solvents consisting of small molecules. The lower lattice energy and the greater solvation energy of salts are required for the higher salt solubility. Generally, the low lattice energy is obtained for salts consisting of large ions. Solvating power of polymer can be achieved by electron donating ability of the polymer. Polymers containing O or N can donate electron pair to the cation of salts through those heteroatoms. For a fixed electron donating ability of the polymer matrix, a smaller cation has a higher binding energy because of stronger electrostatic interaction. Polymer geometry also effects the salt-polymer complex formation. Poly(ethylene oxide) has the most favorable spacing for solvation of salts compared with poly(methylene oxide)[-CH_2-O-] or poly(n-propylene oxide)[-$CH_2CH_2CH_2$-O-] although they have the same electron donating group, ether oxygen.[1] Therefore, as a polymer matrix, poly(ethylene oxide) and poly(propylene oxide) are of interest due to the combination of electron donating ability of the ether oxygen and the optimal spacing of oxygens. In addition, polymer electrolytes based on poly(ethylene succinate)[6-8], poly(β-propiolactone)[9], poly(ethylene imine)[10], polyphosphazenes[11] and others have been reported. As salts capable of forming stable complexes with the polymer, small cations are preferred for better binding energy and large delocalized anions for lower lattice energy. For examples, $LiClO_4$, $LiCF_3SO_3$ and NaSCN have been studied for years.

1.2 Ionic Conductivity of Polymer Electrolyte

Ionic conductivity of the system is determined by the number of ions and the ionic mobility as shown in equation (1.1). In eq.(1.1), n, z, e and μ stand for number of carrier ions, the valency of the carrier ion, the elementary electric charge, and ionic mobility, respectively.

$$\sigma = \Sigma\, n_i\, z_i\, e\, \mu_i \qquad (1.1)$$

As described above, salt solubility is determined by a balance between lattice energy and solvation energy of salts. Since the polymer matrix has a low dielectric constant(ε~5 for polyethers), dissociation of the salt is far from complete.[12-16] Therefore there can exist free ions, solvated ions, and contact ion pairs including multiple aggregates in the polymer matrix. Only free ions and ionic aggregates which have a net charge can contribute to ionic conductivity.[17] As binding energy between ion and polymer increases, the degree of dissociation of the salt increases but too strong binding impedes the movement of ions. Ionic conductivity is in the range of 10^{-3} ~10^{-5} S/cm for poly(ethylene oxide) based polymer electrolytes above the melting temperature depending on the salt species and the salt complex composition.[18-21]

As far as ionic mobility is concerned, it is believed that polymer segmental motion is responsible for ionic transport.[14,22-26] The temperature dependence of the ionic conductivity follows WLF(William-Landel-Ferry, eq. (1.2)) or VTF(Vogel-Tamman-Fulcher, eq. (1.3)) equations for most of the polymer electrolytes studied, usually above the glass transition temperature. In eqn's, (1.2) and (1.3), σ and T_g stand for ionic conductivity and glass transition temperature, respectively. A, B and C are constants. WLF and VTF equations were empirically obtained to describe polymer relaxation and viscosity behavior, respectively which correlate with polymer chain mobility. Therefore the good fit of conductivity data to the WLF or VTF relationship indicates that the ionic conduction process in polymer electrolytes is closely related to the polymer segmental motion.

$$\log \sigma(T)/\sigma(T_g) = -C_1(T-T_g)/(C_2+T-T_g) \qquad (1.2)$$

$$\sigma(T) = AT^{-1/2} \exp[-B / (T-T_g)] \qquad (1.3)$$

Recently, Lin et al.Lin et al.[27] performed molecular dynamics simulations of lithium ions in amorphous poly(ethylene oxide). Their theoretical calculations showed that the lithium

cation moves from one part of the polymer segment at time t_o to another part after Δt by a sliding motion. This result supports the idea that ionic conduction is associated with polymer segmental mobility. Schematic drawing of ion transport in a polymer matrix is shown in Figure 1.1.

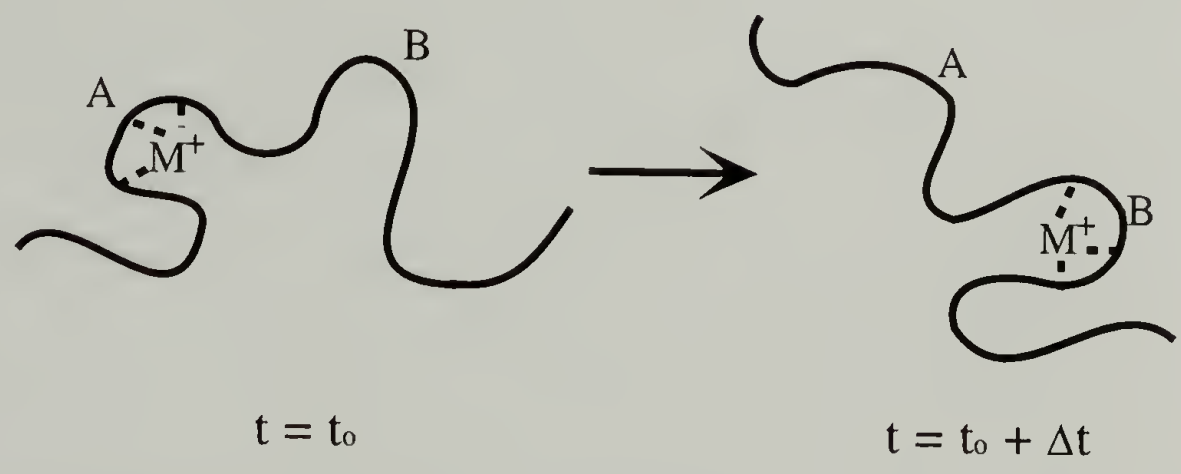

Figure 1.1 Schematic drawing of ionic conduction through polymer segmental motion ; M^+ stands for alkali metal cation.

In contrast with inorganic crystals, ionic conduction in polymer electrolyte does not occur from the defects in the crystalline phase. The studies on poly(ethylene oxide)-salt complexes which are the most widely studied system suggest that poly(ethylene oxide) retains a helical structure with $T_2GT_2G^-$ conformation(T=trans, G=gauche, G^-=gauche minus) and small cations such as Li^+ and Na^+ lie in the helix.[28] It was suggested that ionic transport occurs by an intrahelical hopping process along the helical structure, similar to the mechanism in inorganic substrates[29]. However, an acceptable level of ionic conductivity was achieved above the melting temperature of salt complexed poly(ethylene oxide). Therefore as far as polymer electrolytes are concerned, ionic conduction is believed to take place in the amorphous region of the polymer matrix and is assisted by polymer segmental motion.

1.3 Poly(propylene oxide) based Polymer Electrolytes

Extensive studies on poly(ethylene oxide) complexes of certain salts have been carried out in order to understand the ionic conduction mechanism. However, one problem to get high conductivity and to characterize ionic motion is caused by crystallization of salt complexed poly(ethylene oxide) as well as uncomplexed chains. Since the formation of crystalline phases depends on the concentration of salt, salt species, temperature, preparation methods and so on, ionic conduction behavior is influenced in a complex manner by the formation of crystalline phases.

In order to overcome this problem, much attention has been paid to poly(propylene oxide) as a polymer matrix for ionic conductors.[12,13,15,25,26,30-32] Poly(propylene oxide) has the same structure as poly(ethylene oxide) and also can dissolve alkali metal salts. When atactic poly(propylene oxide) is used as a polymer electrolyte, the resulting poly(propylene oxide)-salt complexes are amorphous and have comparable ionic conductivity with that of the poly(ethylene oxide) complexes. Therefore it can be of great advantage to investigate ionic conduction mechanism of polymer electrolytes directly as a function of salt species, concentration and temperature without considering crystallization effects.

Several types of poly(propylene oxide) based polymer electrolytes have been studied, including linear polymers[25,26], block copolymers[33], and networks[34]. The temperature dependence of the ionic conductivity of these systems complexed with salts is described by the WLF equation. This implies a close relationship between ionic conductivity and the relaxation behavior of the polymer chains.

The ionic conductivity of linear poly(propylene oxide)-$LiClO_4$ complexes measured by Watanabe et al.[25,26] is shown in Figure 1.2 as a function of salt concentration in the oligomeric molecular weight range. Ionic conductivity increases with salt concentration

and reaches 10^{-4}~10^{-6} S/cm and decreases somewhat at higher salt concentrations. This behavior is attributed not to the decrease in the number of free ions but to the decrease in ionic mobility as evidenced by a remarkable increase in viscosity as salt concentration increases. The change in viscosity with salt concentration is considered to be due to the formation of physical crosslinks between ether oxygen and ions. Viscosity data are shown in Figure 1.3.[25,26]

Amorphous complex-forming property and low glass transition temperature of poly(propylene oxide) are advantages to get acceptable ionic conductivity. However, those properties are problem for practical applications because they lead to low mechanical strength. The mechanical strength can be improved by crosslinking and copolymerization. Network polymers[34] have been prepared by the reaction of diol- or triol- terminated poly(propylene oxide) with reagents such as triisocyanate or diisocyanate. Segmented block copolymers, polyether poly(urethane urea)s[33] containing poly(propylene oxide) segments also have been prepared for practical purposes. These systems have been studied in order to understand the ionic conduction mechanism since ionic conductivity is intimately related to the polymer structure. Ionic conductivity was one to two order magnitudes lower than that of the corresponding molecular weight of linear poly(propylene oxide)-salt complexes in network polymer prepared from triol poly(propylene oxide) and diisocyanate.[1] The low conductivity of network based salt complexes was attributed to the absence of macroscopic flow of polymer which occurs in the linear polymer and can be another way to transport ions.

Although it has been well accepted that polymer structure is the most important factor to determine ionic conductivity since ionic mobility as well as the number of carrier ions are dependent on the polymer structure, detailed structural studies are lacking.

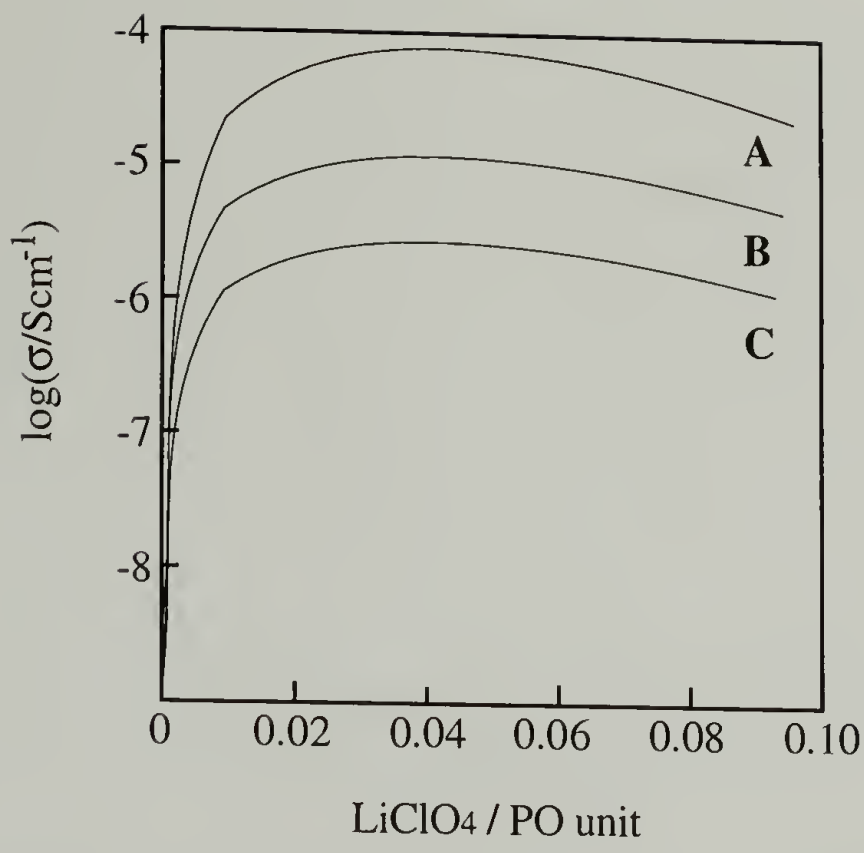

Figure 1.2 Relation between ionic conductivity and salt concentration for PPO-$LiClO_4$ complexes at 25 °C. MW of PPO : A-400, B-1000, C-3000.(from Watanabe et al., ref. 26)

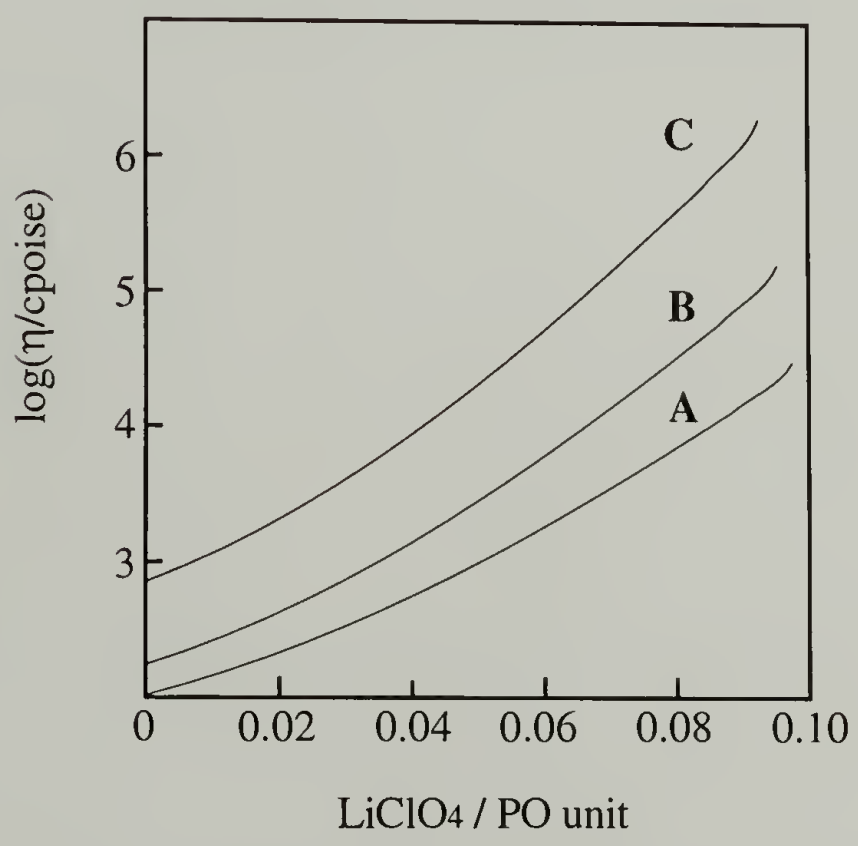

Figure 1.3 Relation between viscosity and salt concentration for PPO-$LiClO_4$ complexes at 25 °C. MW of PPO: A-400, B-1000, C-3000.(from Watanabe et al., ref. 26)

Poly(propylene oxide) based polymer electrolytes also have been studied for more than a decade but the structure effect on the ionic conductivity has not been taken into account at the microscopic level. As a consequence, salt-polymer complex formation and the ionic conduction mechanism have not been carefully characterized yet because of lack of detailed structural information on the polymer matrix in relation to the ionic conductivity.

1.4 Objectives and Overview

On the basis of the brief review discussed above, it is clear that the ionic conductivity of polymer electrolytes is determined by the polymer structure. Poly(ethylene oxide)-salt complexes have been quite well characterized in terms of the chain conformation of the complexes.[35-39] However, almost no information is available for most amorphous polyethers even though it is well accepted that the amorphous region is responsible for ionic conduction. Because of this, sometimes the interpretation of the conductivity data are incorrect. Therefore we would like to estimate the detailed polymer structure effect of the ion solvation as well as the ion mobility on the molecular level in order to understand fully the ionic conduction mechanism in an amorphous polymer matrix.

We studied poly(propylene oxide)-$LiClO_4$ complexes. Although several studies have been carried out on this system[13,15,30-32], very little quantitative structural analysis has been accomplished for poly(propylene oxide) based polymer electrolytes. In chapter 2, we characterize chain conformational changes of atactic poly(propylene oxide) to solvate ions by using Fourier transform Raman spectroscopy and normal coordinate analysis. Chapter 3 and 4 include end group effects on chain flexibility and the relative content of free ions. These studies are very useful to estimate the contribution of each factor, the number of carrier ions and the ionic mobility, to the ionic conductivity of the system. In chapter 5 we study poly(propylene oxide) based networks prepared by reaction with

triisocyanate. We clarify the significant effect of the crosslink point, urethane groups in this case, on the ionic conductivity of the network based polymer electrolytes.

References

(1) MacCallum, J. R.; Vincent, C. A., Ed.; *Polymer Electrolyte Reviews* ; Elsevier Applied Science: London, **1987**; Vol. 1.

(2) MacCallum, J. R.; Vincent, C. A., Ed.; *Polymer Electrolyte Reviews* ; Elsevier Applied Science: London, **1989**; Vol. 2.

(3) Scrosati, B., Ed.; *Second International Symposium on Polymer Electrolytes*; Elsevier Applied Science: London, **1990**.

(4) Watanabe, M.; Ogata, N. *Brit. Polym. J.* **1988**, *20*, 181.

(5) Ratner, M. A.; Shriver, D. F. *Chem. Rev.* **1988**, *88*, 109.

(6) Watanabe, M.; Rikukawa, M.; Sanui, K.; Ogata, N.; Kato, H.; Kobayashi, T.; Ohtaki, Z. *Macromolecules* **1984**, *17*, 2902.

(7) Watanabe, M.; Rikukawa, M.; Sanui, K.; Ogata, N. *J. Appl. Phys.* **1985**, *58*, 736.

(8) Dupon, R.; Papke, B. L.; Ratner, M. A.; Shriver, D. F. *J. Electrochem. Soc.* **1984**, *131*, 586.

(9) Watanabe, M.; Togo, M.; Sanui, K.; Ogata, N.; Kobayashi, T.; Ohtaki, Z. *Macromolecules* **1984**, *17*, 2908.

(10) Harris, C. S.; Shriver, D. F.; Ratner, M. A. *Macromolecules* **1986**, *19*, 987.

(11) Greenbaum, S. G.; Adamic, K. J.; Pak, Y. S.; Wintersgill, M. C.; Fontanella, J. J. *Solid State Ionics* **1988**, *28-30*, 1042.

(12) Kakihana, M.; Schantz, S.; Torell, L. M. *J. Chem. Phys.* **1990**, *92*, 6271.

(13) Schantz, S.; Torell, L. M.; Stevens, J. R. *J. Appl. Phys.* **1988**, *64*, 2038.

(14) McLin, M. G.; Angell, C. A. *J. Phys. Chem.* **1991**, *95*, 9464.

(15) Manning, J.; Frech, R. *Polymer* **1992**, *33*, 3487.

(16) Dupon, R.; Papke, B. L.; Ratner, M. A.; Whitmore, D. H.; Shriver, D. F. *J. Am. Chem. Soc.* **1982**, *104*, 6247.

(17) MacCallum, J. R.; Tomlin, A. S.; Vincent, C. A. *Eur. Polym. J.* **1986**, *22*, 787.

(18) Gray, F. M. *Solid State Ionics* **1990**, *40/41*, 637.

(19) Munshi, M. Z. A.; Owens, B. B. *Polym. J.* **1988**, *20*, 577.

(20) Bruce, P. G.; Evans, J.; Vincent, C. A. *Solid State Ionics* **1988**, *28-30*, 918.

(21) Gorecki, W.; Donoso, P.; Berthier, C.; Mali, M.; Roos, J.; Brinkmann, D.; Armand, M. B. *Solid State Ionics* **1988**, *28-30*, 1018.

(22) Lee, C. C.; Wright, P. V. *Polymer* **1982**, *23*, 681.

(23) Payne, D. R. *Polymer* **1982**, *23*, 690.

(24) Torell, L. M.; Schantz, S. *J. Non-Cryst. Solids* **1991**, *131-133*, 981.

(25) Watanabe, M.; Ikeda, J.; Shinohara, I. *Polym. J.* **1983**, *15*, 175.

(26) Watanabe, M.; Ikeda, J.; Shinohara, I. *Polym. J.* **1983**, *15*, 65.

(27) Lin, B.; Halley, J. W. In *The American Physical Society*; San Jose, California, **1995**; pp 50.

(28) Papke, B. L.; Ratner, M. A.; Shriver, D. F. *J. Electrochem. Soc.* **1982**, *129*, 1434.

(29) Papke, B. L.; Ratner, M. A.; Shriver, D. F. *J. Electrochem. Soc.* **1982**, *129*, 1694.

(30) Frech, R.; Manning, J.; Teeters, D.; Black, B. E. *Solid State Ionics* **1988**, *28-30*, 954.

(31) Frech, R.; Manning, J.; Black, B. *Polymer* **1989**, *60*, 1785.

(32) Manning, J.; Frech, R.; Hwang, E. *Polymer* **1990**, *31*, 2245.

(33) Watanabe, M.; Oohashi, S. I.; Sanui, K.; Ogata, N.; Kobayashi, T.; Ohtaki, Z. *Macromolecules* **1985**, *18*, 1945.

(34) Watanabe, M.; Sanui, K.; Ogata, N.; Kobayashi, T.; Ohtaki, Z. *J. Appl. Phys.* **1985**, *57*, 123.

(35) Papke, B. L.; Ratner, M. A.; Shriver, D. F. *J. Phys. Chem. Solids* **1981**, *42*, 493.

(36) Matsuura, H.; Fukuhara, K. *J. Mol. Struct.* **1985**, *126*, 251.

(37) Maxfield, J.; Shepherd, I. W. *Polymer* **1975**, *16*, 505.

(38) Takahashi, H.; Kyu, T.; Tran-Cong, Q.; Yano, O.; Soen, T. *J. Polym. Sci., Part B* **1991**, *29*, 1419.

(39) Koenig, J. L.; Angood, A. C. *J. Polym. Sci., Part A-2* **1970**, *8*, 1787.

CHAPTER 2

SPECTROSCOPIC ANALYSIS OF CHAIN CONFORMATION OF POLY(PROPYLENE OXIDE) BASED POLYMER ELECTROLYTES

2.1 Introduction

As a matrix for polymer electrolytes, poly(propylene oxide)(PPO) has been studied in order to understand ionic conduction mechanism.[1-8] Because of the property forming an amorphous phase in the presence of salt as well as in pure polymer state, atactic PPO has advantage over poly(ethylene oxide)(PEO) system by removing polymer crystallinity which was an impedance for ionic conduction mechanism study. Although PPO based polymer electrolyte has been interested for more than a decade, only macroscopic properties such as viscosity and ionic conductivity of the system have been reported. Because of the lack of information of microscopic structure of polymer in the presence of salt, clarification of ionic conduction mechanism is still far to be achieved.

Salt solubilization in a polymer matrix is achieved through the solvation of ions by polymer chain. As described in Chapter 1, ether oxygens along the PPO and PEO chains provide electron pair to the cations to form polymer—ion complexes.[9,10] This interaction can cause chain conformational change of polymer matrix. While there are a number of studies focused on the characterization of PEO conformational changes by salt complex formation[11-15], no information is available for PPO chains in the presence of salt.

Vibrational spectroscopy, both infrared(IR) and Raman can be used to characterize conformational changes induced by polymer-salt interactions. Some of vibrational

frequencies are dependent on chain conformations and this dependence is not only limited to the ordered state of polymer but also it is applied to disordered polymer chains. That is the advantage of using vibrational spectroscopy. Several spectroscopic studies have been conducted for PPO based polymer electrolytes but very limited quantitative structural analysis has been carried out.[1-5]

In this study, we utilized Raman spectroscopy to characterize chain conformational change of PPO in the presence of salt, $LiClO_4$. In Raman spectroscopy, molecular vibrational information is acquired from inelastic scattering of incident light and the molecules.[16-18] When a molecule is irradiated by the electromagnetic wave(incident beam) whose electric field strength is E, an electric dipole moment P is induced by equation (2.1).

$$\mathbf{P}=\alpha\mathbf{E} \qquad (2.1)$$

In this equation, α is polarizability tensor since both **P** and **E** are vectors consisting of three components in the x, y, and z directions.[16] The vibration is Raman active if one of components of the polarizability tensor is changed during the vibration.

Chain conformational change of PPO results in the change in polarizability along the chain backbone. Therefore it can be reflected on the Raman spectra. Low frequency Raman bands observed for PPO based electrolytes have considerable contributions from CCO/COC skeletal bending coordinates and can be sensitive to chain conformational changes. These bands exhibited significant frequency shifts and bandwidth changes as a function of salt concentration.[1] The frequency shifts have been interpreted in terms of changing chain stiffness.[5] There are also other new unexplained spectroscopic features present when salts are introduced and a detailed interpretation of PPO structure in the presence of salts has yet to emerge. Since the PPO used for polymer electrolytes has a disordered structure, the obtained vibrational spectra generally consist of overlapping features associated with many different chain conformations. For the analysis of this

complex feature of the spectra in relation to chain conformation, a theoretical normal coordinate analysis(NCA) has been utilized. The basic theory of NCA and the description of the program used in this study can be found in Appendix A.

To reduce the complexity of our analysis, 1,2-dimethoxypropane (DMP) has been utilized as a model compound for PPO. The spectral change obtained for the model compound by salt addition remarkably resembles that obtained for PPO. DMP has the same structure as the chemical repeat unit of poly(propylene oxide).[19] In addition, conformational analysis has revealed that the conformer distribution obtained for DMP was no different from that of the C-C bond along the PPO chain, even though long range interactions are not considered.[19] Although it is difficult to characterize a disordered polymer state utilizing information obtained from a small molecular model, some vibrational modes are sufficiently localized to be used for analysis of common spectroscopic features in both the model and polymer. By analyzing experimental data in conjunction with normal coordinate analysis, chain conformational changes of PPO in the presence of salts can be obtained. Our results are reported herein.

2.2 Materials and Experiments

2.2.1 Preparation of salt complexed hydroxy terminated poly(propylene oxide)

Hydroxy terminated PPO (HPPO) samples of molecular weight 425 (HPPO425), 1000 (HPPO1000), and 4000 (HPPO4000) were obtained from Aldrich Chemical Co. The hydroxy number (Table 2.1) was determined by titration (ASTM D4274). Brief explanation of ASTM D4274 is given in Appendix C.1.

Table 2.1 The hydroxy number of HPPO.

MW	-OH number (mg of KOH/g)*
425	—
1000	111.85
2000	55.56
3000	35.24
4000	26.94

* Determined by titration based on ASTM D4274

Extreme care was exercised to prevent water contamination during sample preparation. HPPO samples received were dried under high vacuum at 70 °C. Lithium perchlorate obtained from Aldrich was also dried at 150 °C under high vacuum for one day, dissolved in fresh dried THF (Aldrich) and then added to the dried HPPO under dry argon gas in a glove bag. The solvent was removed at 60 °C, stored for two days under vacuum and then further dried at 100-130 °C at high vacuum depending on the HPPO molecular weight. Lastly, all samples were dried at room temperature for an additional week at high vacuum. HPPO-$LiClO_4$ complexes were prepared with compositions of molar ratio of lithium cations and propylene oxide unit, $[Li^+]/[-O-] = 0.05, 0.10, 0.15$, and 0.20. 1,2-dimethoxypropane (DMP) was used as received from Aldrich. Lithium complexed DMP's were prepared by dissolving $LiClO_4$ directly into DMP.

2.2.2 Preparation of methoxy terminated poly(propylene oxide)s and their salt complexes

(1) Preparation of MPPO

Methoxy terminated PPO (MPPO) was prepared based on Williamson method[20] in order to examine end group effects. We selected two lowest HPPO's of molecular weights 425 and 1000 as the largest end group effects are expected for these samples. The round bottomed reaction flask containing dried HPPO was connected under dry argon gas to a condenser equipped at the top with a drying agent. The HPPO's had been treated with NaH (Aldrich, 95%) for one day. Excess CH_3I was added by syringe into the flask and the reaction mixture allowed to stand for another day. The NaH residue was killed by MeOH and the mixture separated to MPPO and other side products and impurities by separatory fractionation. MPPO was obtained as a yellow transparent liquid. Reaction scheme is shown in Figure 2.1.

$$HO\text{-}(CH(CH_3)CH_2O\text{-})_nH + NaH \text{ ---> } Na^{+}\text{-}O\text{-}(CH(CH_3)CH_2O^{-}\text{-})_n{}^{+}Na + H_2\uparrow$$

$$Na^{+}\text{-}O\text{-}(CH(CH_3)CH_2O^{-}\text{-})_n{}^{+}Na + CH_3I \text{ ---> } CH_3O\text{-}(CH(CH_3)CH_2O\text{-})_nCH_3 + NaI$$

Figure 2.1 Reaction scheme for preparation of MPPO from HPPO.

(2) Characterization of MPPO

Complete substitution of end group from hydroxy to methoxy has been confirmed by several techniques. Fourier transform infrared(FT-IR) spectra of HPPO and prepared MPPO are shown in Figure 2.2. No detectable intensity in the -OH stretching band were observed and new symmetric alkyl stretching band assignable to $-CH_3$ group connected to the ether oxygen is seen at 2818 cm^{-1}.[17] FT-IR spectra obtained at room temperature by use of an IBM 38 system equipped with a dry nitrogen line and DTGS detector. The FT-

IR spectra were obtained with samples pressed between two potassium bromide plates and 128 scans were signal averaged at a spectral resolution of 2 cm^{-1}. Use of a Bruker FT-NMR (200 MHz) also provided no significant peak indicative of hydroxy groups. The ratio of the number of hydrogens of CH_3 in -O-CH_3 units and -C-CH_3 units calculated by integrating the area under the peaks was obtained as expected for perfect substitution. Polydispersity of sample before and after the reaction was measured by use of a GPC equipped with polystyrene columns and a differential refractometer (Waters). Polydispersity index(PDI) was 1.112 for HPPO and 1.077 for MPPO. No significant change in PDI indicated no polymer degradation. Finally, microanalysis provided no detectable content of sodium and iodine. Microanalysis was carried out at the elemental analysis laboratory in the University of Massachusetts.

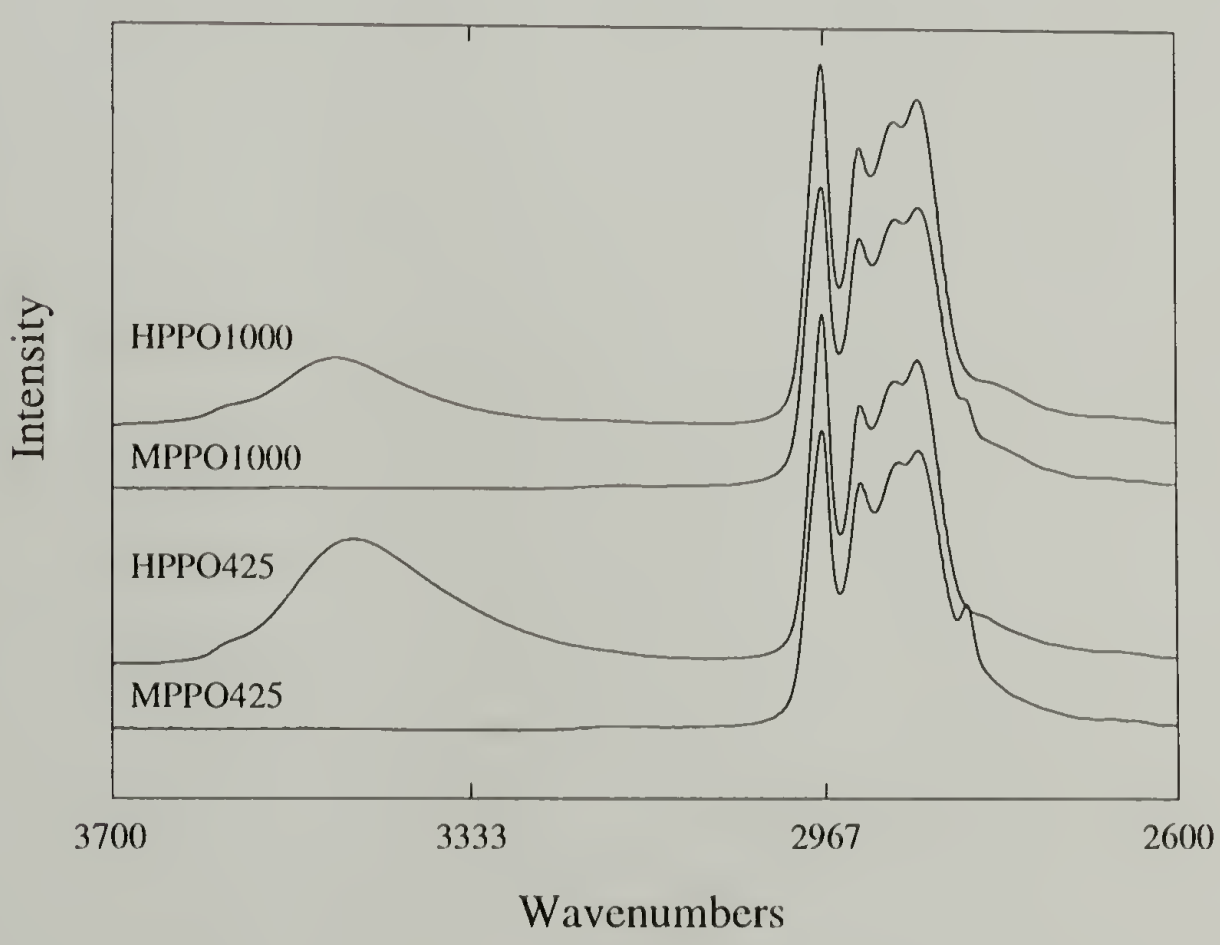

Figure 2.2 FT-IR spectra of HPPO and MPPO for molecular weight 425 and 1000.

(3) Macroscopic phase separation behavior in $LiClO_4$ complexed MPPO

$LiClO_4$ complexed MPPO's were prepared by the same procedure utilized for preparation of salt complexed HPPO's. When MPPO dissolved into the THF solution of $LiClO_4$, the mixture was a homogeneous solution. However, after the solvent was removed, a two layer macroscopic phase separation was found for samples below a certain salt concentration.

Raman spectroscopy, differential scanning calorimetry (DSC), and microanalysis were utilized for characterization of each layer. The upper layer was found to consist of pure MPPO while the bottom layer turned out to be $LiClO_4$-MPPO complex. Glass transition temperature and salt concentration data measured by microanalysis are given in Table 2.2. We should mention that the microanalysis result was only accurate enough to reproduce the known amount of lithium ions within approximately 10~20% of uncertainty. Therefore, within a 20% error range, the salt concentration in the $LiClO_4$-MPPO complexes can be considered to be independent of the initial content of salt and the composition was around 0.15 ± 0.02 in terms of $[Li^+]/[-O-]$. Although the estimated salt concentration is not accurate, since we observed clear phase separation for MPPO425 at an initial salt content, $[Li^+]/[-O-]=0.15$ even though the upper phase was extremely small, while MPPO1000 at the same salt concentration does not phase separate, it seems likely that the stoichiometric salt content in salt complexed MPPO1000 is lower than salt complexed MPPO425. However, because we also found kinetic factors involved in the phase separation process, it is possible for salt complexed MPPO425 and 1000 to have different phase separation rates. We did not study the kinetics of phase separation further. Detailed end group effects will be discussed in Chapters 3 and 4.

Table 2.2 Glass transition temperature(T_g) and salt content([Li^+]/[-O-]) of MPPO and $LiClO_4$-MPPO complexes after phase separation.

	Initial salt concentration	Phase*	Tg(°C)**	[Li^+]/[-O-]***
MPPO425	0.0		-93.4	0.0
	0.05	U	-95.1	0.0
		L	-24.7	0.150
	0.10	U	-92.9	—
		L	-25.5	0.167
	0.15@	U	—	—
		L	-23.8	0.184
	0.20		-8.0	
MPPO1000	0.0		-82.9	0.0
	0.05	U	-81.4	0.0
		L	-16.0©	0.134
	0.10	U	-81.8	—
		L	-17.4©	0.127
	0.15		-8.8	
	0.20		2.3	

* U and L stand for upper phase and lower phase, respectively.
** T_g's have been taken at inflection points and averaged over three measurements.
*** Lithium cation content has been measured by Microanalysis. The estimated values contained 20% of uncertainty.
@ This complex shows a small amount of upper phase portion. Therefore upper phase could not be separated for further measurements.
© Lower phase of $LiClO_4$ complexed MPPO1000 showed two T_g's of pure MPPO and salt containing MPPO right after samples have been prepared. However, as time goes on, further phase separation has been found and the lower phase shows a single T_g.

2.2.3 Experiments

Fourier transform Raman spectroscopy was utilized for the chain conformational study. The use of a long wavelength source removed the influence of fluorescence emitted by some samples during laser excitation with visible light. The spectra were obtained at room temperature using a Bruker FRA 106 spectrometer. A Nd:Yag laser with a wavelength of 1064 nm was used as excitation. The laser output power was maintained at 500 mW. 1024 scans were loaded to obtain an enhanced signal to noise ratio. The excitation collection geometry was 180° and spectral resolution maintained at 4 cm^{-1}. Detailed experimental method is given in Appendix C.2.

Raman spectra were obtained for HPPO's of molecular weight 425, 1000, 2000, 3000, and 4000. All samples exhibit identical features in the observed Raman spectra. Therefore, we report only the spectra obtained for the two extreme molecular weights. Figure 2.3 presents Raman spectra of HPPO425 and HPPO4000 and their salt complexes. Three bands at around 930, 624, and 458 cm^{-1} showing significant intensity change by salt addition are assigned to Raman active vibrational stretching modes of perchlorate anion in polyether medium.[5] Except these bands, rest of bands are all related to the vibrational modes of PPO chains. Similar Raman data obtained for DMP and its salt complexes are shown in Figure 2.4. One interesting region showing spectral changes is that between 700-900 cm^{-1}.[5] The spectra obtained for DMP, HPPO, and their salt complexes in this region are shown in Figure 2.5.

2.3 Results and Discussion

As seen in Figure 2.5, the bands in the 700-900 cm^{-1} region are broad and ill defined in the absence of salt. However, an obvious change in intensity at ca. 810 cm^{-1} is observed with increasing salt concentration. As shown in Table 2.3, these band

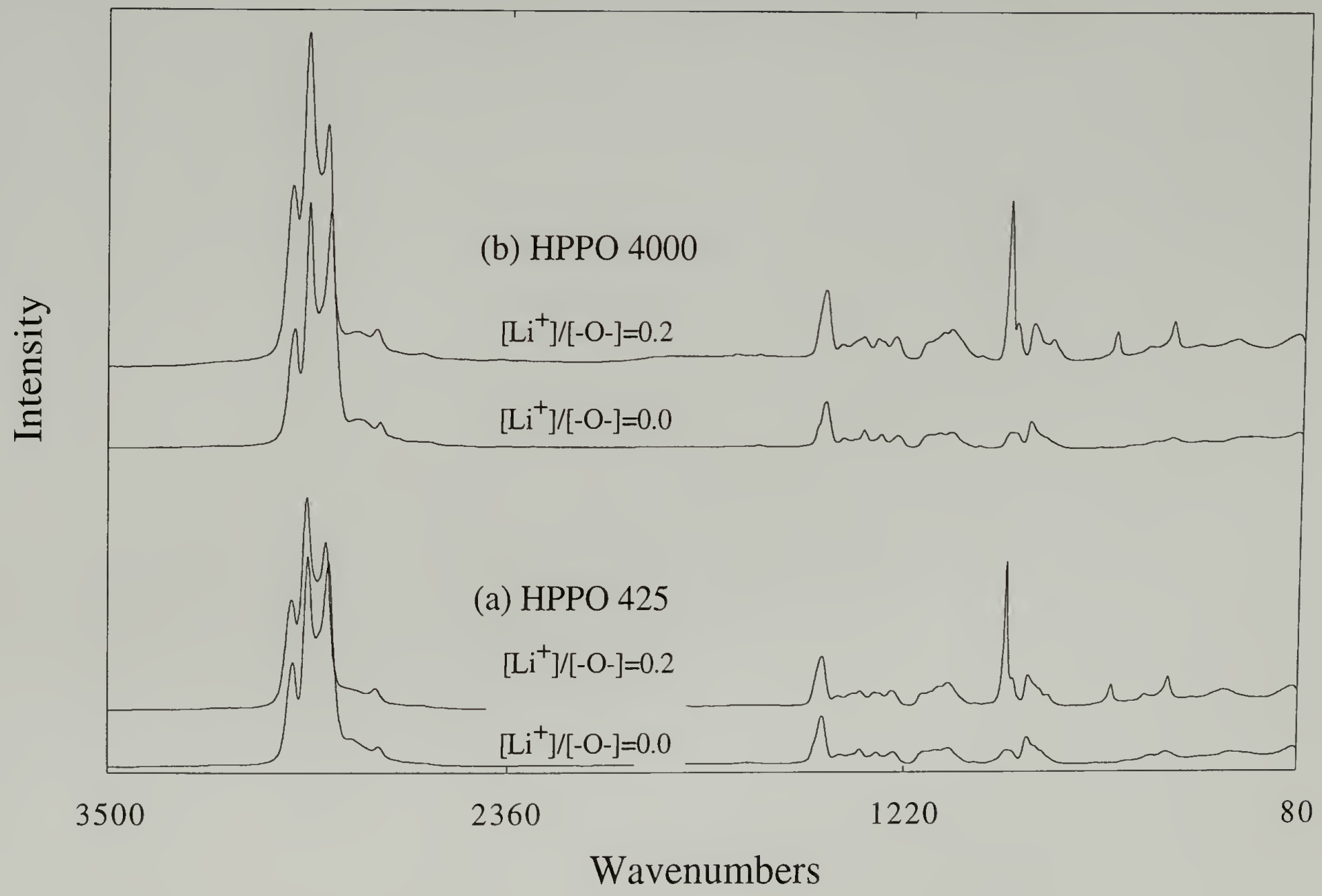

Figure 2.3 Fourier transform Raman spectra of uncomplexed HPPO and HPPO-$LiClO_4$ complex ; Spectral resolution was maintained at 4 cm^{-1} ; Laser power was maintained at 500 mW at the sample.

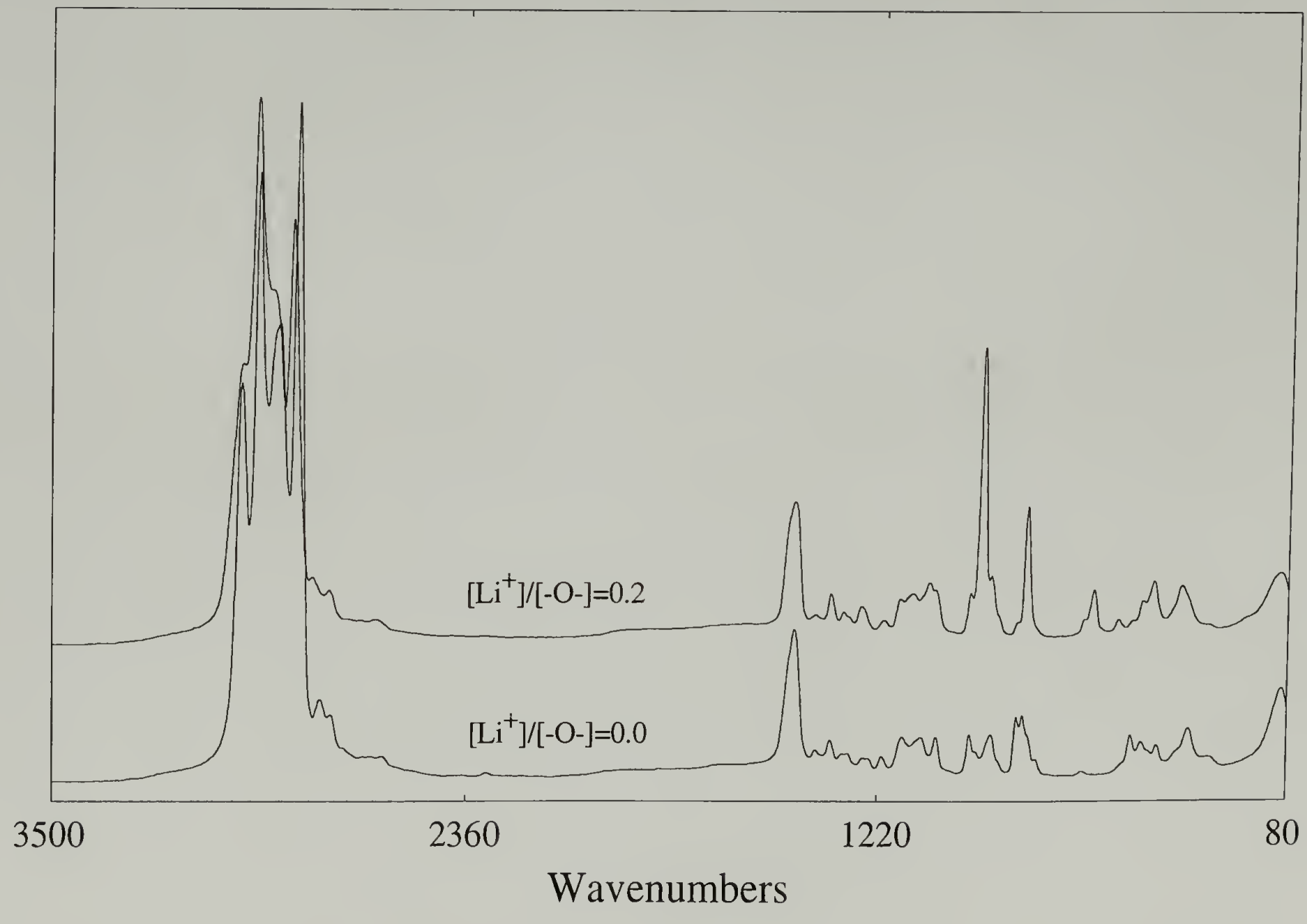

Figure 2.4 Fourier transform Raman spectra of 1,2-dimethoxypropane(DMP) and $LiClO_4$ complexed DMP in the 80-3500 cm^{-1} region.

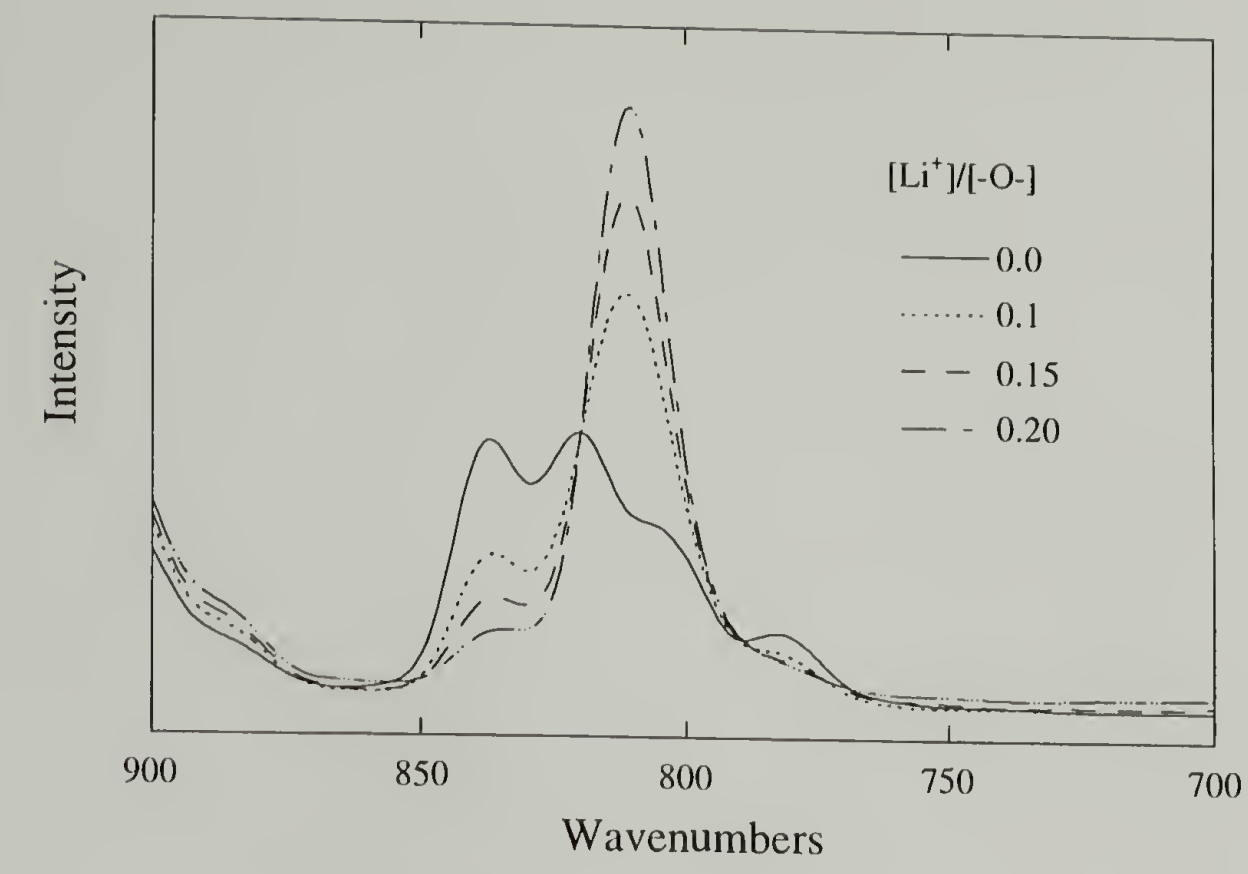

Figure 2.5 Fourier transform Raman spectra over the region between 700-900 cm^{-1} at $[Li^+]/[-O-]$=0 to 0.2 ; (a) DMP, (b) HPPO 4000.

frequencies are independent of molecular weight and therefore must be sufficiently localized to reflect a localized vibrational mode. Although this observation has been mentioned previously,[5] to our knowledge no explanation has been proposed regarding these spectroscopic changes. A new weak shoulder at ca. 851 cm^{-1} appeared in the HPPO-salt complex as seen in Figure 2.5.

Table 2.3 Energy(wavenumbers) at ca. 810 cm^{-1} dependence on salt concentration and chain length.

	DMP	HPPO425	HPPO1000	HPPO4000	MPPO425	MPPO1000
$[Li^+]/[-O-]$			wavenumbers			
0.0	807	—	—	—	807	—
0.05	813	810 (sh)	808 (sh)	810 (sh)		
0.10	811	810	808	809		
0.13*						809
0.15	811	810	808	808		
0.17*					810	
0.20	811	809	808	807		

sh : shoulder.

* : determined by Microanalysis for lower layer of salt complexed MPPO.

HPPO and DMP exhibit significantly different intensity changes as a function of $LiClO_4$ salt concentration. The changes are more dramatic in DMP than in HPPO. The intensity at 810 cm^{-1} normalized to the 624 cm^{-1} assignable to perchlorate anion for HPPO's by changing molecular weight is shown in Figure 2.6. The intensity change is seen to be molecular weight dependent, increasing linearly with increasing chain length. However, the largest change at that particular band observed for DMP compared with any

other HPPO system is contradictory to this molecular weight dependence. It is possible then that there is a contribution from specific interactions between the ions introduced and hydroxy end groups of HPPO's.

The effect of hydroxy end groups was then evaluated by analyzing methoxy substituted PPO's (MPPO). In this study of end group effects, as described above, we have synthesized MPPO's of molecular weights 425 and 1000. These lower molecular weights of PPO's were chosen because larger end group effects were expected in comparison to PPO's of higher molecular weights. As end effects are expected to dominate for HPPO of the lowest molecular weight, we have reported the observed spectra. The Raman spectra of pure MPPO of molecular weight 425 and its salt complexed MPPO are shown in Figure 2.7. Similar to changes observed in the DMP-$LiClO_4$ system, the significant intensity change occurs in the 800 cm^{-1} region. Unlike HPPO of the same molecular weight, the 810 cm^{-1} band becomes dominant in the salt complexed MPPO. Since lithium cation can interact with hydroxy groups as well as ether oxygen, this difference between MPPO and HPPO salt complexes indicates that the intensity change at 810 cm^{-1} results from interaction between the lithium cation and ether oxygen. Also, the molecular weight dependence of the band intensity at 810 cm^{-1} can be explained in terms of the relative content of hydroxy groups. Again, a new band was observed at 853 cm^{-1} in salt complexed MPPO as observed in salt complexed HPPO. An explanation for that spectral change is not available at this point.

In order to analyze spectral changes observed in 800 cm^{-1} region of Raman spectra in the presence of salt in relation to chain conformation, Raman spectra of DMP have been calculated. For numerical analysis of DMP as a model compound, we considered three energy minimum states suggested for the propylene oxide unit. Newman projections of the three states are given in Figure 2.8 for the S-configuration of chiral carbon. Among the three lowest energy states, the gauche α conformation has been suggested to be the most

stable for both DMP and PPO and is attributed to the "gauche oxygen effect".[21-23] Since our experiments reveal great similarity between the spectra obtained for DMP and PPO when both form salt complexes, an analysis of the DMP vibrational spectrum can be used to explain spectral changes occurring in PPO in the presence of salt.

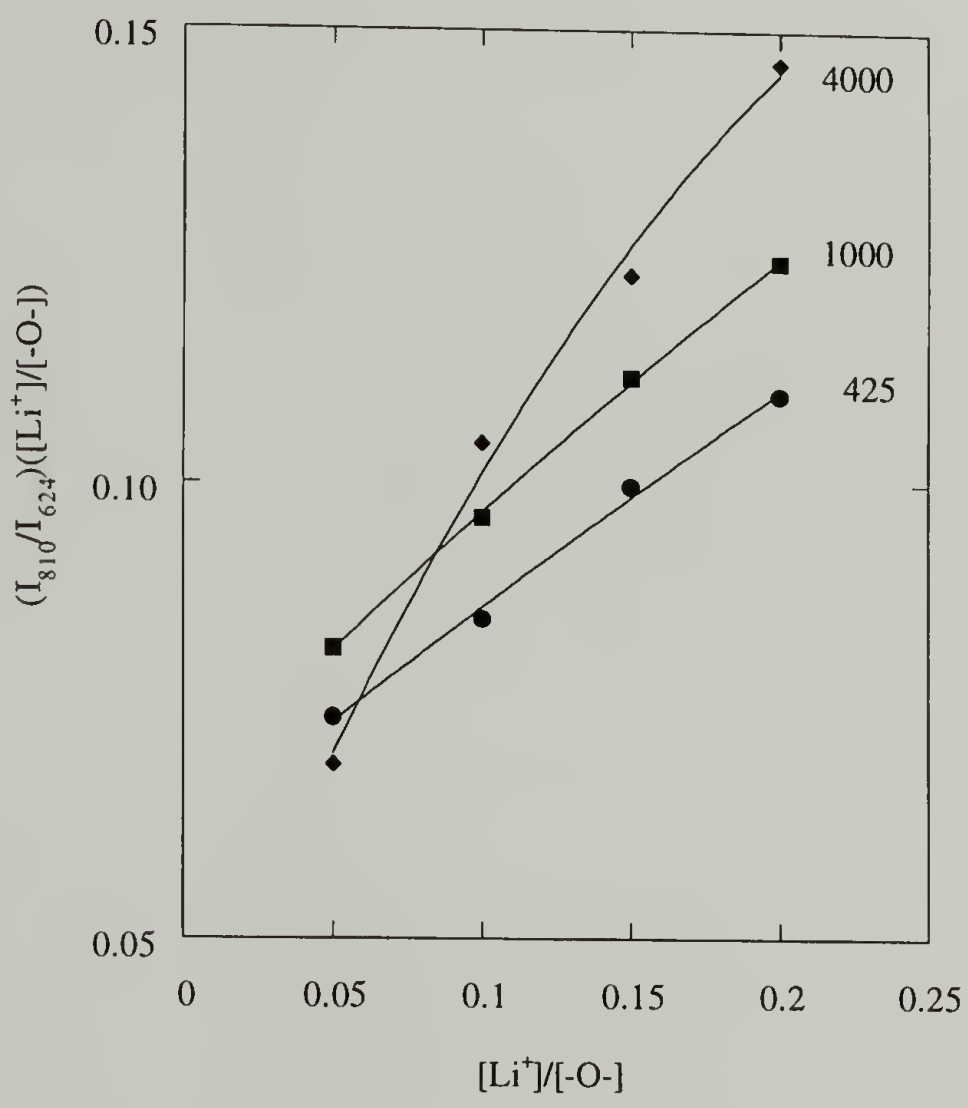

Figure 2.6 The Li^+ concentration dependence of the intensity at ca.810 cm^{-1} for different molecular weight of HPPOs.

The number of normal modes expected for each DMP conformer is 51. In our analysis, all bond angles were assumed to be tetrahedral. C-H, C-O, and C-C bond lengths were assumed to be 1.096, 1.41, and 1.54 Å respectively.[24]

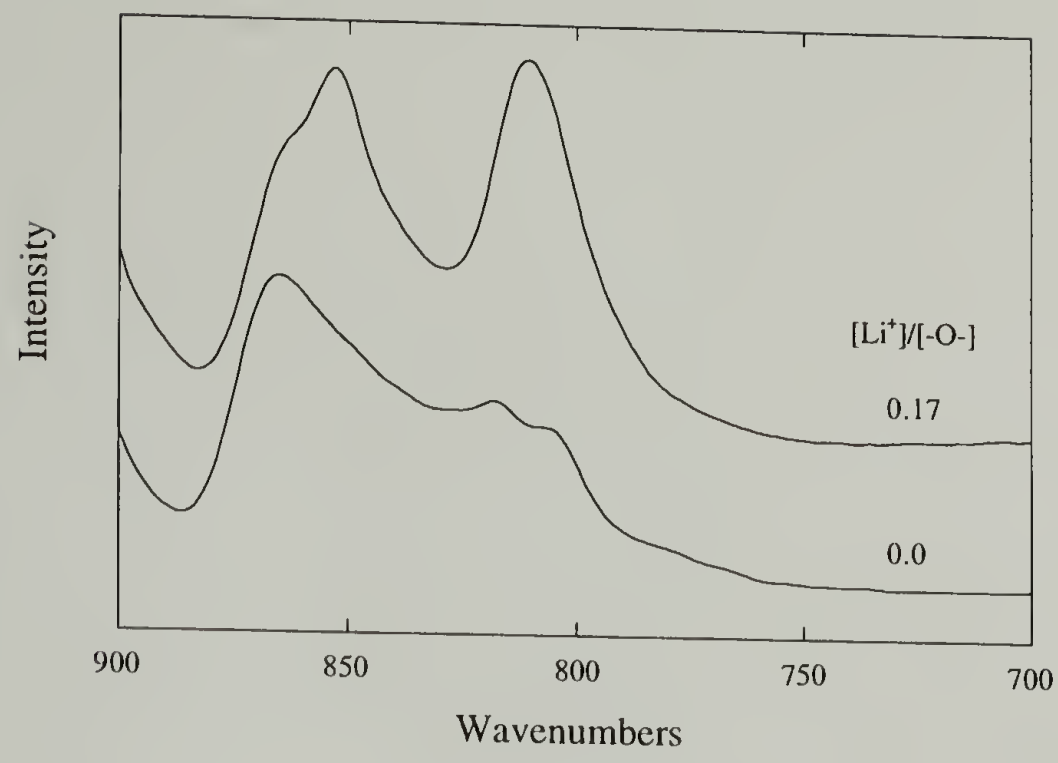

Figure 2.7 Fourier transform Raman spectra of uncomplexed MPPO and $LiClO_4$ complexed MPPO (the lower layer after phase separation) in the 700-900 cm^{-1} ; MW of MPPO=450.

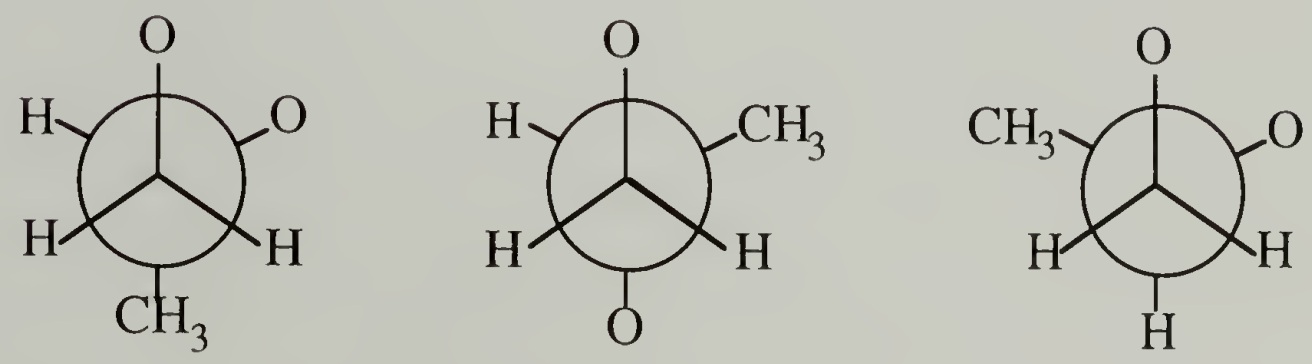

Figure 2.8 Newman projections of three energy minimum states suggested for propylene oxide unit of DMP and PPO for (S)-configuration.

The computer program used in this study has been described earlier.[24-34] The dihedral angles associated with the trans, gauche α, and gauche β states are assigned to 180, 60 and -60, respectively, at the beginning of each calculation. A conformational distribution is

then generated based on the statistical weight expected for the final distribution of the structure. Variations of 5 degrees were used to simulate fluctuations associated with each dihedral angle. The orientation of the end and side methyl groups is fixed. The number of conformers used in the calculation was 3000.

The isotropic Raman spectrum, S(ν), of DMP was approximated based on the equation (A.11). Each conformer C was generated by the probability of each conformation assigned to each bond to obtain the final conformational distribution. C_T is the total number of conformers, i.e. 3000 in our calculation. The conformational probability, i.e. energy difference between trans and gauche conformers of each DMP bond, is adjusted until the most similar Raman spectrum with experimental result is obtained.

Our analysis of calculated Raman spectrum indicates that the C-C and C-O stretching vibrations are the most significant contributors to the isotropic Raman intensity in the range of 700~900 cm^{-1}. Other internal coordinates, such as CH_2 rocking, certainly couple to these stretching coordinates. But the polarizability changes are generally quite small. Their contributions to the overall intensity can thus be ignored.[34-36] The scattering activity of the kth normal mode can then be given by the expression (2.2) based on the equation (A.10),

$$\mathbf{S_k} \propto \left[\sum_{\mathbf{i}} \alpha'_{\mathbf{CO}} \mathbf{L_{ik}} + \sum_{\mathbf{j}} \alpha'_{\mathbf{CC}} \mathbf{L_{jk}} \right]^2 \qquad (2.2)$$

where L_{ik} is the normal coordinate element for the ith C-C stretching internal coordinate and L_{jk} is that for the C-O stretching coordinate, α'_{cc} and α'_{co} are the mean polarizability derivatives associated with C-C and C-O stretching, respectively. The mean polarizability derivative ratio of the C-C to C-O stretch used in this calculation is 2:1. Since the intensity parameters associated with the ether oxygen are not well established, we have determined that ratio based on the bond polarizability values transferred from methyl vinyl ether and

alkanes.[37,38] The values used give the best fit to the data measured. These values are assumed to be insensitive to changes in chain conformation.[34,39] The temperature effects on the occupation probability of various vibrational levels are extremely small for bands in this region and therefore not considered. The calculated spectra are expressed in terms of scattering activity by giving to each frequency a Lorentzian band shape having a FWHM (full width at half maximum) of 8 cm^{-1}.[33] We have determined that $I_{\perp}$ has only limited intensity in the 800 cm^{-1} region. Therefore, we assume that the isotropic Raman spectrum can be approximated to the unpolarized spectra obtained in our Fourier transform instrument.

The calculated isotropic Raman spectra of a chain having certain conformational distribution and one for the $TG_{\alpha}T$ conformation along the -O-C-C-O- bond of (S)-DMP are shown in Figure 2.9. Three bands at 835, 817, and 807 cm^{-1} are calculated for the conformational distribution inserted in Figure 2.9. A single band at 812 cm^{-1} is calculated for the $TG_{\alpha}T$ conformation. On the basis of analysis of the characteristics of normal modes, the lowest frequency component at 807 cm^{-1} (or 812 cm^{-1}) is attributed to trans(O-C)-gauche α (C-C)-trans(C-O)($TG_{\alpha}T$) conformation. The band centered at 817 cm^{-1} has contributions from molecules associated with $G_{\alpha}G_{\alpha}T$ and/or $G_{\beta}G_{\alpha}T$ conformers. In good agreement with a previous study,[40] the main contributor to the band at 835 cm^{-1} was the trans(O-C)-trans(C-C)-trans(C-O)(TTT) conformation of the -O-C-C-O- bond. On the basis of comparison of the relative intensity of the bands associated with different conformations, we conclude that $E_{g\alpha}$ associated with the C-C is -120 cal/mol relative to the trans conformer. The energy difference is smaller than the measured value of DMP in the gaseous phase.[21,23] Once polarizability tensors are determined from earlier studies,[37,38] there are no additional adjustable parameters available to better fit the experimental data.

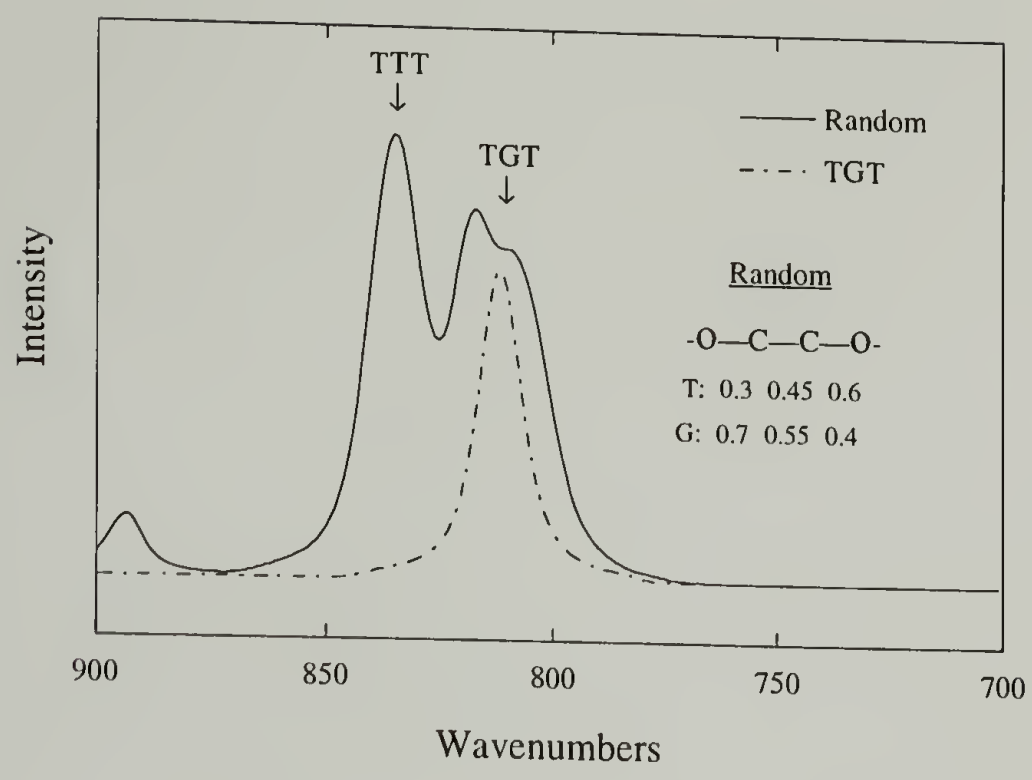

Figure 2.9 The calculated spectra of (S)-DMP obtained for a random conformational distribution and for the $TG_{\alpha}T$ conformation in the 700-900 cm^{-1}.

The normal mode calculation was extended to MPPO having chemical repeat units of (S)-configuration. The fundamental frequencies obtained by calculation in the 800-900 cm^{-1} region are given in Table 2.4. The characteristic band of $TG_{\alpha}T$ conformation at 806 cm^{-1} (811 cm^{-1} for DMP) is clearly separated from bands associated with other conformations, particularly the TTT conformation. The calculated band position of the $TG_{\alpha}T$ conformation obtained for MPPO having more than two units of propylene oxide was found to change slightly (a few wavenumbers) depending on the conformation of the neighbor bonds or structural defects such as head-to-head sequences in our calculation. The band in the 805~810 cm^{-1} can only be associated with a $TG_{\alpha}T$ conformation of -O-C-C-O- bond regardless of chain length.

As can be seen from Figures 2.5 and 2.9, the experimental data for both frequency and intensity can be simulated extremely well by chains having a conformational

distribution such as insertion in Figure 2.9. On the basis of the simulated spectra, observed bands of DMP centered at 836 and 807 cm^{-1} are assigned to TTT and $TG_{\alpha}T$ conformations respectively. As mentioned above, the strong band at 811 cm^{-1} in the DMP-$LiClO_4$ complex can definitely be assigned to the $TG_{\alpha}T$ conformation since the experimental and calculated spectra superimpose nearly exactly. Therefore we conclude that the intensity increase of this band when salt is added is attributed to the increase in the $TG_{\alpha}T$ conformation population induced by interaction between the lithium cation and ether oxygens. This result indicates that the lithium cation prefers to interact with the gauche α conformation of the -C-C- bond. In the absence of salt, the conformational distribution of either PPO or DMP is broad and therefore the corresponding Raman spectra also exhibit broad overlapping bands. When salt is added, the interaction between the lithium cation and ether oxygen narrows the conformational distribution and thus the $TG_{\alpha}T$ conformation is dominant. As expected, the band associated with this conformation then emerges as the principal band in the 800 cm^{-1} region. This assignment can be extended to both HPPO and MPPO systems. As mentioned above, the band frequency assignable to the $TG_{\alpha}T$ conformation of the -O-C-C-O- bond can be changed by a few wavenumbers depending on the conformation of neighboring -O-C-C-O- units.

The small energy (frequency) difference in the bands observed in DMP or PPO versus their corresponding salt complexes can be explained in two ways. First, the frequency shift can be attributed to the change in the valence force field by salt addition. Or, as already experienced by calculation, it can simply be caused by overlapping of broad bands because the exact band position for a certain conformation can be perturbed by the contribution from others when molecules have a broad chain conformational distribution. Our case is close to the latter. In our calculation, we did not take into account the possibility of changes in force constants induced by salt interactions. Since the experimental data can be explained by our calculated results, even with small changes in the

force field, the effects do not appear significant, at least for vibrational modes in the 800 cm^{-1} region.

Table 2.4 Energy of the bands in the 800-900 cm^{-1} region for various conformations calculated by normal coordinate analysis for $CH_3O\text{-}(CH(CH_3)CH_2O\text{-})_n\text{-}CH_3$.

n	Sequence*	Conformation	Wavenumbers
1		TTT	835
		$TG_\alpha T$	812
		$TG_\beta T$	799
		$G_\alpha G_\alpha T$	818
		$G_\beta G_\alpha T$	815
3	H-T-H-T	$(TTT)_3$	861, 847, 825
		$(TG_\alpha T)_3$	870, 839, 806
	H-T-H-H	$TG_\alpha TTG_\beta TTG_\alpha T$	842, 810
		$TG_\alpha TTG_\alpha TTG_\beta T$	857, 814,800
4	$(H\text{-}T)_3$	$(TTT)_4$	862, 856, 841, 823
		$(TG_\alpha T)_4$	875, 856, 830, 806
7	$(H\text{-}T)_6$	$(TTT)_7$	863, 862, 858, 852, 842, 831, 822
		$(TG_\alpha T)_7$	880, 873, 862, 848, 833, 820, 806

* H : Head, T : Tail

2.4 Conclusions

In this study we applied normal coordinate analysis to 1,2-dimethoxypropane and methoxy terminated PPO in order to investigate the chain conformational dependence of Raman bands in the disordered state. We then characterized changes in the conformational distribution of PPO in the presence of $LiClO_4$. An isotropic Raman spectrum for DMP can

be generated by calculation in the 700-900 cm^{-1} region. By comparison of calculated isotropic Raman spectra with experimental results, the characteristic band at ca. 810 cm^{-1} increasing in intensity with salt concentration has been assigned to the $TG_{\alpha}T$ conformation. Studies were extended to MPPO up to 7-mer and consistent results obtained. It was found that the interaction between the lithium cation and ether oxygen predominantly contributes to formation of the gauche α conformation of -C-C- bonds along the backbone. The chain conformational distribution of PPO has been changed to the distribution having increased gauche α conformations of C-C bonds by interaction of Li^{+} and ether oxygen. As confirmed in Fourier transform Raman spectra obtained for an extensive PPO molecular weight range along with calculated results, the characteristic band around 810 cm^{-1} represents a common conformation ($TG_{\alpha}T$) in local bonds of -O-C-C-O- regardless of chain length. Therefore this assignment can be used for information concerning the relative content of the $TG_{\alpha}T$ conformation of propylene oxide units in any PPO system.

References

(1) Frech, R.; Manning, J.; Teeters, D.; Black, B. E. *Solid State Ionics* **1988**, *28-30*, 954.

(2) Frech, R.; Manning, J.; Black, B. *Polymer* **1989**, *60*, 1785.

(3) Manning, J.; Frech, R.; Hwang, E. *Polymer* **1990**, *31*, 2245.

(4) Manning, J.; Frech, R. *Polymer* **1992**, *33*, 3487.

(5) Schantz, S.; Torell, L. M.; Stevens, J. R. *J. Appl. Phys.* **1988**, *64*, 2038.

(6) Watanabe, M.; Ikeda, J.; Shinohara, I. *Polym. J.* **1983**, *15*, 175.

(7) Watanabe, M.; Ikeda, J.; Shinohara, I. *Polym. J.* **1983**, *15*, 65.

(8) Kakihana, M.; Schantz, S.; Torell, L. M. *J. Chem. Phys.* **1990**, *92*, 6271.

(9) MacCallum, J. R.; Vincent, C. A., Ed.; *Polymer Electrolyte Reviews* ; Elsevier Applied Science: London, **1987**; Vol. 1.

(10) Watanabe, M.; Ogata, N. *Brit. Polym. J.* **1988**, *20*, 181.

(11) Takahashi, H.; Kyu, T.; Tran-Cong, Q.; Yano, O.; Soen, T. *J. Polym. Sci., Part B* **1991**, *29*, 1419.

(12) Papke, B. L.; Ratner, M. A.; Shriver, D. F. *J. Phys. Chem. Solids* **1981**, *42*, 493.

(13) Maxfield, J.; Shepherd, I. W. *Polymer* **1975**, *16*, 505.

(14) Matsuura, H.; Fukuhara, K. *J. Mol. Struct.* **1985**, *126*, 251.

(15) Koenig, J. L.; Angood, A. C. *J. Polym. Sci., Part A-2* **1970**, *8*, 1787.

(16) Ferraro, J. R.; Nakamoto, K. *Introductory Raman Spectroscopy*; Academic Press: San Diego, **1994**.

(17) Colthup, N. B.; Daly, L. H.; Wiberley, S. E. *Introduction to Infrared and Raman spectroscopy;* 3rd ed.; Academic press: San Diego, **1990**, pp 327.

(18) Painter, P. C.; Coleman, M. M.; Koenig, J. L. *The theory of vibrational spectroscopy and its application to polymeric materials*; John Wiley & Sons: **1982**.

(19) Abe, A.; Hirano, T.; Tsuruta, T. *Macromolecules* **1979**, *12*, 1092.

(20) Pine, S. H.; Hendrickson, J. B.; Cram, D. J.; Hammond, G. S. *Organic Chemistry;* 4th ed.; McGraw-Hill: New York, **1980**, pp 406.

(21) Hirano, T.; Miyajima, T. *J. Mol. Struct.* **1985**, *126*, 141.

(22) Abe, A.; Tasaki, K. *J. Mol. Struct.* **1986**, *145*, 309.

(23) Miyajima, T.; Hirano, T.; Sato, H. *J. Mol. Struct.* **1984**, *125*, 97.

(24) Snyder, R. G.; Zerbi, G. *Spectrochim. Acta* **1967**, *23A*, 391.

(25) Hallmark, V. M.; Bohan, S. P.; Strauss, H. L.; Snyder, R. G. *Macromolecules* **1991**, *24*, 4025.

(26) Schachtschneider, J. H.; Snyder, R. G. *Spectrochim. Acta* **1963**, *19*, 117.

(27) Schachtschneider, J. H.; Snyder, R. G. *J. Polym. Sci., Part C* **1964**, 99.

(28) Scherer, J. R.; Snyder, R. G. *J. Chem. Phys.* **1980**, *72*, 5798.

(29) Snyder, R. G.; Schachtschneider, J. H. *Spectrochim. Acta* **1963**, *19*, 85.

(30) Snyder, R. G.; Schachtschneider, J. H. *Spectrochim. Acta* **1965**, *21*, 169.

(31) Snyder, R. G. *J. Chem. Phys.* **1982**, *76*, 3921.

(32) Snyder, R. G. *Macromolecules* **1990**, *23*, 2081.

(33) Snyder, R. G.; Kim, Y. *J. Phys. Chem.* **1991**, *95*, 602.

(34) Snyder, R. G. *J. Chem. Soc. Faraday Trans.* **1992**, *88*, 1823.

(35) Snyder, R. G.; Strauss, H. L. *J. Chem. Phys.* **1987**, *87*, 3779.

(36) Snyder, R. G. *J. Mol. Spectroscopy* **1960**, *4*, 411.

(37) Aroney, M. J.; Le Fevre, R. J. W.; Ritchie, G. L. D.; Saxby, J. D. *Aust. J. Chem.* **1967**, *20*, 375.

(38) Denbigh, K. G. *Faraday Soc. Trans.* **1940**, *36*, 936.

(39) Gough, K. M. *J. Chem. Phys.* **1989**, *91*, 2424.

(40) Kawasaki, A.; Furukawa, J.; Tsuruta, T.; Saegusa, T.; Kakogawa, G.; Sakata, R. *Polymer* **1960**, *1*, 315.

CHAPTER 3

END GROUP EFFECT ON THE CHAIN FLEXIBILITY OF POLY(PROPYLENE OXIDE) AND POLY(ETHYLENE OXIDE)

3.1 Introduction

Polymer electrolytes, particularly, polyether-inorganic salt complexes are of interest because of their applications in batteries as solid electrolytes.[1,2] In those systems, it has been shown that the ion transport mechanism is intimately related to the polymer structure. Most studies previously reported in polyether based polymer electrolytes have focused on the structure of the polyether backbone. However, as we reported in Chapter 2, significant end group effects have been observed in the complex formation of oligomeric poly(propylene oxide)(PPO) with $LiClO_4$.[3] Two layer macroscopic phase separation occurrs in the complex based on methoxy terminated PPO(MPPO) while salt complexed hydroxy terminated PPO(HPPO) forms an apparently homogeneous mixture for the molecular weights 425 and 1000. This result definitely shows that the hydroxy end group plays a significant role in the salt-polymer complex formation. In those systems, chain conformational change by salt interaction is also dependent on end groups.[3]

Since polymer segmental motion is known to determine ionic mobility, it is important to estimate the end group effect on the polymer mobility in order to better understand the ionic conduction mechanism in the polymer electrolyte system. Borjesson et al.[4] studied the molecular weight dependence of the structural relaxation behavior of oligomeric HPPO. In their studies, increase in sound velocity and D-LAM frequency with decreasing molecular weight of HPPO is attributed to a decrease in the chain flexibility as

the molecular weight decreases, that is, as the number of hydroxy groups increases. This study suggests that the decrease in the chain flexibility in lower molecular weight HPPO was due to hydrogen bonding interactions. However, the analysis in the D-LAM region of the Raman spectrum was not accurately interpreted although it might not change their conclusions.

In order to estimate chain flexibility, differential scanning calorimetry(DSC) has been utilized. In addition, we suggest that the D-LAM bands in the Raman spectra can be utilized for that purpose. Raman scattering bands in the low frequency region, 200~300 cm^{-1} are known to represent skeletal bending vibrational modes of the chain backbone and their frequencies and band width depend on the chain conformational distribution. The band in this region has been called D-LAM[5-9] which is an abbreviation for disordered longitudinal acoustic mode. As Borjesson et al.[4] and Schantz and his co-workers[10] suggested, the D-LAM band frequency reflects chain stiffness. The band in the 200~400 cm^{-1} region for HPEO of molecular weight 600 is interpreted as a D-LAM band by Snyder et al.[8] They studied the effect of water on the D-LAM band of HPEO and observed a shift to higher frequencies and a band narrowing. These changes are assigned to an increase in gauche conformations and chain stiffness of HPEO due to the presence of water.

In this study, we utilized D-LAM bands as well as glass transition temperature(T_g) to re-estimate end group effects in PPO from a chain flexibility point of view by directly comparing HPPO and MPPO instead of changing chain length. We tried to characterize the bands in the 200~300 cm^{-1} region more carefully. Also, we studied end group effects in poly(ethylene oxide)(PEO) by comparing hydroxy(HPEO) and methoxy(MPEO) end groups. From the comparison studies of end group effects between PPO and PEO, we could deduce the $-CH_3$ side group effect on the chain flexibility of PPO.

3.2 Materials and Experiments

Hydroxy terminated PPO(HPPO), PEO(HPEO) and methoxy terminated PEO(MPEO) were obtained from Aldrich and Fluka Chemical Co. Methoxy terminated PPO(MPPO) of molecular weights 425 and 1000 was prepared as described in Chapter 2.2.2. Isotactic PPO(IsoPPO) of molecular weight M_n 710(M_w/M_n=1.3) was donated by the Dow Chemical Co. IsoPPO has hydroxy groups at the ends. Tacticity is 95% isotactic and regioselectivity is 80% of head-to-tail. Those samples were used as received without further purification. In order to prevent water contamination during sample preparation, PPO samples were dried under high vacuum at 70 °C and PEO's were dried by exposing them to molecular seives(3 Å) for 1 week before use.

Dispersive Raman spectra were taken for HPPO of molecular weight 1000 using a vertically polarized Spectra Physics model 165-08 Argon ion laser and U-1000 double monochromator. The excitation wave length of the Argon laser line was 514.5 nm. A Newport Model RSA-2 polarizer was used to select linearly polarized scattered light. The scattered light was collected at 90° geometry by Pentax lens and detected by a cooled photomultiplier. The power at the sample was 100 mW and the data points were taken every 0.25 cm^{-1} for 3 seconds per point at slit size 200μm for four horizontal slits. Vertical slits were opened completely. This condition for data collection corresponds to the spectral resolution of 2~3 cm^{-1}.[11] The frequency reading from the monochomator was corrected by taking the spectrum of CCl_4. CCl_4 gives five bands in the 400~500 cm^{-1} region. The strongest band of CCl_4 at 459.6 cm^{-1} was used to define the frequency corrected. Also, the intensity of the band at 459.6 cm^{-1} was used to maximize the signal by adjusting the position of lens in the optical collection system.

For D-LAM studies for the other samples, dispersive Raman data were difficult to obtain since some of the samples exhibit fluorescence when excited with laser excitation in the visible region. This difficulty was overcome by using long wavelength excitation in

Fourier transform Raman spectroscopy. In order to get consistency, Fourier transform Raman spectroscopy was carried out on every sample at the same conditions. These spectra were obtained at room temperature using a Bruker FRA 106 spectrometer. Nd:Yag laser(wave length : 1064 nm) was used as excitation. Laser output power was maintained at 500 mW. 1024 scans were loaded in order to get enhanced signal to noise ratio. The excitation collection geometry was 180° and spectral resolution maintained at 4 cm^{-1}. Detailed procedure is given in Appendix C.2.

Differential scanning calorimetry(DSC) was performed with a Dupont instrument 2910. Data were taken from -150 °C to room temperature at 20 °C/min heating rate under N_2 gas. The temperature was calibrated at -87 °C and 156.6 °C by cyclohexane and indium. Samples for DSC measurements were prepared in the glove box under argon gas stream and transferred to DSC sample cell in the desiccator. Glass transition temperatures were determined at inflection points of the step change in the thermograms.

3.3 Results and Discussion

The molecular weight dependence of the T_g for HPPO is depicted in Figure 3.1. As clearly seen in Figure 3.1, there is no significant molecular weight dependence of the T_g for HPPO's even in such a low molecular weight range. It is unusual because it has been known that the T_g is dependent on molecular weight of the polymer below degrees of polymerization of several hundreds on the basis of free volume theory.[12,13] It is interesting to compare this result with the T_g behavior of HPEO in this low molecular weight range. Faucher and his coworkers measured T_g for HPEO by mechanical loss and broadline nuclear magnetic resonance(NMR).[14] They found a significant molecular weight dependence of T_g in the molecular weight range of 10^2~10^4. This is in contrast with the

behavior of HPPO in similar molecular weight range although both HPEO and HPPO have similar structure.

The anomalous T_g behavior of low molecular weight of HPPO can be attributed to hydrogen bonding interactions since the hydroxy end group density increases with decreasing molecular weight. It can be the effect of an apparent molecular weight increase by end to end hydrogen bonding interactions or physical crosslink formation by interaction between hydroxy groups and ether oxygens. However, neither effect can explain the discrepancy in the T_g behavior of HPEO and HPPO since they both have the same geometry and particularly the same hydroxy group at the chain end. One thing different between HPEO and HPPO is the $-CH_3$ side group in HPPO. When the hydroxy group interacts with the ether oxygen, that interaction can cause restriction of the segmental motion by steric hindrance due to the $-CH_3$ side group. It has been supported by comparing with MPPO. By changing the hydroxy to the methoxy group, T_g was decreased by 20 °C for molecular weight 425 and 12 °C for 1000(Figure 3.1). Although we have only two data points for MPPOs, significant molecular weight dependence of the T_g is observed by removing hydroxy end groups. It is difficult to measure T_g of MPEO due to the fast crystallization. Although there are several techniques which are available to estimate T_g, instead of using conventional methods, we used low frequency region of Raman spectra to examine the discrepancy shown in HPEO and HPPO.

FT-Raman spectra of HPPOs in the low frequency range, 100~400 cm^{-1} are compared in Figure 3.2 for molecular weight 425(HPPO425), 1000(HPPO1000), 2000(HPPO2000), 3000(HPPO3000), and 4000(HPPO4000). The band in the 200~300 cm^{-1} region shifts to lower frequency as molecular weight of HPPO increases although it is difficult to define band frequencies due to their broadness. Although the bands in this region have been known to be D-LAM for various polymers[8], we tried to characterize the bands in this region more carefully. For that purpose, polarized experiment has been taken

by using dispersive Raman spectroscopy. Figure 3.3 shows parallel(//) and perpendicularly(⊥) polarized Raman scattering bands of HPPO1000. Complete polarization of the band supports that this band is the D-LAM band because D-LAM band is known to have a low depolarization ratio.[8] The vibrational bands in this region represent the skeletal bending mode. The band frequency shift can occur by changes in the force constant for the vibrational bending mode and/or changes in chain conformational distribution.[8] D-LAM band frequency is also known to be inversely proportional to the square of n, the number of skeletal atoms in the chain for n-alkane systems.[7] Borjesson et al.[4] claimed that the D-LAM frequencies for HPPO are proportional to $1/n^2$ and so these bands are D-LAM bands. But it is questionable how they determined the band frequencies.

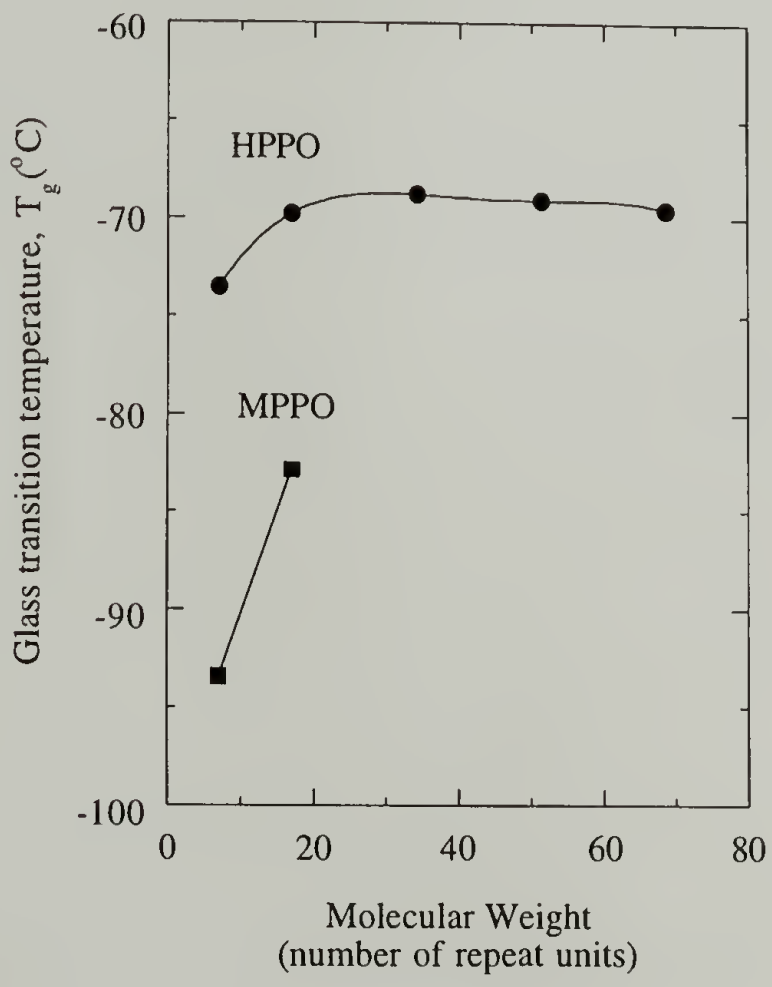

Figure 3.1 Glass transition temperature of HPPO and MPPO by changing molecular weight.

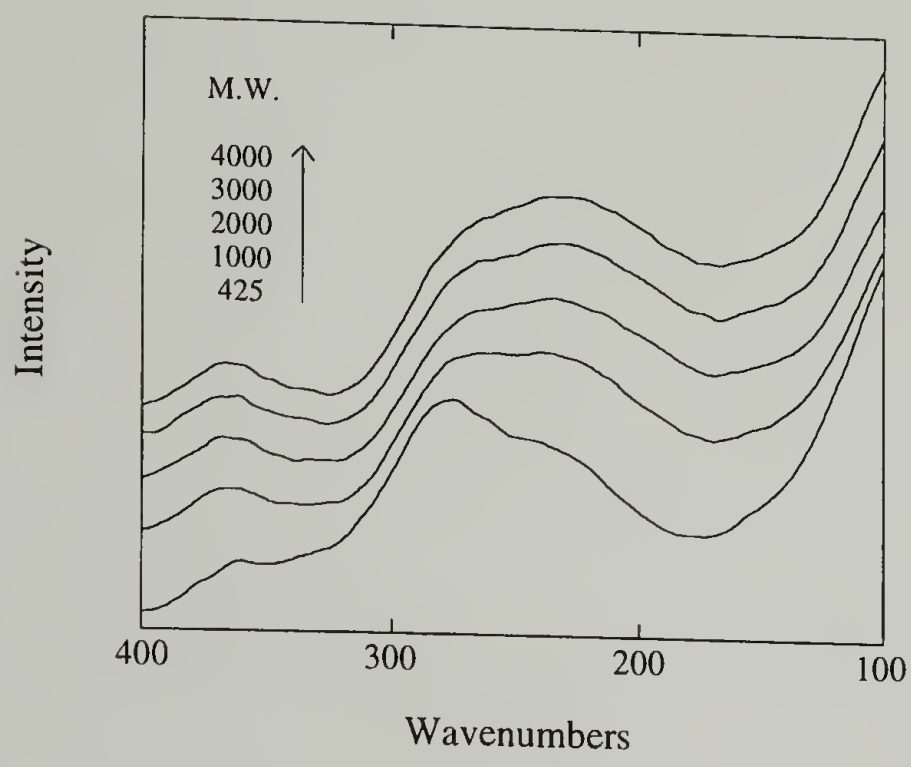

Figure 3.2 Molecular weight dependence on the D-LAM bands of HPPO.

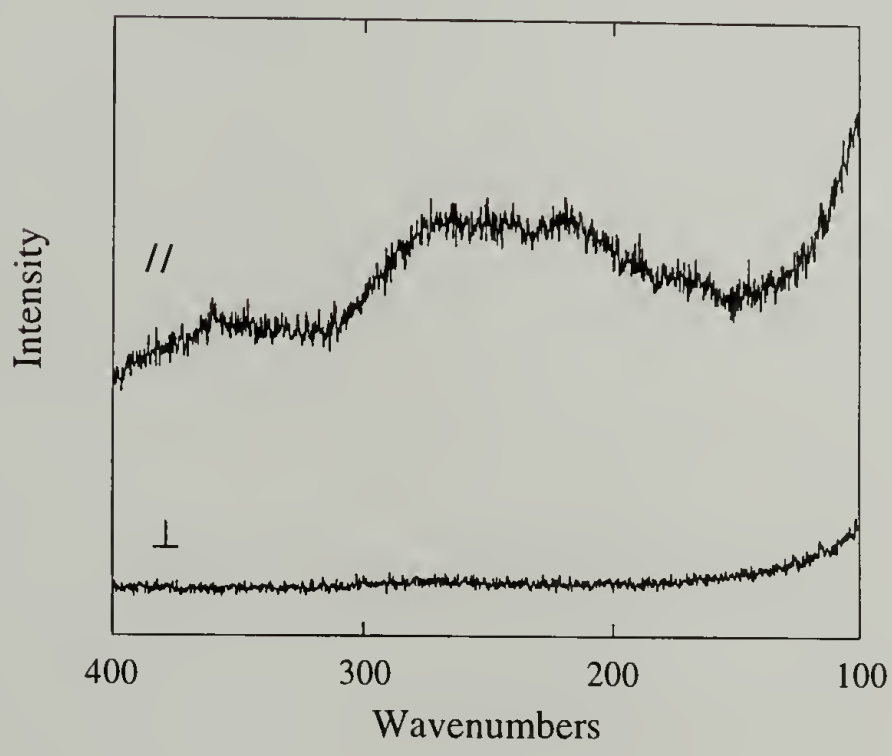

Figure 3.3 Dispersive Raman spectra of HPPO1000 ; // - parallel and ⊥ - perpendicularly polarized.

We have to point out the doublet feature of the bands observed in this region. HPPO425 shows a distinguishable doublet feature and the relative intensity of the lower frequency side band increases as the molecular weight of HPPO increases. Since the relative intensity of these two components of the band as well as the band frequency is dependent on molecular weight, i.e. concentration of hydroxy groups in this case, it is necessary to estimate the end group effect.

Figure 3.4 compares FT-Raman spectra of MPPO with those of HPPO for the molecular weight 425 and 1000. The higher frequency sides of the D-LAM bands were 275 and ca. 258 cm^{-1} for HPPO425 and HPPO1000, respectively. The frequency shift to lower values for MPPOs has been observed to be ca. 15 cm^{-1} for molecular weight 425 and ca. 3 cm^{-1} for 1000 in the higher frequency side as well as lower frequency side. Therefore 17 cm^{-1} difference between the D-LAM bands of HPPO425 and HPPO1000 was reduced to 5 cm^{-1} between MPPO425 and MPPO1000. Since frequency shift was proportional to the density of hydroxy end groups, our spectroscopic results also indicated the significant effect of hydrogen bonding interaction and it was in good agreement with DSC results. Because it was extremely difficult to determine the band frequencies for each components of the doublet above molecular weight 1000, we could not estimate molecular weight dependence of the frequencies. However, it is unlikely to follow the relationship obtained for n-alkanes.[7]

It is clear that the doublet feature of the band in this region still exists for MPPOs as seen in Figure 3.4. Therefore the relative intensity change with change in molecular weight of HPPO was not caused by difference in relative content of hydroxy end groups which can result in the change in chain conformational distribution and then the shape and frequency of D-LAM bands. These changes can not result from a molecular weight distribution effect either since our polymers have a quite narrow molecular weight distributions(=1.06~1.11). In order to estimate whether the molecular weight dependence

of the doublet is related to the configuration of the chains, we compared atactic HPPO(HPPO) with isotactic HPPO(IsoPPO). FT-Raman spectra of HPPO and IsoPPO of molecular weight around 700 are shown in Figure 3.5. The relative intensity of the lower frequency side increases in IsoPPO compared with HPPO. Therefore the relative intensity change in the doublet of the bands can be, in part, attributed to changes in the isotactic content of the different molecular weight PPO"s. 20% of structural defects such as head to head or tail to tail connection in IsoPPO also can contribute to the spectral change. In fact, the band of IsoPPO710 was also not homogeneous. This might be due to the presence of structural defects, broad molecular weight distribution(=1.3) or overlap of two different vibrational modes. However, the differences in structural defects among HPPOs is going to be negligible because HPPO's prepared with a base catalyst hardly have head to head or tail to tail contents.[15,16] At this point, we can only conclude that we have found a molecular weight dependence of the band shape in the D-LAM region in atactic PPO's and it was not due to the hydrogen bonding interaction effect. We suggest that the complexity of the bands in this region is caused by the intrinsic properties of the chains such as the configurational distribution of propylene oxide units. Further studies are required for more detailed interpretation.

For comparison with PPO, we measured the FT-Raman spectra of HPEO and MPEO for molecular weight 400. As seen in Figure 3.6, spectral changes in 200~300 cm^{-1} region of the Raman spectra by changing the end group from -OH to -OCH_3 are negligible compared with the significant changes shown in HPPO versus MPPO for molecular weight 425. The band in this region has been reported as a D-LAM by Snyder et al.[8] We have found that the band frequency at maximum intensity in this region for MPEO400 was 3 cm^{-1} higher than that of HPEO400 which is in contrast with the end group effect found in PPO. Since the bands span a quite broad range from 200 to 350 cm^{-1}, the scattering intensity in the 300~350 cm^{-1} region can affect the frequency of the band at 200~300 cm^{-1} if we assume that this broad band consists of one at 300~350 cm^{-1} and the other at

200~300 cm^{-1}. Therefore we attribute the higher frequency shift of the band at 200~300 cm^{-1} for MPEO to an artifact due to band overlap since the relative scattering intensity of these two components is changed by changing the end group. The scattering in the 300~350 cm^{-1} region might be a part of the D-LAM as suggested by Snyder et al.[8] or caused by a localized bending mode. We do not have any explanation for it at this moment.

The frequency shift of D-LAM bands can be caused by changes in chain conformational distributions and/or changes in the force constant for the skeletal bending motion. Snyder et al. concluded in the study of the D-LAM band of polyethers that the band frequency shift due to changes in the force constant can be expected to be less than 15 cm^{-1} and if it is caused by chain conformational change, greater than 20 cm^{-1}.[8]

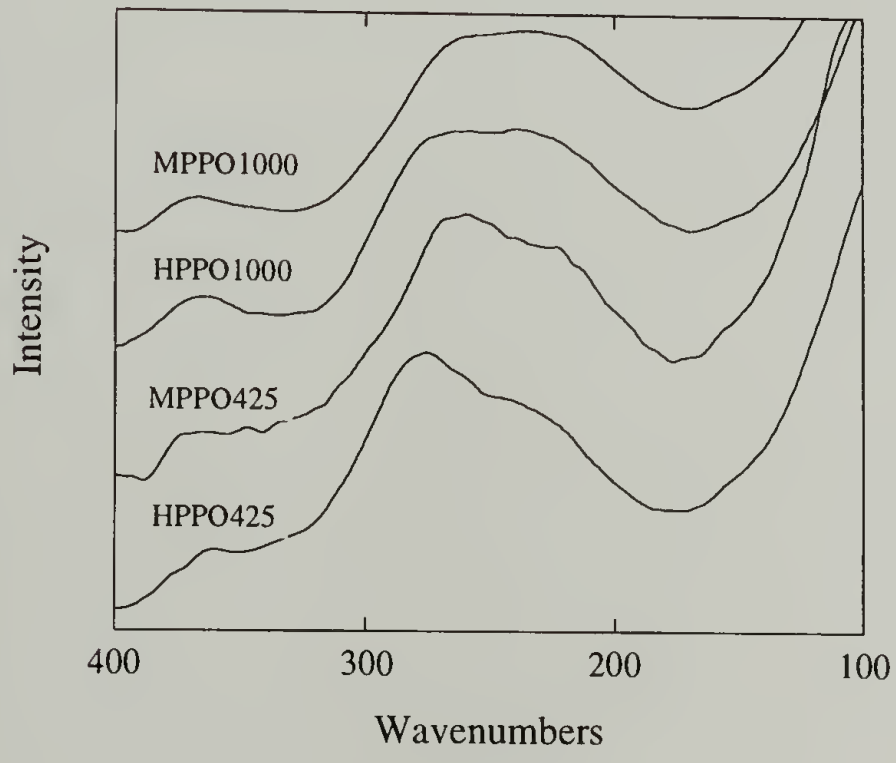

Figure 3.4 End group effect on the D-LAM bands of poly(propylene oxide).

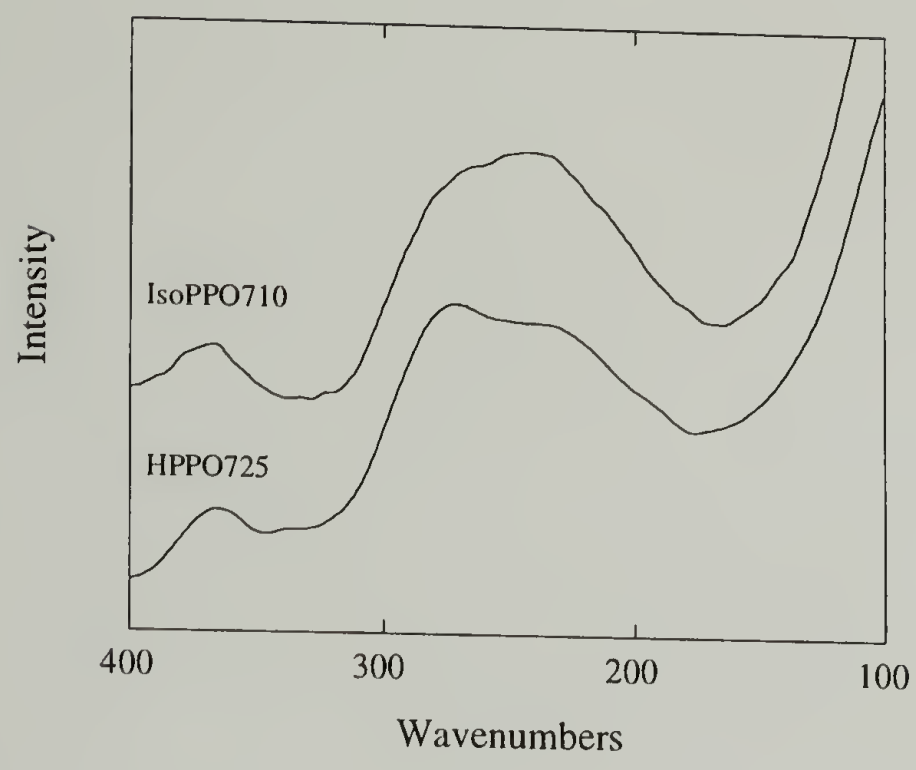

Figure 3.5 Tacticity effect on the D-LAM bands for HPPO of molecular weight ca.700.

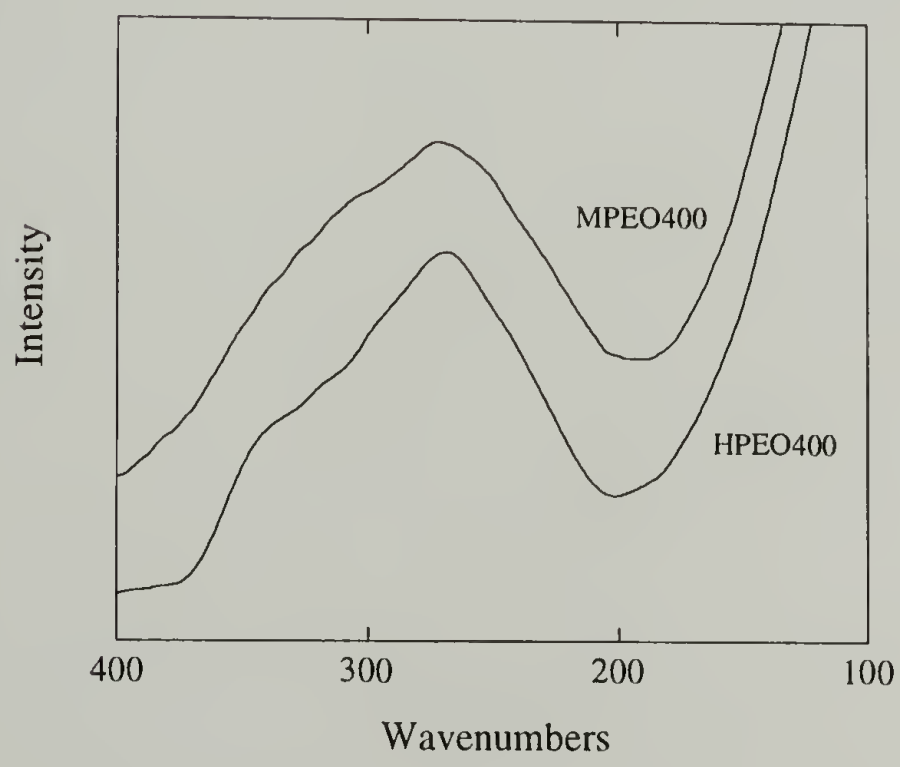

Figure 3.6 FT-Raman spectra of HPEO and MPEO in D-LAM frequency region.

Since the D-LAM band shift was dependent on the density of hydroxy end groups for PPO, it can be due to the change in conformational distribution or force constant for bending motion by hydrogen bonding interaction. However, since end group dependence is not observed for PEO, it is probably not simply due to a hydrogen bonding interaction but the -CH_3 side group effect should be considered. CH_3 side groups in the chemical repeat units of PPO instead of the hydrogen in PEO can introduce steric hindrance in chain segmental motion when hydroxy groups interact with ether oxygens. Therefore the spectroscopic observations can be assigned to the restriction of the skeletal bending motion of the chain due to the interaction of the hydroxy groups with the ether oxygens in the presence of the -CH_3 side group. This restriction on the chain segmental mobility may also cause the unusual behavior of T_g for HPPO. The comparison study of PPO versus PEO provides useful information to understand the side group effect.

3.4 Conclusions

End group effect on the chain flexibility has been studied by vibrational spectroscopic analysis in the low frequency region(D-LAM) of FT-Raman spectra and the glass transition temperature(T_g) behavior measured by DSC. T_g behavior shown for HPPOs depending on molecular weight and end group has been explained by the presence of a hydrogen bonding interaction between hydroxy end groups and ether oxygens. This interaction increases chain stiffness due to the steric hindrance caused by the -CH_3 side group. For the HPEOs which do not have any side group, no such end group effect is observed. CH_3 side group effect also is reflected in the D-LAM band. A significant end group effect on the band frequency exists in PPO but not in PEO. As a consequence, the side group effect on chain flexibility has been proven through comparison studies of PPO and PEO. The increased chain flexibility introduced by replacing hydroxyl end groups in PPO with methoxy end groups might contribute to the increased ionic conductivity of PPO

based polymer electrolytes since the chain segmental mobility is the predominant factor in determing ionic conductivity of the polymer electrolyte system. We studied the end group effect on the ionic conductivity of polymer electrolytes and report the results in the next chapter.

References

(1) MacCallum, J. R.; Vincent, C. A., Ed.; *Polymer Electrolyte Reviews* ; Elsevier Applied Science: London, **1987**; Vol. 1.

(2) MacCallum, J. R.; Vincent, C. A., Ed.; *Polymer Electrolyte Reviews* ; Elsevier Applied Science: London, **1989**; Vol. 2.

(3) Yoon, S.; Ichikawa, K.; MacKnight, W. J.; Hsu, S. L. *Macromolecules* **1995**, *28*, 4278.

(4) Borjesson, L.; Stevens, J. R.; Torell, L. M. *Physica Scripta* **1987**, *35*, 692.

(5) Hallmark, V. M.; Bohan, S. P.; Strauss, H. L.; Snyder, R. G. *Macromolecules* **1991**, *24*, 4025.

(6) Scherer, J. R.; Snyder, R. G. *J. Chem. Phys.* **1980**, *72*, 5798.

(7) Snyder, R. G. *J. Chem. Phys.* **1982**, *76*, 3921.

(8) Snyder, R. G.; Wunder, S. L. *Macromolecules* **1986**, *19*, 496.

(9) Snyder, R. G.; Strauss, H. L. *J. Chem. Phys.* **1987**, *87*, 3779.

(10) Schantz, S.; Torell, L. M.; Stevens, J. R. *J. Appl. Phys.* **1988**, *64*, 2038.

(11) Strommen, D. P.; Nakamoto, K. *Laboratory Raman Spectroscopy*; John Wiley & Sons: New York, **1984**, pp 21.

(12) Sperling, L. H. *Introduction to physical polymer science;* 1st ed.; Wiley: New York, **1986**, pp 272.

(13) Aklonis, J. J.; MacKnight, W. J. *Introduction to Polymer Viscoelasticity;* 2nd ed.; John Wiley and Sons: New York, **1983**, pp 77.

(14) Faucher, J. A.; Koleske, J. V.; Santee, E. R., Jr.; Stratta, J. J.; Wilson, C. W. *J. Appl. Phys.* **1966**, *37*, 3962.

(15) Price, C. C.; Spector, R.; Tumolo, A. L. *J. Polym. Sci., Part A-1* **1967**, *5*, 407.

(16) Price, C. C.; Tumolo, A. L. *J. Polym. Sci., Part A-1* **1967**, *5*, 175.

CHAPTER 4

END GROUP EFFECT ON THE IONIC CONDUCTIVITY OF POLY(PROPYLENE OXIDE) BASED POLYMER ELECTROLYTES

4.1 Introduction

In Chapter 3, the end group effect on the chain flexibility of poly(propylene oxide)(PPO) and poly(ethylene oxide)(PEO) is reported. The increased glass transition temperature(T_g) in hydroxy terminated poly(propylene oxide)(HPPO) compared to methoxy terminated poly(propylene oxide)(MPPO) is attributed to the hydrogen bonding interaction between hydroxy end groups and ether oxygens. This interaction reduced chain segmental motion in HPPO due to steric hindrance introduced by the methyl side group whereas it did not effect the chain flexibility of HPEO.

Polyethers are a matrix for polymer electrolytes.[1-5] It is known that chain segmental motion of the host polymer determines ionic mobility in the polymer electrolyte system.[6-11] Therefore chain flexibility changes depending on the type of present end group will affect the ionic conductivity of the system. Since the ionic conductivity of the system is determined by ionic mobility and number of free ions, the relative content of carrier ions as well as chain mobility is another factor to determine the ionic conductivity of the system. Since hydroxy end groups have higher polarity than methoxy groups, the degree of dissociation of the salt is greater in the HPPO matrix than the MPPO matrix. It already has been proven that lithium cations interact with hydroxy groups as well as ether groups in HPPO-$LiClO_4$ complexes.[12-14] Therefore the change in end group from hydroxy to methoxy has two contradictory effects on ionic conductivity. One is the positive effect

from increased chain mobility, the other is the negative contribution due to a smaller number of carrier ions. Compared with PPO, since we have found negligible end group effects on the chain flexibility of PEO on the basis of Fourier transform Raman spectroscopy, the end groups might have different effects on the ionic conduction mechanism in PPO and PEO.

In this study, we purpose to estimate the end group effect on the ionic conductivity of PPO based polymer electrolytes in the presence of $LiClO_4$ by comparing hydroxy with methoxy end groups. Impedance spectroscopy is utilized to measure the conductivity of the system. Qualitative content of free ions relative to the amount of solvent separated ions and contact ion pairs are estimated by analyzing the Raman scattering band of the perchlorate anion symmetric stretching mode in the 900 cm^{-1} region. The band at 930~931 cm^{-1} is assigned to free perchlorate anion and that at 938~939 cm^{-1} to solvent separated anions in the polyether matrix.[15] Information about chain segmental mobility is deduced from glass transition temperatures measured by differential scanning calorimetry(DSC).

4.2 Materials and Experiments

All of the polyethers and salt complexes were prepared as described in previous Chapters. As we pointed out in Chapter 2, two layer macroscopic phase separation occurs for MPPO-$LiClO_4$ complexes and the salt composition of MPPO-salt complexes(bottom layer) is constant at $[Li^+]/[-O-]$ = ca. 0.15 ± 0.02 independent of initial salt concentration. The salt complexed MPPO of $[Li^+]/[-O-] = 0.17$ for MPPO425 and 0.13 for MPPO1000 were used for this study(refer to Table 2.2).

Fourier transform Raman spectra were obtained as descirbed in Appendix C.2. Laser output power is maintained at 500 mW. 1024 scans were loaded in order to get

enhanced signal to noise ratio. The excitation collection geometry was 180° and spectral resolution maintained at 2 cm^{-1} to get better resolution of bands. As explained in Appendix C.2, 2 cm^{-1} was the maximum resolution we can achieve with Bruker FRA 106 spectrometer. Band deconvolution to separate the Raman band(931 cm^{-1}) of free perclorate ion from the other components was carried out using a commercial package *Lab Calc* purchased from Galactic Industries. Band shape used was a mixture of gaussian and Lorentzian functions. Without any fixed parameters such as band position, width, or shape, band deconvolution has been simulated to get the best fit. Relative intensity was then measured as integrated area of individual peaks deconvoluted.

Ionic conductivity* was estimated from the impedance diagram obtained using platinum electrodes with a Hewlett 4192A LF-impedance analyzer over the frequency range 5Hz to 13 MHz at 1 V amplitude. Cell design is shown in Figure 4.1. Measurement was performed under an argon gas stream to prevent moisture effects. Samples were sandwiched between two thin flat platinum electrodes with a spacer made of teflon to control the sample thickness and to avoid pressure effects. Since some of our samples were flowed out from the electrodes slowly, the cell(Figure 4.1) was positioned vertically during the measurement. In this way, the viscosity of samples was enough to keep them in the cell. Absolute values of impedance($|Z|$) and phase difference(θ) were measured. The real and imaginary parts of the impedance were calculated from $|Z|\cos\theta$ and $|Z|\sin\theta$, respectively to get the impedance diagram. The detailed method to determine impedance of the system is given in Appendix C.3.

Differential scanning calorimetry(DSC) was performed with a Dupont instrument 2910. Empty cell was scanned with heating rate 20 °C for baseline correction under N_2 gas

---

* Ionic conductivity was measured in Dr. Allcock's Laboratory (PennState University) with assistance from a student, M. Napierala and Dr. O'Connor.

flow. The temperature was calibrated at -87 °C and 156.6 °C by cyclohexane and indium at same condition. Samples for DSC measurement were prepared in the glove box under argon gas stream and transferred to DSC sample cell in the desiccator. Data were taken from -100 °C to 80 °C at 20 °C/min heating rate under N_2 gas. Glass transition temperatures were determined at inflection points of the step change in the thermograms.

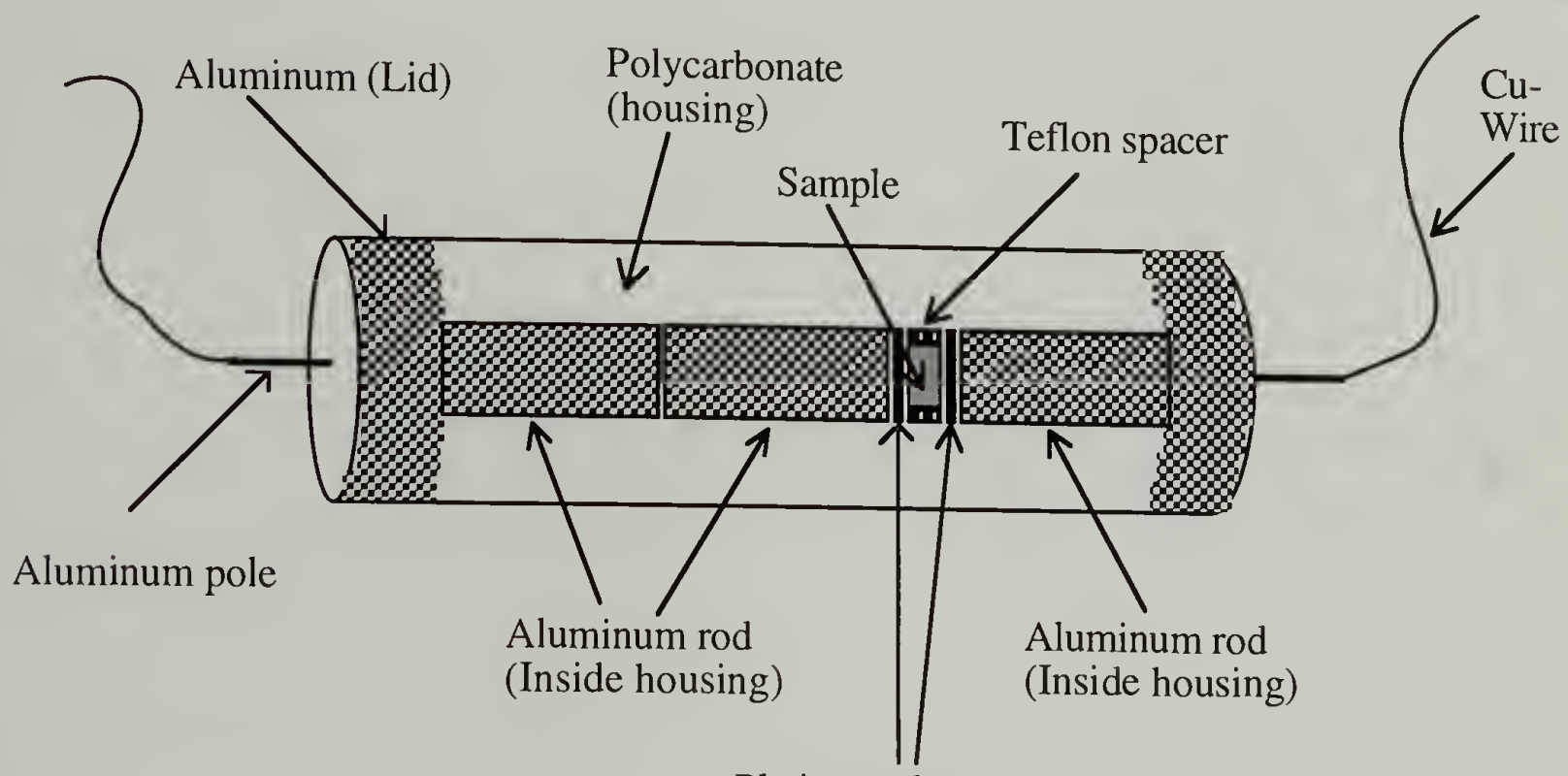

Figure 4.1 Schematic drawing of the cell for impedance measurement.

4.3 Results and Discussion

A remarkable end group effect is observed in PPO-$LiClO_4$ complexes. As we mentioned in our previous study[12] and the experimental section in this report, clear macroscopic phase separation occurs when $LiClO_4$ is dissolved in MPPO while no such phase separation occurs in salt complexed HPPO of molecular weight 425 and 1000. In contrast with this result, no end group effect is observed in PEO-$LiClO_4$ complexes so far as macroscopic phase separation is concerned.

Vachon et al.[16] suggested that polymer structure can affect the cation-oxygen binding energy in their study of microphase separation behavior in polyether complexed with alkali metal salts. They confirmed that the cation-oxygen binding energy is lower in PPO than in PEO. It has been suggested that the balance between the long range coulombic interaction and cation-oxygen binding energy determines the degree of phase separation. For the particular behavior of PPO and PEO based alkali metal complexes, such an interpretation seems to apply.

First of all, the macroscopic phase separation in MPPO-$LiClO_4$ compared with its absence in methoxy terminated PEO(MPEO)-$LiClO_4$ can be explained due to the lower binding energy of the lithium cation-ether oxygen in MPPO compared to the MPEO. In the MPPO complex case, the long range coulombic interaction energy is larger than the cation binding energy to the ether oxygen. As a result, salt complexed microdomains aggregate to form a separated phase from the uncomplexed phase. However such a phase separation phenomenon was not found in either HPPO or HPEO based salt complexes. We suggest that this is because of the hydroxy end group effect. In our previous study, we proved that the lithium cation interacted with hydroxy groups as well as ether oxygens.[12] If this interaction is preferred over the cation-ether oxygen interaction, the differences between the ethylene oxide and propylene oxide units interaction with the cation will contribute less. This result implies that cation-hydroxy binding is stronger than cation-ether oxygen interaction. Therefore microphase separation observed for HPPO4000[16] but not for HPPO425 and 1000 can be attributed to the higher density of hydroxy groups in the lower molecular weight HPPOs which provide stronger interactions with the cation than the ether oxygens.

The symmetric stretching region of the perchlorate anion in the FT-Raman spectrum is utilized to estimate the qualitative content of free ions versus solvent separated or contact ion pairs. Figure 4.2 shows curve deconvolution results in the 910~960 cm^{-1} range for

HPPO4000 at $[Li^+]/[-O-]=0.2$. Only two bands are taken into account , one for free ions at 931 cm^{-1} and another for other types of ions at 939 cm^{-1}. We did not try to separate the broad band centered at 939 cm^{-1} into solvent separated ion(938 cm^{-1}) and contact ion pairs(948 cm^{-1}).[15] Since the center of the band frequency was close to solvent separated one, we treat the band at 939 cm^{-1} as the solvent separated one. Also, multiple aggregations of ions were not taken into account in this analysis. Although this method might not be accurate enough for a quantitative estimation of each type of ion, spectroscopic analysis is easy to use for a qualitative estimation of the relative free ion content, at least for a comparison study among similar systems.

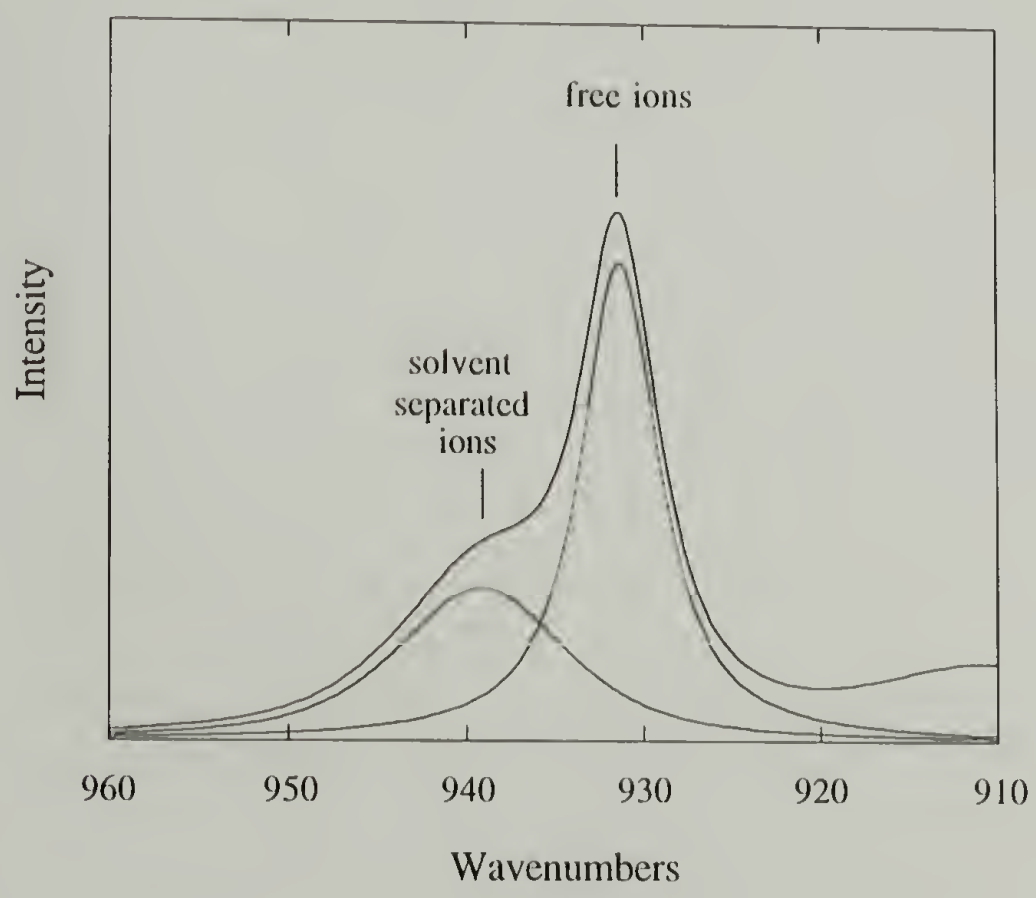

Figure 4.2. Curve deconvolution of symmetric stretching band of ClO_4^- for HPPO4000 at $[Li^+]/[-O-] = 0.2$.

The integrated area under each band was divided by the total curve area estimated in the spectral region of 910~960 cm^{-1} and then normalized with respect to salt concentration to estimate each ion content. Relative content of free and solvent separated ions for HPPO and MPPO are compared in Figure 4.3 as a function of molecular weight. As expected, the relative content of free ions was higher in the HPPO having the higher content of hydroxy groups. For MPPO's, no molecular weight dependence is found. Therefore the number of free ions in the system is influenced by the concentration of hydroxy groups and this result indicates the better solvation power of the hydroxy group for the lithium cation than ether oxygen. Since HPPO4000 shows very close agreement in free and solvent separated ion contents with those for MPPO, the hydroxy end group effect may be negligible above that molecular weight.

Figure 4.4 shows the relative content of each type of ion in HPEO and MPEO. The same spectral analysis was applied and band frequencies for free and solvent separated perchlorate ions were the same as those for PPO within 1 cm^{-1} range. Unfortunately, we could not compare HPEO400 with the corresponding MPEO400 at high salt concentrations because the anomalous scattering background observed in MPEO400 precluded proper spectral analysis . However, since the estimated values of the ion contents were the same as those for MPEO500 at $[Li^+]/[-O-]=0.02$ and 0.05, we assume the results obtained for MPEO500 are valid for MPEO400. The lack of molecular weight dependence on the concentration of ions exhibited by MPPO supports this assumption. Basically, a similar hydroxy end group effect is observed.

It is interesting to compare the relative content of free ions in the PPO and PEO matrix. HPEO shows a somewhat higher free ion concentration in low salt concentration range but almost the same content of free ions compared to the HPPO as the salt concentration increases. This is also the case for the methoxy terminated ones. This result indicates that PPO and PEO have similar abilities for solvation of perchlorate anions

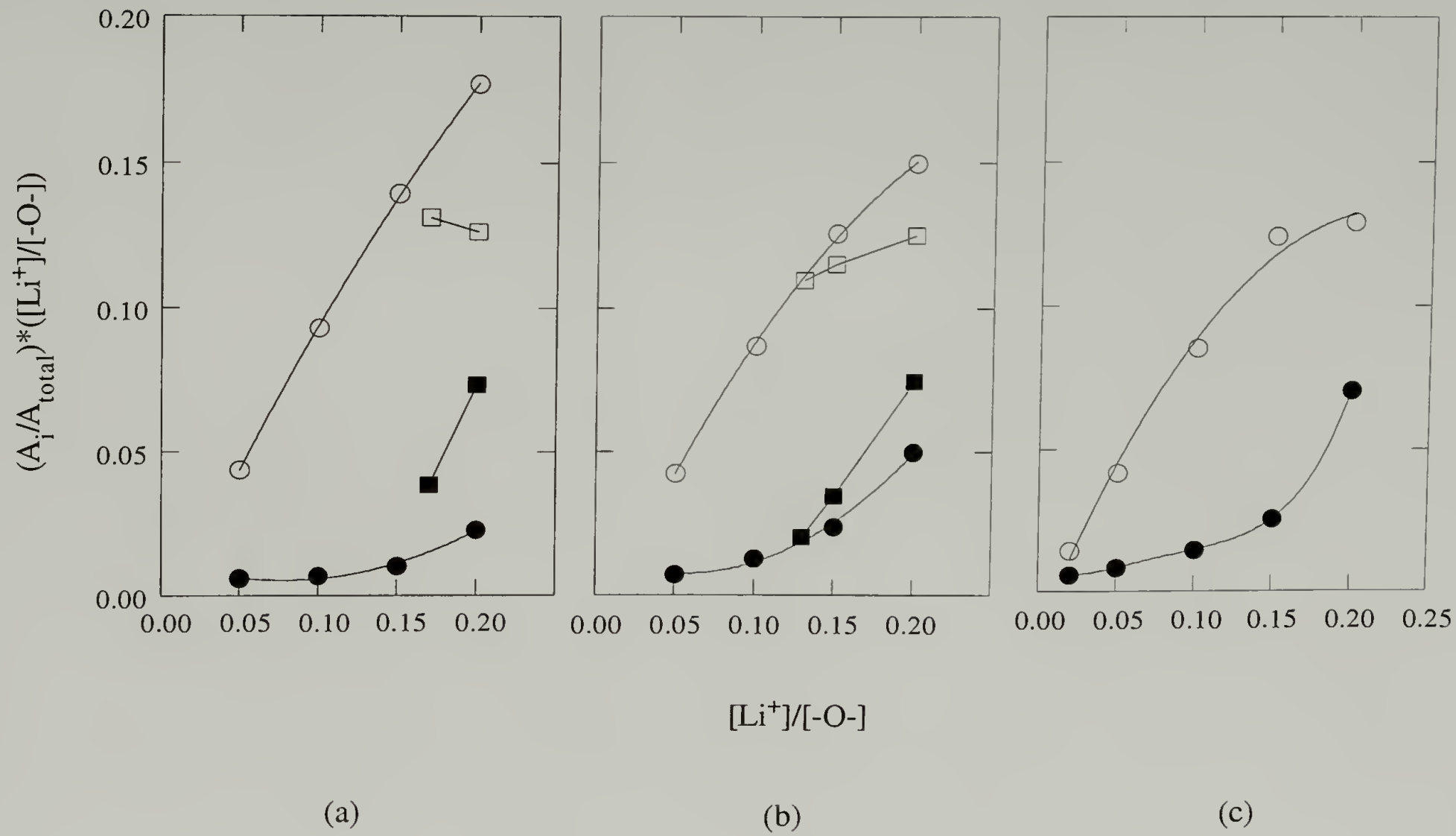

Figure 4.3 Dependence of the relative content of free ions(i=F, 931 cm^{-1}) and solvent separated ion pairs(i=S, 939 cm^{-1}) on $[Li^+]/[-O-]$ concentration estimated by curve deconvolution of ClO_4^- stretching bands for poly(propylene oxide)-$LiClO_4$ complexes.

MW—(a) 425, (b) 1000 and (c) 4000 ; —o— HPPO (F) —●— HPPO (S) —□— MPPO (F) —■— MPPO (S)

although the binding energy of lithium cation-ethylene oxide units is stronger than that of lithium cation-propylene oxide. Therefore it seems likely that the number of free ions only depends on the concentration of hydroxy groups of the system.

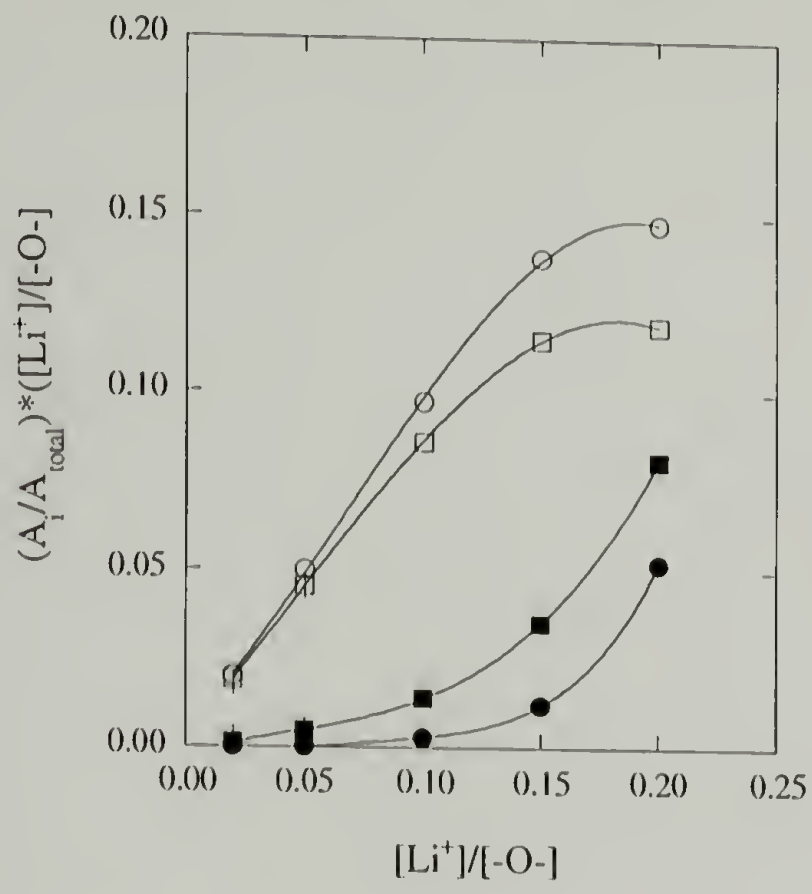

Figure 4.4 Dependence of the relative content of free ions(i=F, 931 cm^{-1}) and solvent separated ion pairs(i=S, 939 cm^{-1}) on $[Li^+]/[-O-]$ concentration estimated by curve deconvolution of ClO_4^- stretching bands for poly(ethylene oxide)-$LiClO_4$ complexes.

MW—400 ; —o— HPEO (F) —●— HPEO (S) —|— MPEO (F, S)

MW— 500 ; —⊟— MPEO (F) —■— MPEO (S)

One way to estimate chain flexibility is to measure glass transition temperature(T_g). The T_g's for HPPOs are shown in Table 4.1. As salt concentration increases, T_g increases. We have found two T_g's for HPPO4000 at $[Li^+]/[-O-]=0.05$ and this result is in good agreement with Vachon and his coworker's.[16] We compared T_g's of HPPO-$LiClO_4$ complexes with T_g's of the salt complexed phase of MPPO. The lower phase of $LiClO_4$-MPPO425 complex showed T_g at -29.5 ± 3 °C and -16 ± 3 °C for MPPO1000 with 20

°C/min heating rate. Reproducibility of T_g was not very good. However, the range of fluctuation observed is not unusual in T_g measurements. If we compare HPPO and MPPO at comparable salt concentrations, $[Li^+]/[-O-]=0.15$, MPPO shows a lower T_g than HPPO although the difference of the T_g between salt complexed MPPO and HPPO is smaller than in the pure ones. This result indicates increased chain flexibility in MPPO compared to HPPO not only in the pure polymer but also in the presence of salt.

Table 4.1 Glass transition temperature(°C) of hydroxy terminated poly(propylene oxide) by changing molecular weight and $LiClO_4$ concentration.

$[Li^+]/[-O-]$	HPPO425	HPPO1000	HPPO4000	HPPO4000
0.0	-74.1	-71.2	-70.0	
0.02			-67.8	
0.05	-56.6	-59.0	-65.6	-24.2
0.10	-32.6	-29.3		-14.2
0.15	-17.8	-4.2		10.1
0.20	-3.6	14.1		29.0

Therefore there are two contradictory factors which can affect the ionic conductivity of the system by switching end group from hydroxy to methoxy. One is the positive contribution of increased chain mobility and the other is the negative effect due to a decrease in the number of free ions. The relative contribution of each factor can be qualitatively estimated by comparing the ionic conductivity of HPPO and MPPO based polymer electrolytes. Specific ionic conductivity(σ)'s of $LiClO_4$ complexed HPPO and MPPO were determined by analyzing impedance diagrams(Figure 4.5) and values are given

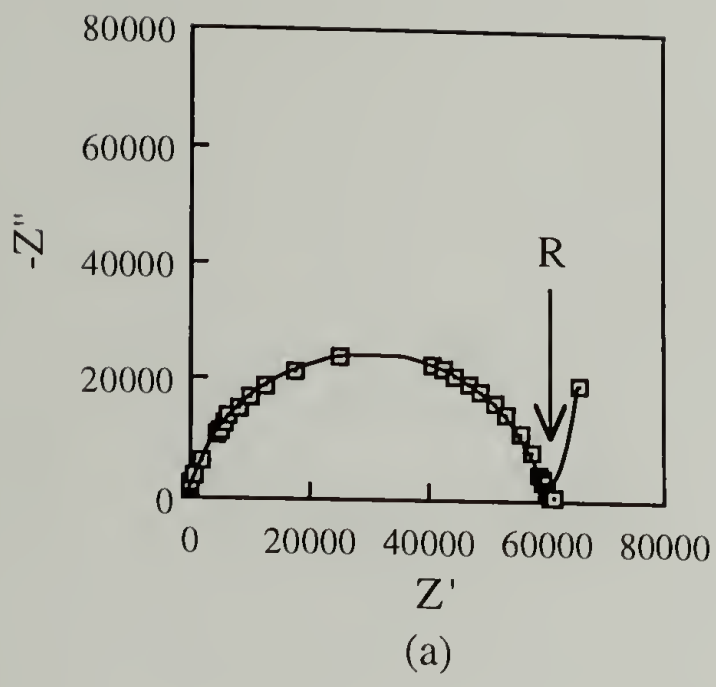

(a)

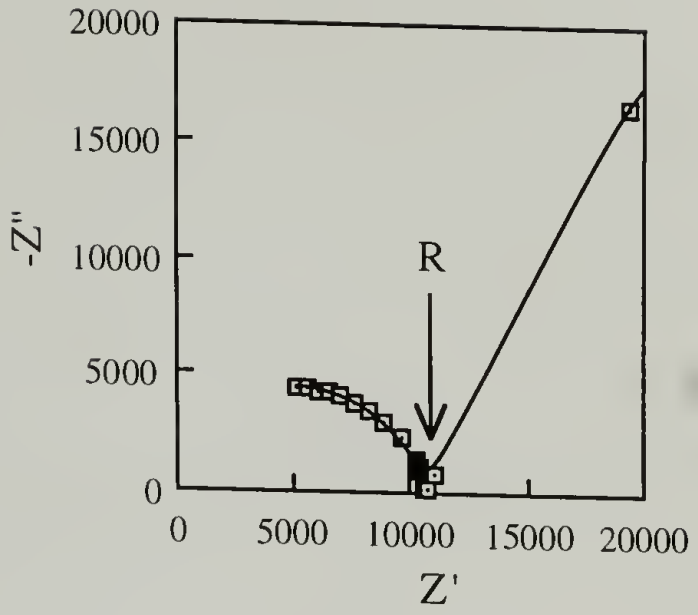

(b)

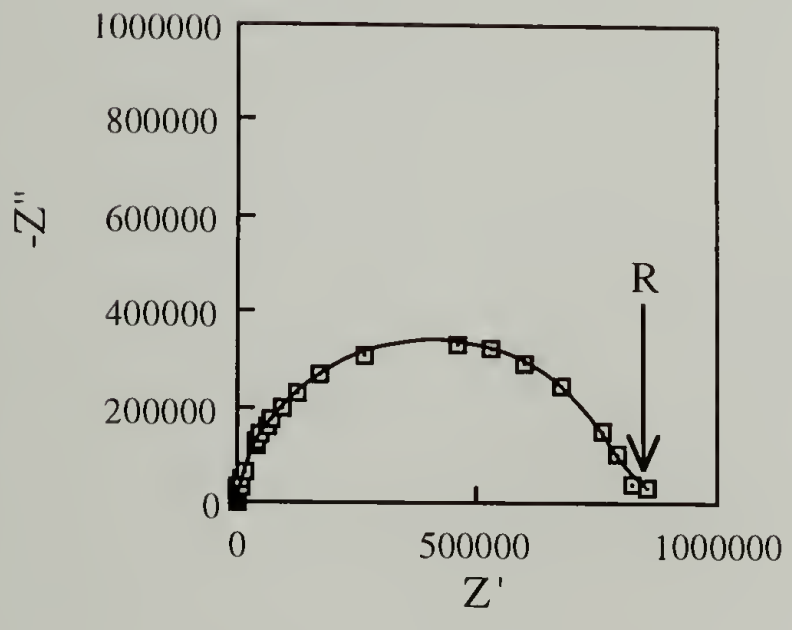

(c)

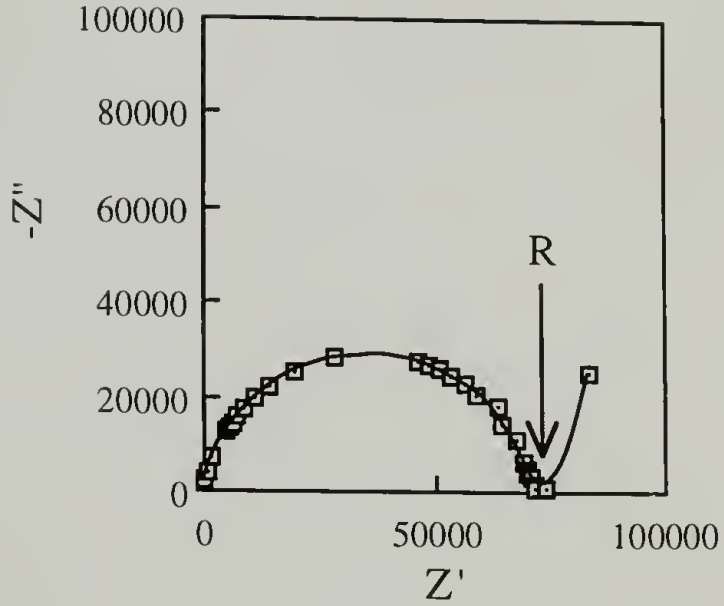

(d)

Figure 4.5 Impedance diagrams for (a) HPPO425, $[Li^+]/[-O-]=0.15$, (b) MPPO425, $[Li^+]/[-O-]=0.17$, (c) HPPO1000, $[Li^+]/[-O-]=0.15$, and (d) MPPO1000, $[Li^+]/[-O-]=0.13$.

in Table 4.2. Specific ionic conductivity is calculated from equation (4.1), where R, A, and l stand for resistance, electrode area contacting with sample, and sample thickness, respectively. Resistance of the systems is estimated from the impedance diagram at the low frequency limit where the imaginary part of the impedance disappears.

$$\sigma = l/RA \qquad (4.1)$$

Table 4.2 Specific ionic conductivity(σ) of poly(propylene oxide)-$LiClO_4$ complexes depending on end group.

	$[Li^+]/[-O-]$	$\sigma(Scm^{-1})$
HPPO425	0.05	1.7×10^{-5}
HPPO425	0.15	4.5×10^{-6}
HPPO1000	0.15	3.4×10^{-7}
MPPO425	0.17*	2.6×10^{-5}
MPPO1000	0.13*	1.5×10^{-6}

* Salt concentration was estimated by Microanalysis. The values contain 20% of uncertainty.

Ionic conductivity's of HPPOs obtained at room temperature were a little bit lower than previously reported values[10,11] but they are in reasonable agreement. The lower ionic conductivity at higher salt concentration can be attributed to the reduced chain segmental mobility as evidenced by the increased T_g. For MPPO425, ionic conductivity at $[Li^+]/[-O-] = 0.17$ has been estimated. Compared with HPPO425 of similar salt concentration, $[Li^+]/[-O-] = 0.15$, MPPO complex showed about one order of magnitude higher ionic conductivity

than HPPO complex. Ionic conductivity of MPPO1000 complex at $[Li^+]/[-O-]=0.13$ also was higher than that of HPPO1000 at $[Li^+]/[-O-]=0.15$. As we showed above, chain flexibility which has been suggested to be associated with ion mobility was increased in MPPO complexes while the number of free ions was decreased compared to the HPPO complexes. Since the ionic conductivity is proportional to the ionic mobility and number of ions(eq.(1.1)), these results indicate that increased chain mobility was the predominant factor contributing to the increase in the ionic conductivity in spite of the reduced number of carrier ions.

4.4 Conclusions

In this study, the end group effect on the ionic conductivity of $LiClO_4$-poly(propylene oxide) complexes has been investigated by estimating the number of free ions and the ionic mobility separately. We assume that ionic mobility can be represented by chain segmental mobility, reflected by the glass transition. The number of free ions is decreased while chain segmental mobility is increased by changing the end group from hydroxy to methoxy. The ionic conductivity of the salt complexed methoxy terminated poly(propylene oxide) is increased by about one order of magnitude compared to the corresponding hydroxy terminated one. This result indicates that the effect of increased chain segmental mobility overwhelms the effect of the decreased number of free ions on the ionic conductivity of the system.

References

(1) MacCallum, J. R.; Vincent, C. A., Ed.; *Polymer Electrolyte Reviews* ; Elsevier Applied Science: London, **1987**; Vol. 1.

(2) MacCallum, J. R.; Vincent, C. A., Ed.; *Polymer Electrolyte Reviews* ; Elsevier Applied Science: London, **1989**; Vol. 2.

(3) Scrosati, B., Ed.; *Second International Symposium on Polymer Electrolytes*; Elsevier Applied Science: London, **1990**.

(4) Watanabe, M.; Ogata, N. *Brit. Polym. J.* **1988**, *20*, 181.

(5) Ratner, M. A.; Shriver, D. F. *Chem. Rev.* **1988**, *88*, 109.

(6) Lee, C. C.; Wright, P. V. *Polymer* **1982**, *23*, 681.

(7) McLin, M. G.; Angell, C. A. *J. Phys. Chem.* **1991**, *95*, 9464.

(8) Payne, D. R. *Polymer* **1982**, *23*, 690.

(9) Torell, L. M.; Schantz, S. *J. Non-Cryst. Solids* **1991**, *131-133*, 981.

(10) Watanabe, M.; Ikeda, J.; Shinohara, I. *Polym. J.* **1983**, *15*, 175.

(11) Watanabe, M.; Ikeda, J.; Shinohara, I. *Polym. J.* **1983**, *15*, 65.

(12) Yoon, S.; Ichikawa, K.; MacKnight, W. J.; Hsu, S. L. *Macromolecules* **1995**, *28*, 4278.

(13) Frech, R.; Manning, J.; Black, B. *Polymer* **1989**, *60*, 1785.

(14) Manning, J.; Frech, R.; Hwang, E. *Polymer* **1990**, *31*, 2245.

(15) Schantz, S.; Torell, L. M.; Stevens, J. R. *J. Appl. Phys.* **1988**, *64*, 2038.

(16) Vachon, C.; Vasco, M.; Perrier, M.; Prud'homme, J. *Macromolecules* **1993**, *26*, 4023.

CHAPTER 5

FOURIER TRANSFORM RAMAN SPECTROSCOPIC STUDY OF POLY(PROPYLENE OXIDE) BASED MODEL NETWORK ELECTROLYTE

5.1 Introduction

Polymer based electrolytes have generated great interest from both fundamental and applied points of view.[1] Particularly, linear polyether based polymer electrolytes have been widely investigated to understand the relationship between polymer structure and ionic conductivity. Recently, network polymer based electrolytes have been of interest because of their inherent advantages such as dimensional and thermal stability in spite of their lower ionic conductivity as compared to the corresponding linear polymer based electrolytes.[1,2]

The network derived from poly(propylene oxide) with multi-functional isocyanates has been used as a model network polymer because atactic poly(propylene oxide) has a narrow molecular weight distribution giving a homogeneous structure. The ionic conductivity of these network polymer electrolytes has been determined previously and the temperature dependence of the ionic conductivity was described using the Williams-Landel-Ferry (WLF) equation.[1,3] This suggests that the ionic conductivity is mainly associated with local segmental motions of polymer chains. Furthermore, it has been shown that there are two distinct dielectric relaxation processes in this particular network polymer, one of which is related to the ether units and the other of which is associated with the urethane groups.[4] Also, in impedance measurements of poly(propylene oxide) based network polymer containing $LiClO_4$, it has been suggested that both the ether units in the network chains and the urethane groups at the crosslink points contribute to the ionic conductivity of

the system.[5] Further studies at the molecular level are needed, however, to differentiate ionic conduction processes coupled with urethane and ether groups.

In order to investigate the crosslinking effect on the ionic conduction mechanism in network based polymer electrolytes, it is necessary to separate the ionic interactions with the crosslink points from those of the poly(propylene oxide) network chains and to clarify the relationships between polymer structure and electrical properties of these systems. One of the best techniques for this is Raman spectroscopy. It has been verified that the Raman technique, especially in the low to mid-frequency region, can be employed to investigate specific interactions between ions and polymer chains as well as chain conformational distribution.[6-15] In Chapter 2, we have characterized the chain conformational changes occurring in poly(propylene oxide) chains as a result of interactions with salt by analyzing the 800 cm^{-1} region of the Raman spectrum.[16] In addition to the changes observed in this region, the characteristic bands which might be sensitive to the conformational and/or compositional changes were recognized in the low frequency region of the Raman spectrum. The bands at ca. 360 and 500 cm^{-1} appear to be associated with conformational changes of poly(propylene oxide) as a result of complexation with the ions. In addition, several well assigned localized vibrations exist which can be used to provide information regarding interactions between specific functional groups and ions. For example, the characteristic carbonyl stretching region in the 1700 cm^{-1} region can provide information about changes in the carbonyl group in the urethane unit as a result of interaction with ions.

In this Chapter, we report Raman spectroscopic studies of the model networks of atactic poly(propylene oxide) with different molecular weights end-linked with tri-functional isocyanate. By comparing with linear poly(propylene oxide)'s complexed with $LiClO_4$, we investigate the crosslinking effect on the interaction between ions and the network and thus the mechanism of ionic conduction in the poly(propylene oxide) based network polymer electrolytes.

5.2 Materials and Experiments

Linear hydroxy terminated poly(propylene oxide)(HPPO) and salt complexed HPPO have been prepared as described in previous chapters. Poly(propylene oxide) based network crosslinked with triisocyanate was synthesized. The crosslinking agent, tris(4-isocyanatophenyl) thiophosphate(triisocyanate) is supplied as the ethyl acetate solution by Bayer Chemical Co. The yellow ethyl acetate solution of triisocyanate was concentrated to about one-third of the volume and kept in the refrigerator to get triisocyanate recrystallized as described previously.[Feger, 1984 #3] After the crystals were filtered from the solution, they were recrystallized in the dry toluene. Finally obtained crystals were dissolved in benzene and freeze-dried. Network films were prepared by dissolving 1/3 mole of purified triisocyanate into 1/2 mole of pre-dried HPPO under vacuum at 90 °C until the solution becomes clear. The slightly yellow and transparent solution is poured on to glass plate and then cured at 90 °C under vacuum for 3 days. The obtained films then were washed with THF by Soxhlet extractor in order to remove any unreacted reactants. The chemical structures of the triisocyanate and the network are shown in Figure 5.1. Network samples prepared from HPPO425, HPPO1000 and HPPO4000 are designated as NPPO425, NPPO1000 and NPPO4000, respectively.

The salt complexed network films are prepared by swelling the films in anhydrous THF solutions of lithium perchlorate with different concentrations for 1 day and drying at 60 °C under vacuum for 1 week and further drying at 130 °C for 5 hrs. The concentration of lithium perchlorate in the films were determined by microanalysis and was represented by the molar ratio of lithium cation to ether oxygen, i.e. $[Li^+]/[-O-]$.

Fourier transform(FT) Raman spectroscopy has been utilized to characterize these systems. Experimental conditions and procedure are same as described in Appendix C.2. FT-Raman spectra were obtained at room temperature and spectral resolution maintained at

4 cm^{-1}. Raman spectra of HPPO1000 and NPPO1000 and their salt complexes are shown in Figure 5.2.

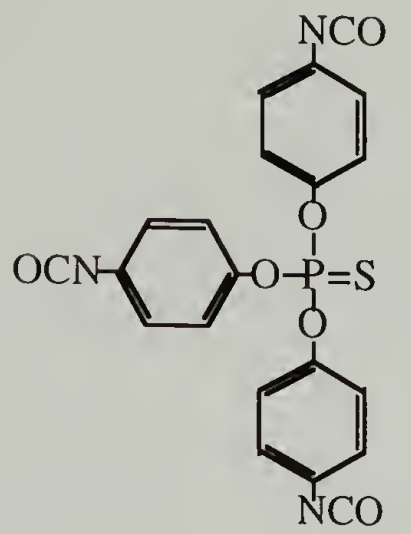

(a)

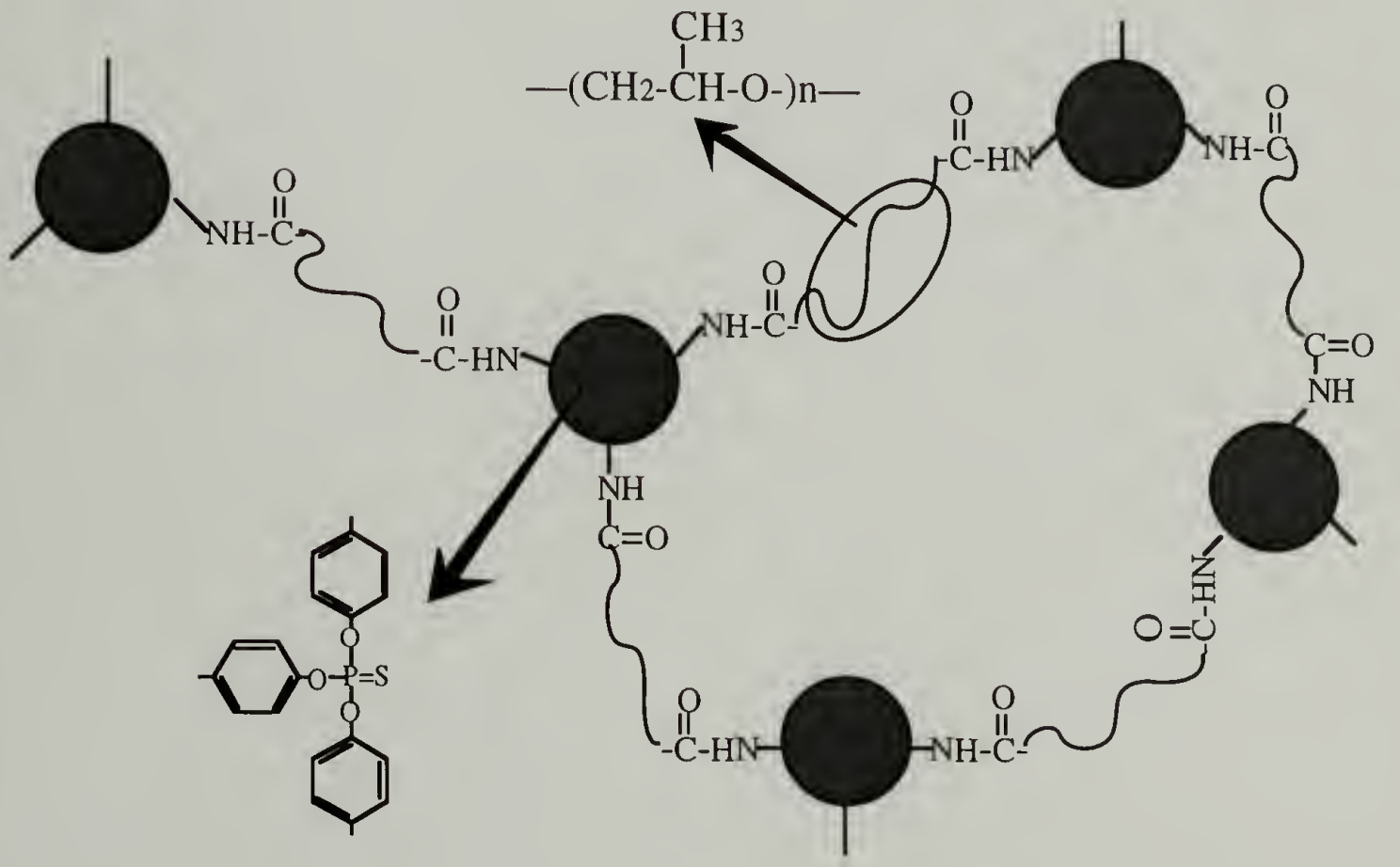

(b)

Figure 5.1 The chemical structure of (a) tris(4-isocyanatophenyl) thiophosphate and (b) poly(propylene oxide) based network.

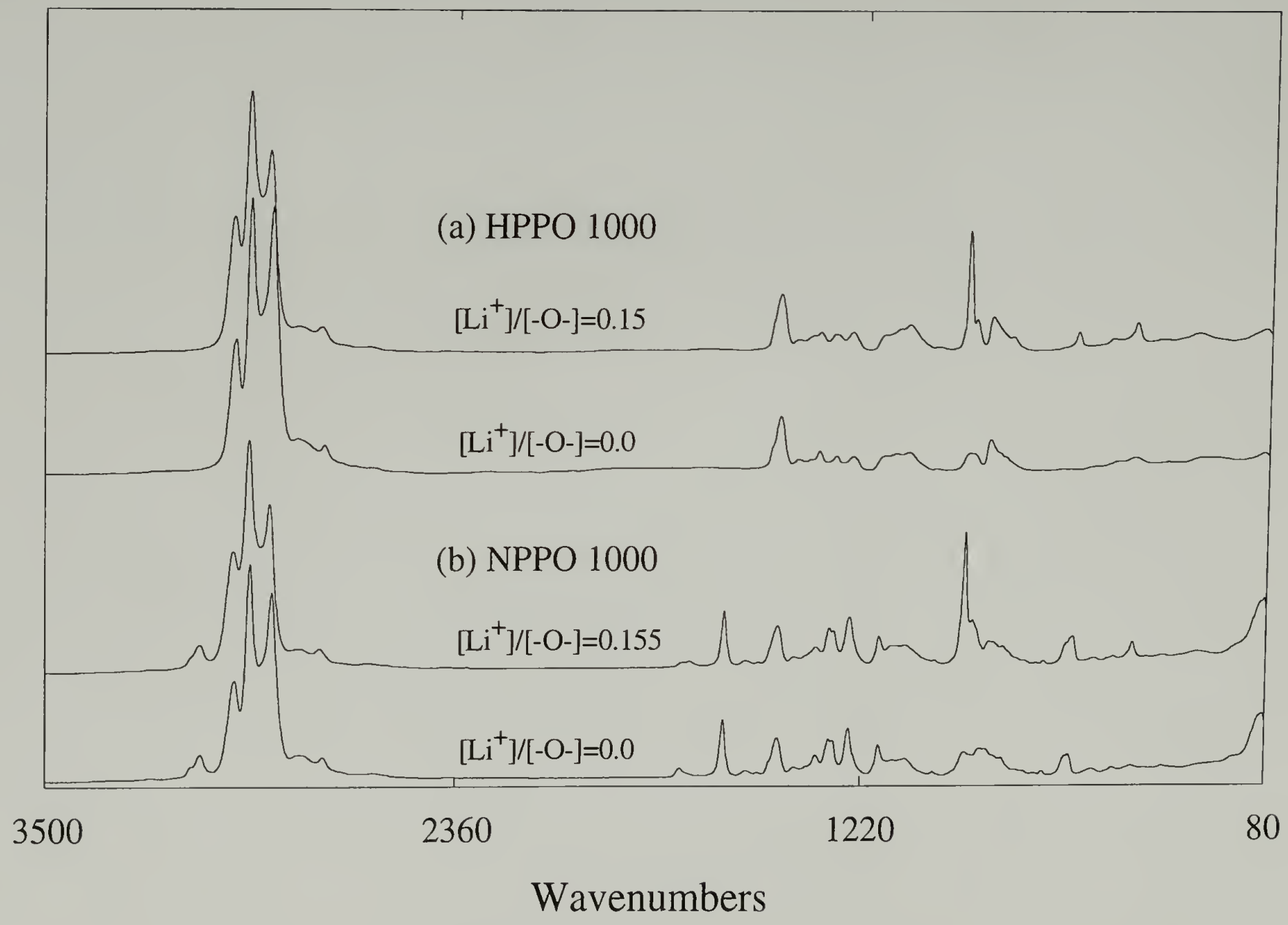

Figure 5.2 Raman spectra of HPPO1000 and NPPO1000 and their salt complexes in the 3500~80 cm^{-1} range.

Band deconvolution to separate multiple components of carbonyl stretching bands was carried out using a commercial package *Lab Calc* purchased from Galactic Industries. Band shape used was a mixture of Gaussian and Lorentz functions. This program provides the capability to fix, if necessary, any of the parameters used to describe band position, width, or shape. Relative intensity was then measured as integrated area of individual peaks deconvoluted.

5.3 Results and Discussion

The network derived from the reaction of the hydroxy groups of poly(propylene oxide) and the isocyanate contains urethane groups at the crosslink points. Figure 5.3 shows the Raman spectrum in the carbonyl stretching band region of the urethane group as a function of salt concentration for NPPO1000. Without salt, the strongest band is assigned to the free carbonyl stretching mode at 1730 cm^{-1} and the weak shoulder to the hydrogen bonded one at ~1710 cm^{-1}.[17-19]

In the salt-network complexes, a specific interaction between the salt and urethane is evidenced by the increased intensity in the 1700~1710 cm^{-1} region with increased salt concentration while the intensity of the free carbonyl stretching band at 1730 cm^{-1} decreases. Further quantitative analysis has been performed utilizing the band deconvolution technique for the multiple components observed in the 1700~1730 cm^{-1} region. Three peaks are considered for salt-NPPO complexes and two for NPPO without salt. Without fixing any of the fitting parameters, the spectrum was deconvoluted into the bands at 1731 (band 1) and 1711 cm^{-1} (band 2) for NPPO1000 without salt. The series of band deconvolution results for spectra obtained as a function of salt concentration are shown in Figure 5.4. In the presence of salt, we have deconvoluted the various components by fixing only the band position at 1711 cm^{-1} with a width of ~25cm^{-1} for the

hydrogen bonded carbonyl stretching component. Best fit can only be achieved by adding a third component at 1700~1703 cm^{-1}. It can be clearly seen in Figure 5.4 that the intensity of this third component increases with a corresponding decrease in intensity of band 1 as a function of increasing salt concentration. No significant change was observed in the intensity of band 2 as compared with changes found for bands 1 and 3. We therefore conclude that lithium cations interact mostly with free carbonyl groups and that interaction is characterized by the new carbonyl stretching component at 1700 cm^{-1}.

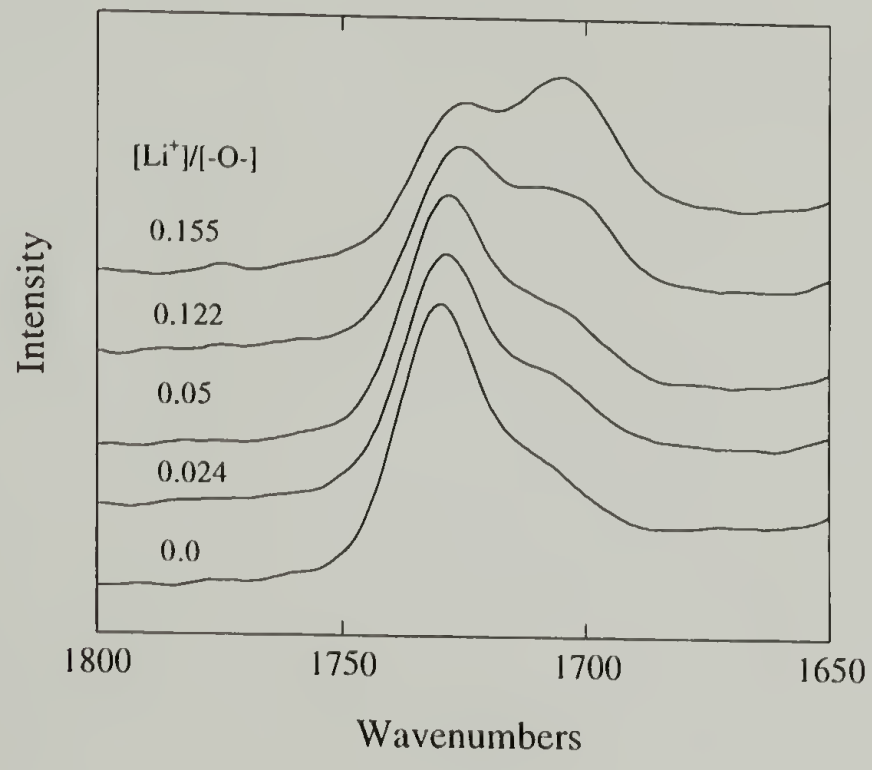

Figure 5.3 Raman spectra of NPPO1000 in the carbonyl stretching region as a function of salt concentration.

Because conformationally sensitive backbone skeletal modes in mid-to-low frequency region all exhibit large changes in polarizability, Raman spectroscopy has been particularly useful in providing polymer microstructural information.[16,20,21] Figure 5.5 shows the 700~900 cm^{-1} region of the Raman spectrum of HPPO1000 with changing salt concentration, $[Li^+]/[-O-] = 0.0$ to 0.2. The intensity of the 810 cm^{-1} band increases with

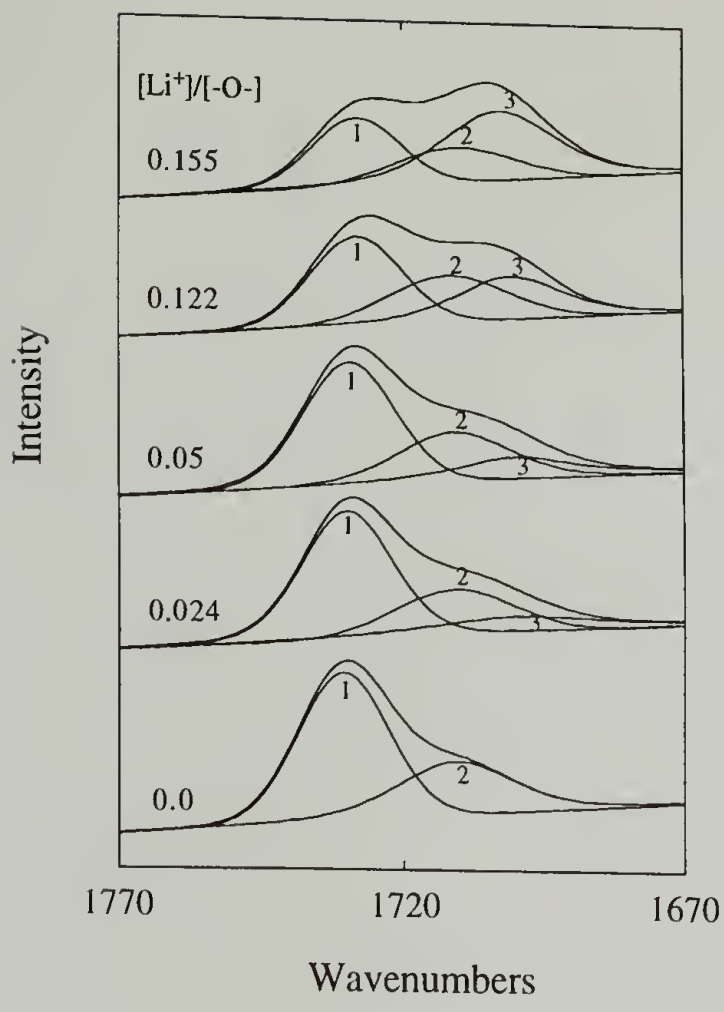

Figure 5.4 Deconvoluted results for the carbonyl stretching bands of NPPO1000.

increasing salt concentration. This band at 810 cm^{-1} has been assigned to the $TG_{\alpha}T$ conformation of propylene oxide unit and the intensity increase indicates an increase in the $TG_{\alpha}T$ conformation population of the poly(propylene oxide) chain induced by the interaction between the lithium cation and the ether units.[16] We do not suggest the presence of long range order due to this increase in the $TG_{\alpha}T$ conformation, however. In the same frequency region, Raman spectra of NPPO1000, NPPO4000 and their salt complexes are shown in Figure 5.6. Compared with HPPO1000, a relatively smaller intensity change of the 810 cm^{-1} band is shown in NPPO1000. In contrast with NPPO1000, NPPO4000 which has lower crosslink density shows an intensity change in the 810 cm^{-1} band comparable to that of the corresponding linear poly(propylene oxide), HPPO4000(Figure 2.5(b)).[16]

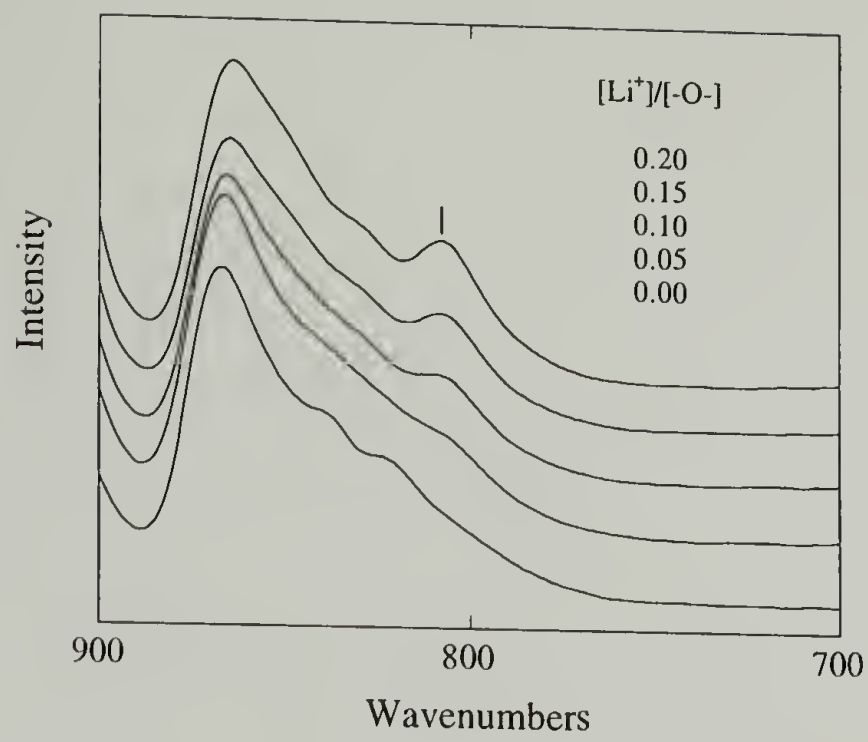

Figure 5.5 Raman spectra of HPPO1000 in 700~900 cm^{-1} region as a function of salt concentration.

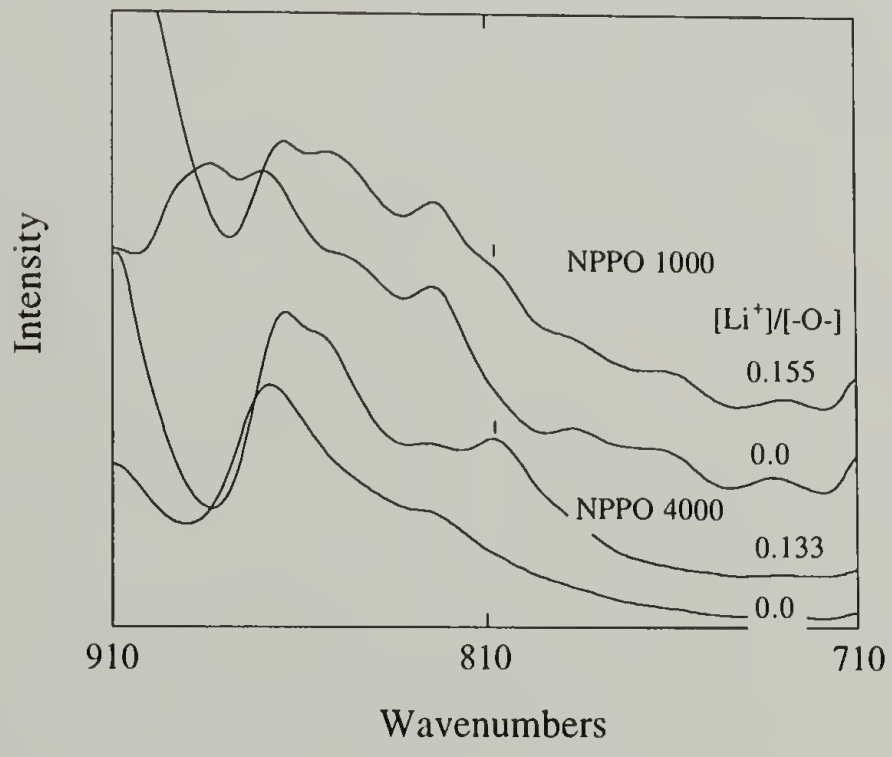

Figure 5.6 Raman intensity of the bands at 810 cm^{-1} for NPPO1000 and NPPO4000.

In addition, characteristic differences between linear and network polymers are observed at ca. 360 and 500 cm^{-1}. The bands in the 300~500 cm^{-1} region are assignable to the COC/CCO bending vibrational mode.[21] The HPPO1000 (Figure 5.7(a)) has broad features at around 364 and 503 cm^{-1} while NPPO1000 (Figure 5.7(b)) shows narrower bands at higher frequencies centered at 370 and 510 cm^{-1}, respectively. The sharpening of the bands for the network indicates a better defined chain conformational distribution. The higher frequency as observed in the network polymer might indicate a change in the conformational distribution.[21] It should be mentioned that the size of these crosslinking groups is extremely large, if comparable to the molecular dimensions of these low molecular weight poly(propylene oxide) chains. Therefore, the presence of the crosslinking groups can influence the conformational distribution of the connecting poly(propylene oxide) chains.[4,22] As expected, the smaller the molecular weight of poly(propylene oxide) chains, the greater are the effects.

With increasing salt concentration, a relative intensity increase at ca. 388 and 526 cm^{-1} is observed in linear poly(propylene oxide) and these new growing bands dominate in the high salt concentration range as shown in Figure 5.7(a). However, the Raman bands of NPPO1000 in this region show almost no change at low salt content. With increasing salt content, only moderate changes in intensity at ca. 380 and 520 cm^{-1} are observed but still the bands at ca. 371 and 512 cm^{-1} are dominant (Figure 5.7(b)). The frequency shift might represent a change in conformational distribution. The normal coordinate calculation for methyl isopropyl ether by Snyder et al.[21] shows a conformational dependence on frequencies in the 300~500 cm^{-1} region. The calculated frequencies for the C_1 species(TT) are 372 and 492 cm^{-1} and 385 and 569 cm^{-1} for the C_s species(GT). These bands are assigned to the vibrational mode of the COC bending and asymmetric skeletal bending of the isopropyl group.[21]

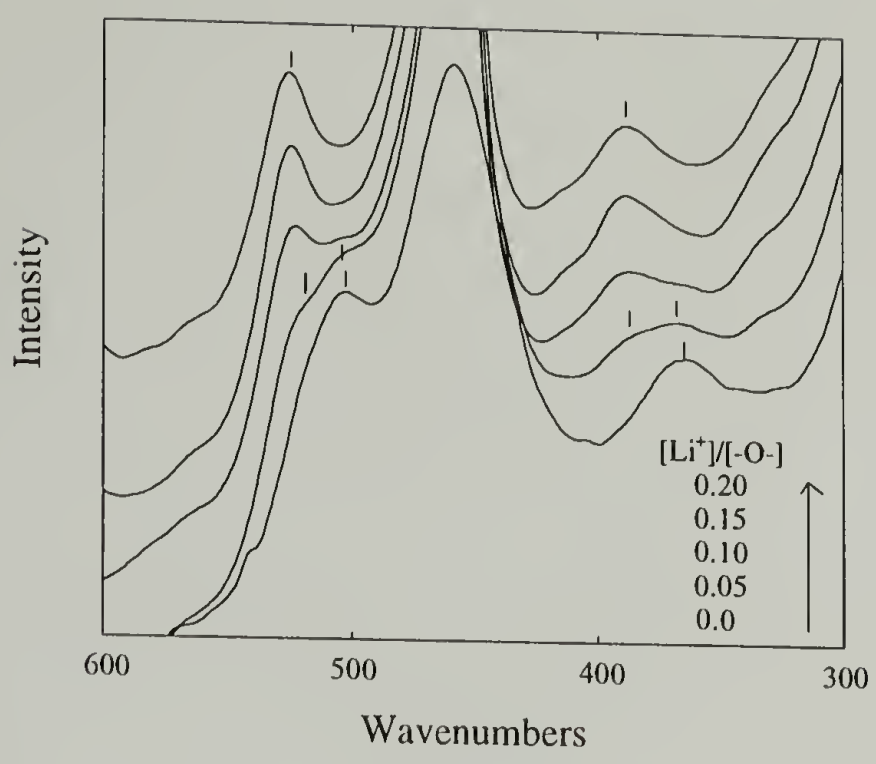

(a)

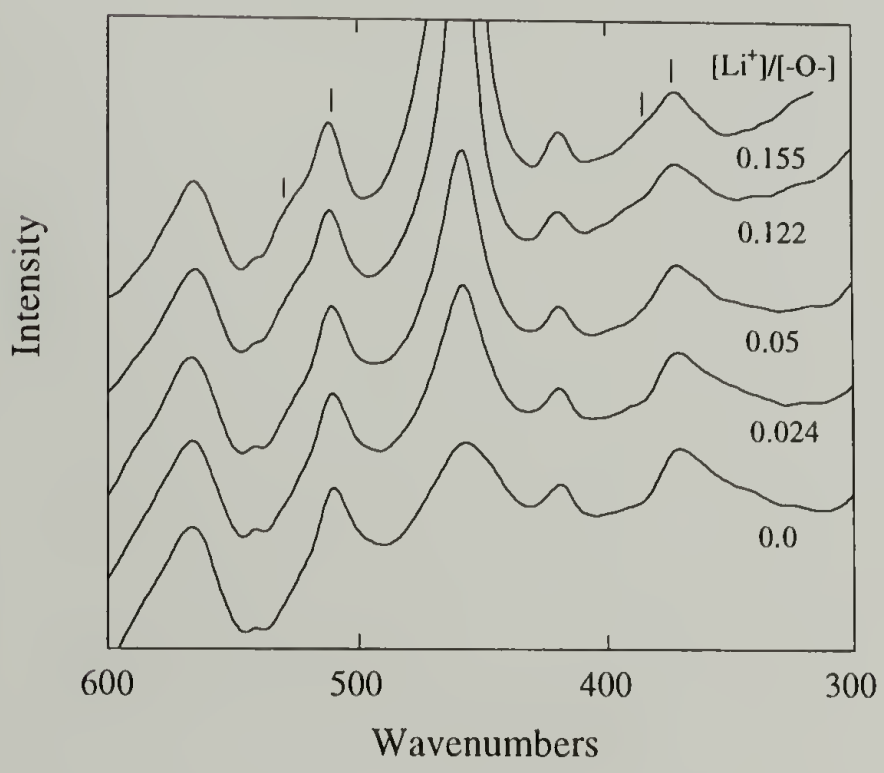

(b)

Figure 5.7 Raman spectra of (a) HPPO1000 and (b) NPPO1000 in the 600-300 cm^{-1} region as a function of salt concentration.

The Raman spectrum of 1,2-dimethoxypropane(DMP), which has one isopropyl group, as a model compound for poly(propylene oxide) has been utilized in this study. As shown in Figure 5.8, Raman bands for 1,2-dimethoxypropane were observed at 358 and 520 cm^{-1} at room temperature. With increasing salt concentration, intensity increases at 380 and 557 cm^{-1} occur. On the basis of Snyder's assignment,[21] this spectral change might be related to the conformational change of the -O-C-C-O- backbone caused by the interaction with lithium cations. Also, our previous study which showed an increase of the $TG_{\alpha}T$ conformation of the -O-C-C-O- backbone with increasing salt concentration supports this interpretation.[16] Although there is a frequency difference among the molecules, this interpretation can be extended to a poly(propylene oxide) chain having the same chemical structure as DMP. Therefore the higher frequency shift of bands at ca. 360 and 500 cm^{-1} in the presence of salt can be attributed to conformational changes of poly(propylene oxide) chains interacting with salt and the discrepancy in the spectroscopic changes between HPPO1000 and NPPO1000 indicates the difference in the degree of chain conformational change of poly(propylene oxide) in the two systems.

The Raman spectrum of NPPO4000 in this region (Figure 5.9) shows the bands at 371 and 507 cm^{-1} which are a few wavenumbers higher than the bands at 367 and 500 cm^{-1} in HPPO4000. This difference was also observed in NPPO1000 as compared to HPPO1000, indicating changes in the chain conformational distribution of poly(propylene oxide) or constraint by network formation. On the other hand, unlike the lower molecular weight poly(propylene oxide) chains, the spectral change of NPPO4000 by salt addition shows almost no difference to that of HPPO4000 in this region.

This result is in good agreement with the spectral change observed at 810 cm^{-1} for these systems. It has been found in our previous study that the intensity change of the 810 cm^{-1} band was proportional to the salt concentration in HPPO based polymer

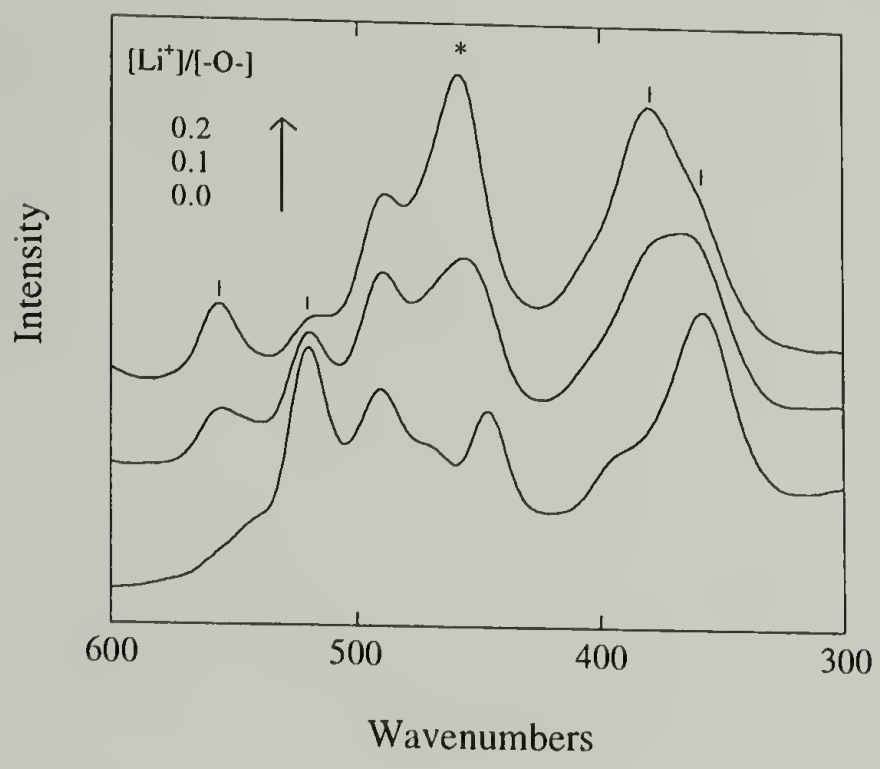

Figure 5.8 Raman bands of DMP in the 600-300 cm^{-1} range as a function of salt concentration ; * designates anion(ClO_4^-) band.

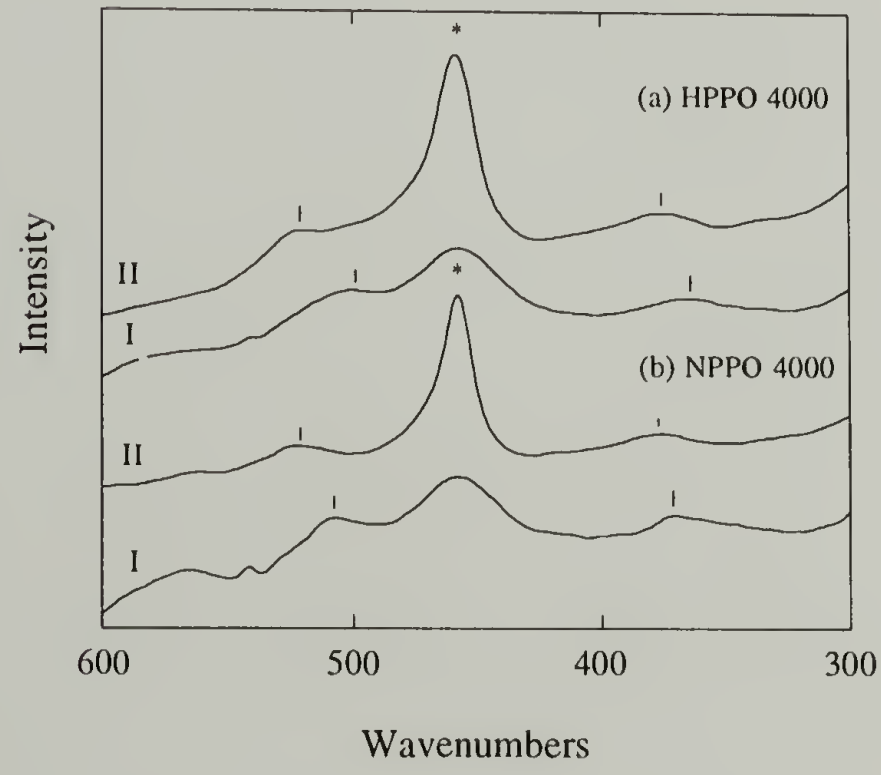

Figure 5.9 Raman spectra of HPPO4000 and NPPO4000 in the range of 600~300 cm^{-1} ; $[Li^+]/[-O-]$ = 0.0 (I), 0.133 (II) for NPPO ; 0.0(I), 0.10 (II) for HPPO ; * designates anion(ClO_4^-) band.

electrolytes.[16] Also, the spectral change in the 300~500 cm^{-1} region is dependent upon salt concentration. Since both Raman scattering band regions represent characteristic vibrational modes of poly(propylene oxide) chains, relative intensity changes of those bands indicates the proportion of poly(propylene oxide) chains interacting with the ions through changes in chain conformation by solvation of ions. Therefore the smaller intensity changes observed in the networks based on the short chain length (mol. wt. 1000) of poly(propylene oxide) means that there is a low local concentration of lithium cations interacting with ether oxygen although the total salt concentration based on the number of ether units is the same as that in linear poly(propylene oxide) based polymer electrolyte. From the crosslink density dependence of the spectral change in the 800 and 300~500 cm^{-1} region, depletion of salt associated with ether units in the network of low molecular weight poly(propylene oxide) chains can be attributed to the interaction of the lithium cation with the urethane group of the crosslink point. As mentioned earlier, additional evidence for this is found in the intensity increase in the 1700 cm^{-1} region.

If lithium cations are distributed between urethane and ether units only on the basis of the statistical weight of the two components, the local content of lithium cations should be much higher along the poly(propylene oxide) chains and reflected in changes of the skeletal modes even for NPPO1000 of high crosslink density. The molar content of the ether units to urethane groups is 8:1 for NPPO1000. This is contrary to our observations. Therefore, our spectroscopic observations suggest that Li^+ ions interact preferentially with the urethane crosslinks. NPPO4000 which has much low urethane content compared to NPPO1000 also showed significant changes in the 1700 cm^{-1} region, as much as those observed in NPPO1000 as seen in Figure 5.10. This observation provides further evidence for the greater solvation ability of the urethane group for the lithium cation than the ether unit. It is true, however, because of the large size of the junction points, that the chain conformation between network junction points may not be the same as for linear

polymers and also chain flexibility must be reduced for specially low molecular weight of poly(propylene oxide). Therefore these changes may restrict solvation of Li^+ ions by ether oxygens. At this moment, we do not have quantitative analysis.

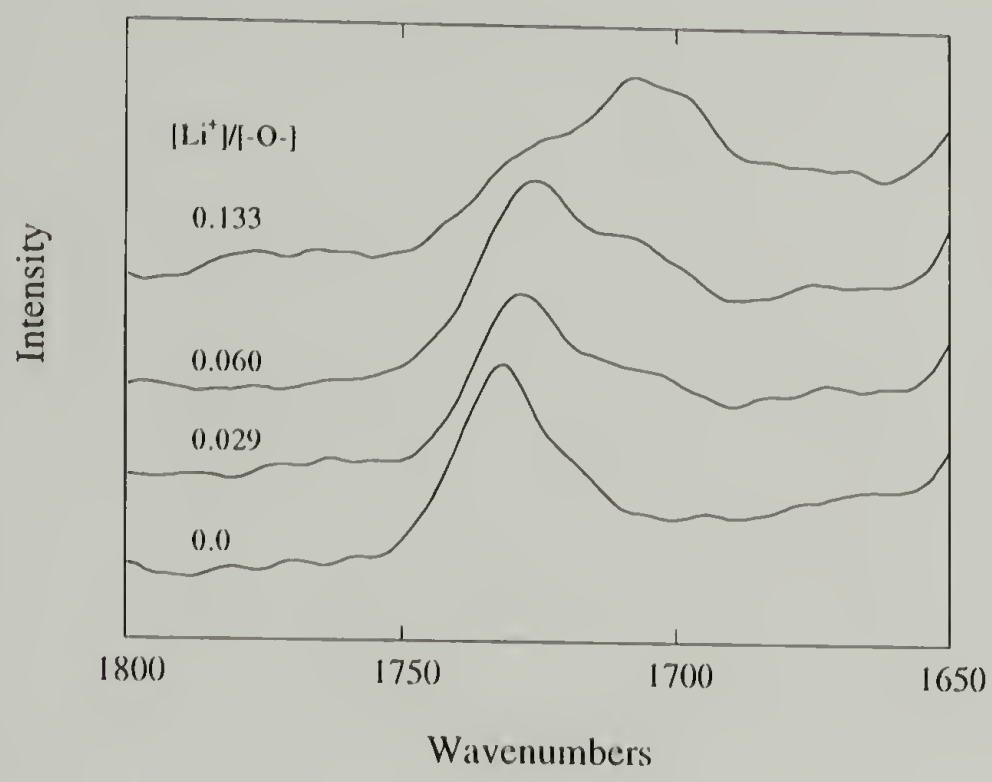

Figure 5.10 Raman spectra of NPPO4000 in the carbonyl stretching region as a function of salt concentration.

Ichikawa et al. studied ionic motions in the same network based polymer electrolytes.[5] They found that the complex impedance diagram of NPPO1000 was a superposition of two semicircles having different relaxation times. On the other hand, the corresponding diagram of NPPO4000 was found to be a single semicircle. By applying normalization of the imaginary part of the complex impedance and the Cole-Cole distribution function, the two relaxation processes observed in NPPO1000 were analyzed. The higher frequency process was found to be related to the ether units and the lower frequency process was assigned to relaxation involving the urethane groups.

The salt dependence of the relative relaxation strength of the higher frequency process showed a difference between NPPO1000 and NPPO2000. While NPPO2000 shows a decrease in the relative relaxation strength with increasing salt concentration, there was no change up to salt concentration, $[Li^+]/[-O-] = 0.07$ for the NPPO1000. Since the relaxation strength is proportional to both the number of dipoles and the strength of the dipole, the relaxation strength change of the higher frequency process is related to the changes in the ether dipoles due to the interaction with lithium cations. Therefore no change in the relaxation strength below $[Li^+]/[-O-] = 0.07$ for the NPPO1000 indicates no significant influence on the ether units by lithium cations which reflects a depletion of lithium cations associated with the poly(propylene oxide) chain of the NPPO1000. These results are in good agreement with our vibrational spectroscopic studies indicating preferred interactions of lithium cations with the urethane group.

Until now, it has been concluded that the lower ionic conductivity in network based polymer electrolytes is due to their reduced chain segmental motion compared to that of the linear polymer.[1] This may be true for the case of networks having long enough chains (≥ MW 3000) between crosslink points so that the effect of crosslinking agent can be ignored.[22] However, for the case of short chains, a crosslinking agent consisting of polar groups which can interact with ions can play an important part in ionic conduction as shown in the isocyanate based network used in our study.

Since urethane groups have a different interaction strength with lithium cations compared to ether groups, the number of carrier ions and the ionic mobility which determine ionic conductivity must be dependent upon crosslink density. Based on the equation derived by Barker et al.[23], the number of carrier ions(n) for a monovalent salt in a polymer is determined by the lattice energy of the salt (U) and the relative dielectric constant (ε) of the polymer at the temperature T by the equation (5.1).[24] In this equation, N_o is

$$n = N_o \exp(-U/2\varepsilon kT) \qquad (5.1)$$

a constant and k stands for the Boltzman constant. The dielectric relaxation measurements carried out previously showed that urethane groups contribute to increasing the dielectric constant of the system.[4] Therefore urethane groups can generate more carrier ions than ether groups because of their higher ε. Even though the urethane group can generate more carriers than the ether group, the higher binding energy between the urethane group and the lithium cation can cause reduced ionic mobility. The contribution of the urethane group to ionic conductivity is determined by the balance of forces between the lattice energy of the salt and the binding energy of the salt to the urethane group. Therefore the lower ionic conductivity in NPPOs compared to HPPOs complexed with $LiClO_4$ should be interpreted as arising from the higher binding energy of the urethane group with the lithium cation in addition to any restrictions on chain mobility of poly(propylene oxide) as a result of network formation in this particular system.

5.4 Conclusions

Vibrational spectroscopy results correlate well with the dielectric relaxation behavior of oligomeric poly(propylene oxide) based networks formed by end linking them with triisocyanate. When lithium perchlorate is dissolved in linear and network species, ionic conductivity is observed and this is generally lower in the networks than in the linear oligomers. The complex impedance behavior of these systems exhibit two conductivity regions for the network and Fourier transform Raman results confirm that these are associated with the complexation of the lithium cation with the ether group of the chains on one hand and with the urethane group of the crosslink points on the other. The lithium cations interact more strongly with the urethane groups than with the ether oxygen groups.

References

(1) MacCallum, J. R.; Vincent, C. A., Ed.; *Polymer Electrolyte Reviews* ; Elsevier Applied Science: London, **1987**; Vol. 1.

(2) Watanabe, M.; Ogata, N. *Brit. Polym. J.* **1988**, *20*, 181.

(3) Williams, M. L.; Landel, R. F.; Ferry, J. D. *J. Am. Chem. Soc.* **1955**, *77*, 3701.

(4) Ichikawa, K.; MacKnight, W. J. *Polymer* **1992**, *33*, 4693.

(5) Ichikawa, K.; Dickinson, L. C.; MacKnight, W. J.; Watanabe, M.; Ogata, N. *Polymer* **1992**, *33*, 4699.

(6) Takahashi, H.; Kyu, T.; Tran-Cong, Q.; Yano, O.; Soen, T. *J. Polym. Sci., Part B* **1991**, *29*, 1419.

(7) Papke, B. L.; Ratner, M. A.; Shriver, D. F. *J. Phys. Chem. Solids* **1981**, *42*, 493.

(8) Maxfield, J.; Shepherd, I. W. *Polymer* **1975**, *16*, 505.

(9) Matsuura, H.; Fukuhara, K. *J. Mol. Struct.* **1985**, *126*, 251.

(10) Koenig, J. L.; Angood, A. C. *J. Polym. Sci., Part A-2* **1970**, *8*, 1787.

(11) Frech, R.; Manning, J.; Teeters, D.; Black, B. E. *Solid State Ionics* **1988**, *28-30*, 954.

(12) Frech, R.; Manning, J.; Black, B. *Polymer* **1989**, *60*, 1785.

(13) Manning, J.; Frech, R.; Hwang, E. *Polymer* **1990**, *31*, 2245.

(14) Manning, J.; Frech, R. *Polymer* **1992**, *33*, 3487.

(15) Schantz, S.; Torell, L. M.; Stevens, J. R. *J. Appl. Phys.* **1988**, *64*, 2038.

(16) Yoon, S.; Ichikawa, K.; MacKnight, W. J.; Hsu, S. L. *Macromolecules* **1995**, *28*, 4278.

(17) Bandekar, J.; Klima, S. *J. Mol. Struct.* **1991**, *263*, 45.

(18) Bandekar, J.; Kilima, S. *Spectrochim. Acta.* **1992**, *48A*, 1363.

(19) Sung, C. S. P.; Schneider, N. S. *Macromolecules* **1975**, *8*, 68.

(20) Snyder, R. G. *J. Chem. Soc. Faraday Trans.* **1992**, *88*, 1823.

(21) Snyder, R. G.; Zerbi, G. *Spectrochim. Acta* **1967**, *23A*, 391.

(22) Dickinson, L. C.; Morganelli, P.; Chu, C. W.; Petrovic, Z.; MacKnight, W. J.; Chien, J. C. W. *Macromolecules* **1988**, *21*, 338.

(23) Barker, J., R. E.; Thomas, C. R. *J. Appl. Phys.* **1964**, *35*, 3203.

(24) Watanabe, M.; Sanui, K.; Ogata, N.; Kobayashi, T.; Ohtaki, Z. *J. Appl. Phys.* **1985**, *57*, 123.

CHAPTER 6

OVERALL CONCLUSIONS AND FUTURE WORK

6.1 Overall Conclusions

In this dissertation, chain conformation of atactic poly(propylene oxide) in the poly(propylene oxide)-$LiClO_4$ complexes and polymer structural effects on the ionic conductivity in polymer electrolytes have been investigated at the molecular level. Linear and network poly(propylene oxide) based polymer electrolytes have been studied.

In Chapter 2, Fourier transform Raman spectroscopy and normal coordinate analysis have been utilized to explore the chain conformational changes of poly(propylene oxide) in the presence of $LiClO_4$. Spectral changes were observed at 810 cm^{-1} as salt concentration increases. By utilizing the model compound, 1,2-dimethoxypropane(DMP), the bands in the 800 cm^{-1} region have been characterized to represent C-C/C-O stretching vibrational modes. The intensity increase at 810 cm^{-1} has been attributed to the increase of $TG_\alpha T$(trans-gauche α-trans) conformation of propylene oxide units by complex formation with $LiClO_4$. Also, Raman scattering bands centered at 817 cm^{-1} and 835 cm^{-1} have been assigned to $G_\alpha G_\alpha T$ and/or $G_\beta G_\alpha T$ and TTT conformation of the -O-C-C-O- bond, respectively. In salt complex formation of poly(propylene oxide), end group effects on the chain conformational change has been found by comparing hydroxy terminated PPO(HPPO) and methoxy terminated PPO(MPPO). The interaction of lithium cation with ether oxygen caused a chain conformational change of the propylene oxide unit to $TG_\alpha T$ while that with hydroxy end group did not contribute to $TG_\alpha T$ formation.

In Chapter 3, the end group effect on the chain flexibility of poly(propylene oxide) in the oligomeric molecular weight range has been studied. The glass transition temperature(T_g) of HPPO was higher than that of MPPO and the difference of T_g between HPPO and the corresponding molecular weight of MPPO increased with number of hydroxy groups. Unusually, HPPO showed no significant molecular weight dependence on T_g in such a low molecular weight range. In contrast, a greater molecular weight dependence was reported for poly(ethylene oxide) having hydroxy end groups in a similar molecular weight range. D-LAM bands of Raman spectra have been utilized to understand the differences between end group effects in poly(propylene oxide) and poly(ethylene oxide). Poly(propylene oxide) showed a significant frequency shift of the D-LAM band by changing end group while there was no noticeable band shift found in poly(ethylene oxide). Band frequency of D-LAM bands is known to depend on the chain conformational distribution and force constant of the skeletal bending motion. Therefore the lower frequency shift of D-LAM band for poly(propylene oxide) compared to poly(ethylene oxide) on changing hydroxy to methoxy end group is attributed to the increased chain flexibility resulting in easier bending motion on the basis of T_g behavior. In HPPO, the interaction between hydroxy end group and ether oxygen caused steric hindrance in the intramolecular chain segmental motion due to the $-CH_3$ side group of propylene oxide unit. However, this hydrogen bonding interaction did not affect the chain segmental mobility in poly(ethylene oxide).

In Chapter 4, the end group effect on the ionic conductivity of linear poly(propylene oxide)-$LiClO_4$ complexes was studied by analyzing the ionic mobility and number of ions separately. Ionic mobility was estimated indirectly by measuring chain flexibility. Differential scanning calorimetry was used to measure T_g's for estimation of chain segmental mobility. Symmetric stretching Raman scattering bands of perchlorate anion were used to estimate the number of free ions. MPPO-$LiClO_4$ complexes showed lower T_g's and fewer free ions than HPPO-$LiClO_4$ complexes. Ionic conductivity was one order

of magnitude higher in MPPO than HPPO based polymer electrolytes measured by impedance analyzer. This result indicated that increased chain flexibility was the predominant factor to determine ionic conductivity of MPPO based polymer electrolytes in spite of the decreased number of charge carriers compared to HPPO based polymer electrolytes.

In Chapter 5, Raman spectroscopic studies of the model network derived from poly(propylene oxide) with tris(4-isocyanatophenyl) thiophosphate(triisocyanate) in the presence of salt, $LiClO_4$ are carried out by changing salt concentration and molecular weight of poly(propylene oxide). The spectral analysis in the frequency region of 800 cm^{-1} and 300~500 cm^{-1} representing characteristic vibrational modes of poly(propylene oxide) chains showed the salt to interact preferentially with the crosslink points, i.e. the urethane groups rather than the ether groups of the poly(propylene oxide) chain. Also, the relative intensity changes on the 1700 cm^{-1} carbonyl stretching region with increasing salt concentration provided a direct indication of the salt interaction with the urethane groups. Previously, an impedance spectroscopic study suggested that there are two ionic conduction mechanisms related to the ether units and the urethane groups, respectively. Our spectroscopic studies proved this hypothesis. Therefore ionic conductivity in this particular network based polymer electrolyte is determined by the combination of two mechanisms, one coupled to the poly(propylene oxide) chains and the other the urethane groups present at the crosslink points. The higher binding ability of urethane group to the lithium cation can restrict ionic mobility.

6.2 Future Work

This study re-examined detailed polymer structure effect on the ionic conductivity of the linear and network types of poly(propylene oxide)-$LiClO_4$ complexes. However,

estimated ionic mobility and number of charge carriers which determine ionic conductivity was obtained indirectly by thermal and spectroscopic studies. Therefore, for quantitative analysis of ionic conduction mechanism in the conjunction with polymer structure, electrical properties of the systems should be characterized in detail.

A polymer electrolyte consists of a polymer which has dielectric properties and ions which give rise to conductivity. In order to characterize the total electrical properties of polymer electrolytes, it is required to know the electrical properties of each of the components of the system. Impedance measurements as a function of frequency are known to be the best way to accomplish this. In this study, we reported a few data obtained from impedance measurement but for more useful information regarding ionic conduction mechanism, the temperature dependence of ionic conductivity(σ) should be examined.

There are a few methods available to determine ionic mobility(μ). Representative methods developed for polymer electrolyte systems are the direct current(dc) method and the isothermal transient ionic current method. The way these methods work is by measuring the current change of the system with time by applying a constant voltage. By analyzing the time dependence of the current obtained by using an ion-blocking electrode and an ion-reversible electrode, ionic mobility and therefore transference number, $t_+=\mu_+/(\mu_+ + \mu_-)$ can be determined.

From the measured ionic conductivity and mobility, the number of carrier ions(n) can be calculated by equation (1.1). It is interesting to compare n values calculated from equation (1.1) with the relative content of free ions determined by the vibrational spectroscopic study for comparison of HPPO and MPPO based electrolytes.

Besides clarifying ionic conduction mechanism, further quantitative analysis of vibrational spectra of poly(propylene oxide) should be conducted to fully characterize

amorphous poly(propylene oxide) chain itself. Particularly, D-LAM band of poly(propylene oxide) should be analyzed to investigate long range chain conformational distribution depending on end group, tacticity and regioselectivity of the chain as well as salt concentration. Also, more detailed spectral analysis in 800~900 cm^{-1} region is required to clarify the spectral change observed at around 850 cm^{-1} with increase of salt concentration. These studies are going to be very useful to characterize poly(propylene oxide) chains in the wide variety of their applications. Particularly, poly(propylene oxide) has been used as a soft segment of polyurethane but no characterization on soft segment has been conducted yet because of lack of detailed structure information of amorphous polymer chains. Therefore it is going to be a breakthrough for full characterization of those systems consisting of amorphous poly(propylene oxide).

APPENDIX A

NORMAL COORDINATE ANALYSIS(NCA)

A.1 Theoretical Background

The origin of the vibrational spectrum is the change in energy of nuclear vibrations upon interaction with radiation of suitable frequency. A molecule having N nuclei has 3N degrees of freedom in 3-dimensional space. There are 3N-6 vibrational degrees of freedom for non-linear molecules which are equal to the number of normal modes of vibration. A normal mode of vibration is such a motion that each atom is oscillating about its equilibrium position with different amplitudes but with the same frequency and phase during the vibration. Normal coordinate analysis is a mathematical treatment of the normal modes of vibration to determine the forms and frequencies. The frequencies are proportional to the energies of normal vibrations.

NCA is based on the several assumptions. First of all, this method uses the Born-Oppenheimer approximation that assumes the motion of nuclei during vibrations are so slow compared to the motions of electrons. Based on this assumption, a nuclear vibration can be described using electron distribution of the equilibrium configuration. In this analysis, the forces acting between nuclei are assumed to follow Hooke's law and the motion of each atom is assumed to be simple harmonic. In order to calculate frequencies and forms of normal modes, it is needed to set up potential(V) and kinetic(T) energy expressions associated with the total energy of nuclear vibration. With 3N coordinates q_i, where i = 1,2,3,.....and 3N, V and T are expressed by equation (A.1).

$$2V=\sum_{i=1}^{3N}\sum_{j=1}^{3N} f_{ij}q_iq_j \quad \text{and} \quad 2T=\sum_{j=1}^{3N} m_j\dot{q}_j^2 \tag{A.1}$$

In this equation, f_{ij} is a force constant and m_j is an atomic mass. Then the equation of motion for the vibration can be expressed by equation (A.2) based on Newton's law.

$$\sum_{j=1}^{3N} m_j\ddot{q}_j+\sum_{j=1}^{3N} f_{ij}q_j=0 \tag{A.2}$$

By solving this equation of motion, the general solution(A.3) is obtained which describes simple harmonic motion with a frequency ν equal to $\lambda^{1/2}/(2\pi)$, a maximum displacement A_j and a phase constant α.

$$q_j=A_j\sin(\lambda^{1/2}t+\alpha) \quad \text{where } \lambda^{1/2}=2\pi\nu \tag{A.3}$$

Substituting equation (A.3) into (A.2), we get the equation (A.4) in terms of f_{ij} and m_i. By solving these 3N equations, eigenvalues(vibrational frequencies) and eigenvectors(forms of normal modes) are obtained. 6 of 3N frequency values are zero for nonlinear finite molecules because they are associated with the translational and rotational motions.

$$\sum_{j=1}^{3N}\left(f_{ij}-m_j\lambda\right)A_j=0 \tag{A.4}$$

Therefore, if we have force constants and atomic masses, we can calculate vibrational spectra of any kinds of molecules, in theory.

The basic principles described above can be applied to all methods of calculating vibration frequencies. As a simple and familiar coordinate, Cartesian coordinates can be used to describe normal vibrational modes. However, in actual calculation, it is inconvenient to express such changes in interatomic distances or bond angles during vibrations. Internal coordinates were introduced to describe these displacements. In the

internal coordinate space, the physical interpretation of the potential energy terms is most straight forwarded. In 1953, E. B. Wilson, Jr. set up the equation of motion with internal coordinates suitable for high speed computation. If **R** represents a vector of internal coordinates and **X** Cartesian coordinates, the relation between two coordinates will be of the form (A.5), where **B** is the rectangular matrix of the transformation .

$$\mathbf{R} = \mathbf{BX} \qquad \text{(A.5)}$$

With internal coordinates, then, the potential energy V is expressed as follows when **R'** denotes the transpose of **R**.

$$\mathbf{2V}=\sum_{ij} F_{ij}R_iR_j \qquad \text{or} \qquad \mathbf{2V=R'FR} \qquad \text{(A.6)}$$

For the description of kinetic energy **T** in internal coordinates, the **G** matrix is defined in equation (A.7) where **B'** is transpose matrix of the **B** matrix defined above and $\mathbf{M^{-1}}$ is the inverse of the diagonal matrix of the masses, containing entries $1/m_j$ along the main diagonal and zeros elsewhere.

$$\mathbf{G} = \mathbf{BM^{-1}B'} \qquad \text{(A.7)}$$

Then kinetic energy is obtained in terms of **G** and **R**.

$$\mathbf{2T}=\sum_{ij}\left(G^{-1}\right)_{ij}\dot{R}_i\dot{R}_j \quad \text{or} \qquad \mathbf{2T=\dot{R}'G^{-1}\dot{R}} \qquad \text{(A.8)}$$

In the equation (A.8), $\mathbf{G^{-1}}$ stands for the inverse of the **G** matrix. Now, equation (A.6) can be expressed in terms of F_{ij} and $G^{-1}{}_{ij}$ instead of f_{ij} and m_{ij} . By solving secular equation (A.9), vibrational frequencies are obtained.

$$|\mathbf{F} - \mathbf{G^{-1}}\lambda| = 0 \qquad \text{or} \qquad |\mathbf{GF} - \mathbf{E}\lambda| = 0 \qquad \text{(A.9)}$$

In this equation, **E** represents the 3N-6 x 3N-6 unit matrix and **GF** is called Wilson's GF matrix.

By use of Wilson's GF matrix method, NCA has been extensively used since the early '60s. In '60s and '70s, the extension of Wilson's GF method was made by Tadokoro,[1] Miyazawa,[2] Zerbi,[3,4] Snyder,[5-8] Schachtschneider[9,10] and many others in order to utilize normal vibrational method to describe vibrational behavior of longer chain of molecules(polymer) and better understand experimental observations of infrared and Raman spectra. Those methods were applicable only for a specific and regular chain conformation. Further development has been achieved by R. Snyder et al. since early '80s. Snyder and coworkers tried to understand some features of vibrational spectra of disordered states of oligomeric range of molecules as well as ordered state.[11-13] They recently developed a set of programs capable of reproducing observed vibrational spectra for both ordered and disordered oligomeric systems.[14] Chain conformation is generated based on the rotational isomeric state model with the specific number of isomeric states governed by the energy differences of the states. With a surprisingly small number of parameters, it has been possible to reproduce remarkably accurate experimental infrared and Raman spectra of disordered chains. Snyder and coworkers analyzed the low frequency (0-600 cm^{-1}) Raman spectra of n-alkanes in the liquid state.[14] Subsequently, this method was applied for analysis of the low frequency Raman spectrum of molten state isotactic polypropylene and successfully demonstrated that the vibrational spectroscopic analysis can be used to identify the correct model governing the chain.[15] This method has been extended to analysis of higher frequency vibrations (0-1500 cm^{-1}) of liquid n-alkanes as well.[16]

A.2 Description of a Program for NCA

The program used in this study was written by R. Snyder and modified by D. Cates* based on Wilson's GF method. This program is design to solve the secular equation in the Cartesian coordinates or Cartesian mass-weighted coordinates. The secular determinant is traditionally built up in the internal coordinates as discussed above. However, for linear polymers, a severe redundancy condition arises when internal coordinates are used. When the internal coordinates are transferred into local symmetry coordinates at each center along the chain backbone, one redundancy condition arises on the angle variations at each center. For example, the sum of all six angle variations about a single sp^2 carbon atom must vanish. If the chain contains N such atoms, then there are N redundancy conditions which must be accommodated in the computation. Cartesian coordinates are much less complicated to use when the number of such centers exceeds the number of rotations and translations. Additionally, the force field is uniquely defined when expressed in Cartesian coordinates, and is independent of the particular selection of internal coordinates made by the individual investigator.

By giving structure parameters such as bond length, bond angle, dihedral angle, and atomic mass and information of bond connections, the program generates Cartesian coordinates for each atom of a molecule and internal coordinates. The **B** matrix is in turn determined by both Cartesian and internal coordinates. As a feature of the program, it possesses a generator and specific database for making **F** matrix. The generator automatically chooses the proper force constants from the well-defined database with given force field. Then vibrational frequencies and normal modes are obtained by solving the

---

* We wish to acknowledge assistance from Drs. Snyder and Cates, U. C. Berkeley, in working with their normal coordinate analysis program.

secular equation written in Cartesian coordinates. In this step, these normal modes are described in the Cartesian coordinates.

This program is designed to calculate not only frequencies but also scattering activity(or intensity) of each normal mode. The isotropic Raman spectrum is particularly useful for the study of chain conformation because it can be easily simulated through calculation and can also be obtained experimentally. Isotropic Raman spectrum is obtained by subtracting $I_{\perp}$ from $\sigma I_{//}$, where $I_{\perp}$ and $\sigma I_{//}$ are the parallel and perpendicular components of Raman intensity. The constant σ is adjusted to separate the isotropic and anisotropic components within 10% of the theoretical value of 4/3. For the calculation of isotropic Raman intensity, a simple bond polarizability model is used and polarizability changes in the x, y, z directions are assigned to be same. In this step, the normal modes are redefined in internal coordinates. Then, the scattering activity of normal mode k is given by equation (A.10), where L_{ik} is the normal coordinate element for the ith internal coordinate of M normal vibration and L_{jk} is that for the N, α'_M and α'_N are the mean polarizability derivatives associated with M and N vibrations, respectively.

$$S_k \propto \left[\sum_i \alpha'_M L_{ik} + \sum_j \alpha'_N L_{jk} \right]^2 \qquad \text{(A.10)}$$

The program is able to generate thousands of conformers using a Monte Carlo method for a given conformational distribution. A conformational distribution can be defined in two ways in this program. One is based on the Flory's RIS(rotational isomeric state) model[17] and the other is by assigning a conformational probability to each bond. With given conformational distributions, the spectrum, $S(\nu)$ is obtained by summing each isotropic Raman spectrum, $S^C(\nu)$ of the constituent conformer C. In the equation (A.11), ν is frequency and C_T is the total number of conformers.This program also allows fluctuation of dihedral angle during the random generation of conformers.

$$S(\nu) \propto \sum_{C=1}^{C_T} S^C(\nu) \qquad (A.11)$$

In order to evaluate the program for the use of ether molecules, we calculated vibrational frequencies of simple ethers, dimethyl ether and methyl isopropyl ether. In this analysis, all bond angles were assumed to be tetrahedral. C-H, C-O, and C-C bond lengths were assumed to be 1.096, 1.41, and 1.54 Å respectively.[18] The dihedral angles associated with the trans, gauche +, and gauche – states are assigned to 180, 60 and -60, respectively. The set of valence force fields used in these calculations were obtained from an earlier study of ten simple ether systems.[18] Upon applying corrected nomenclature for some force constants presented previously, the earlier results[18] were duplicated. The corrections for the force constants are summarized in Table A.1. Input and output data for

Table A.1 Corrections to the earlier force field used to calculate small ether systems.

Force constant	Group	Coordinates * and values	Corrected coordinates and values
$H\alpha$	CH_3-C	∠HCC, 0.540	∠HCH, 0.540
$F\sigma$	CH_3-O	∠HCO, ∠HCO, -0.023	∠HCO, ∠HCO, -0.029
$f_{\mu\theta^g}$	CH-O-C	∠HCO, ∠COC, 0.004	∠HCO, ∠COC, -0.112
$f_{\mu\theta^t}$	CH-O-C	∠HCO, ∠COC, -0.112	∠HCO, ∠COC, 0.004

* Spectrochim. Acta **1967**, *23A* , 391 : Table 7

dimethyl ether are given in Appendix B together with a schematic drawing of a structure of the molecule. The numbers marked on each atoms indicate atom numbers. In the output, the set of valence force constants used for frequency calculation of dimethyl ether is included. These force constant values are used for all other ether molecules analyzed in this study. Brief descriptions for each parameters used in the input are also given in Appendix B.

APPENDIX B

INPUT AND OUTPUT OF DIMETHYL ETHER

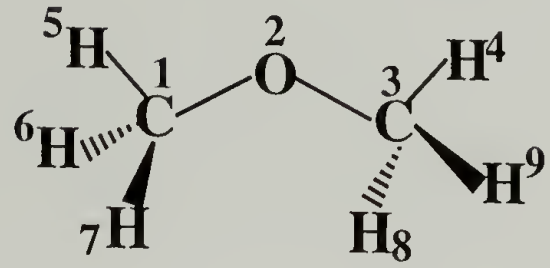

Structure of dimethyl ether

B.1 Input

```
DIMETHYL ETHER
TOPOVIB1
      1  0  0  0  2
12
    1.096          1.41          1.54          0            60           -60
  180              1.008145    12.003844   15.994915   120          -120
9  8  0  2
1  0  0  0  0  0  0  9
2  1  0  0  2  0  0 10
3  2  1  0  2  4  0  9
4  3  2  1  1  4  7  8
5  1  2  3  1  4  7  8
6  1  2  3  1  4  6  8
7  1  2  3  1  4  5  8
8  3  2  1  1  4  5  8
9  3  2  1  1  4  6  8
2  8  2  1  1  1  1  1  1
1  2  2  3  3  4  1  5  1  6  1  7  3  8  3  9
1  1  0
2  1  0
0
```

B-2. Output

<PROGRAM TOPOVIB1>

DIMETHYL ETHER
TOPOVIB1

NUMBER OF CONFORMERS = 1 IFS = 0 IFR = 0 IFU = 0 IFL = 2

CONFORMERS ARE DEFINED.

LIST OF STRUC. PAR. (SPAR(I) :

```
  1.096000    1.410000   1.540000   0.000000   60.000000
-60.000000  180.000000   1.008145  12.003844   15.994915
120.000000 -120.000000
```

NOAT = 9 NOBOND = 8 NOOP = 0 NT = 2

CART INPUT FOLLOWS

```
 1   0   0   0    0.000000    0.000000    0.000000   12.003844
 2   1   0   0    1.410000    0.000000    0.000000   15.994915
 3   2   1   0    1.410000    0.000000    0.000000   12.003844
 4   3   2   1    1.096000    0.000000  180.000000    1.008145
 5   1   2   3    1.096000    0.000000  180.000000    1.008145
 6   1   2   3    1.096000    0.000000  -60.000000    1.008145
 7   1   2   3    1.096000    0.000000   60.000000    1.008145
 8   3   2   1    1.096000    0.000000   60.000000    1.008145
 9   3   2   1    1.096000    0.000000  -60.000000    1.008145
```

PRINCIPAL CARTESIAN COORDINATES

ATOM NO.	X	Y	Z	MASS
1	0.000000	0.000000	0.000000	12.003844
2	1.410000	0.000000	0.000000	15.994915
3	1.880000	1.329361	0.000000	12.003844
4	2.976000	1.329361	0.000000	1.008145
5	-0.365333	-1.033319	0.000000	1.008145
6	-0.365333	0.516659	-0.894880	1.008145
7	-0.365333	0.516659	0.894880	1.008145
8	1.514667	1.846020	-0.894880	1.008145
9	1.514667	1.846020	0.894880	1.008145

ATOM KINDS

```
2   8   2   1   1   1   1   1   1
```

BOND PAIRS

1 2 2 3 3 4 1 5 1 6 1 7 3 8 3 9

TORSIONS

#	KBON	KBTOR	KTNUM	KARTAU	ANGTAU
1	1	1	0	0	0.00
2	2	1	0	0	0.00

TORSIONAL COORDINATES. NT = 2

1	4	5	1	2	3
1	0	6	1	2	3
1	0	7	1	2	3
2	4	4	3	2	1
2	0	8	3	2	1
2	0	9	3	2	1

INTERNAL COORD. WITH TORSIONS DEFINED IN A STRETCH FORMAT

NO.	NCOD	N1	N2	N3	N4
1	1	4	3	0	0
2	1	5	1	0	0
3	1	6	1	0	0
4	1	7	1	0	0
5	1	8	3	0	0
6	1	9	3	0	0
7	1	1	2	0	0
8	1	2	3	0	0
9	2	6	1	7	0
10	2	5	1	7	0
11	2	5	1	6	0
12	2	5	1	2	0
13	2	6	1	2	0
14	2	7	1	2	0
15	2	8	3	9	0
16	2	4	3	9	0
17	2	4	3	8	0
18	2	4	3	2	0
19	2	8	3	2	0
20	2	9	3	2	0
21	2	1	2	3	0
22	4	1	2	0	0
23	4	3	2	0	0

VFF USED =
VFF FOR ALIPHATIC ETHERS

NOF = 62

FORCE CONSTANTS

NO.	F.NO.	VAL.	ANGLE	KODE	K1	K2	K3	K4	K5	K6	K7	K8	K9	K10	ZFACT
1	1	4.688913	0.0	1	1	2	0	0	0	1	1	8	0	0	1.0000
2	2	4.626027	0.0	1	1	2	0	0	0	1	2	8	0	0	1.0000
3	3	4.687947	0.0	1	1	2	0	0	0	2	2	8	0	0	1.0000
4	4	4.699000	0.0	1	1	2	0	0	0	1	1	2	0	0	1.0000
5	5	4.554000	0.0	1	1	2	0	0	0	1	2	2	0	0	1.0000
6	6	5.089538	0.0	1	2	8	0	0	0	0	0	0	0	0	1.0000
7	7	4.260643	0.0	1	2	2	0	0	0	0	0	0	0	0	1.0000
8	8	-0.056653	0.0	5	1	1	0	0	0	0	0	0	0	0	1.0000
9	9	-0.045928	0.0	5	2	2	0	0	0	0	0	0	0	0	1.0000
10	10	0.043000	0.0	5	4	4	0	0	0	0	0	0	0	0	1.0000
11	11	0.006000	0.0	5	5	5	0	0	0	0	0	0	0	0	1.0000
12	12	0.287786	0.0	5	6	6	0	0	0	0	0	0	0	0	1.0000
13	13	0.101000	0.0	5	7	7	0	0	0	0	0	0	0	0	1.0000
13	13				7	6									
14	14	0.508315	0.0	2	1	2	1	1	8	0	0	0	0	0	1.0000
15	15	0.880377	0.0	2	1	2	8	1	1	0	0	0	0	0	1.0000
16	16	0.470743	0.0	2	1	2	1	2	8	0	0	0	0	0	1.0000
17	17	0.752041	0.0	2	1	2	2	1	8	0	0	0	0	0	1.0000
18	18	0.901226	0.0	2	1	2	8	1	2	0	0	0	0	0	1.0000
19	19	0.961034	0.0	2	1	2	8	2	2	0	0	0	0	0	1.0000
20	20	0.717575	0.0	2	1	2	2	2	8	0	0	0	0	0	1.0000
21	21	0.540000	0.0	2	1	2	1	1	2	0	0	0	0	0	1.0000
22	22	0.645000	0.0	2	1	2	2	1	1	0	0	0	0	0	1.0000
23	23	0.550000	0.0	2	1	2	1	2	2	0	0	0	0	0	1.0000
24	24	0.656000	0.0	2	1	2	2	1	2	0	0	0	0	0	1.0000
25	25	1.312698	0.0	2	2	8	2	0	0	0	0	0	0	0	1.0000
26	26	1.181530	0.0	2	2	2	8	0	0	0	0	0	0	0	1.0000
27	27	1.071146	0.0	2	2	2	2	0	0	0	0	0	0	0	1.0000
28	28	0.386511	0.0	8	6	18	0	0	0	0	0	0	0	0	1.0000
28	28				6	15									
28	28				6	19									
29	29	0.477749	0.0	8	7	17	0	0	0	0	0	0	0	0	1.0000
29	29				7	20									
30	30	0.328000	0.0	8	7	24	0	0	0	0	0	0	0	0	1.0000
30	30				7	22									
31	31	0.079000	0.0	9	7	24	0	0	0	0	0	0	0	0	1.0000
31	31				7	20									
32	32	0.483320	0.0	8	6	25	0	0	0	0	0	0	0	0	1.0000
33	33	0.617508	0.0	8	6	26	0	0	0	0	0	0	0	0	1.0000
34	34	0.402996	0.0	8	7	26	0	0	0	0	0	0	0	0	1.0000
35	35	0.417000	0.0	8	7	27	0	0	0	0	0	0	0	0	1.0000
36	36	-0.029413	0.0	11	15	15	8	2	0	0	0	0	0	0	1.0000
37	37	-0.004602	0.0	11	18	18	8	2	0	0	0	0	0	0	1.0000
38	38	0.104538	0.0	11	17	17	2	2	0	0	0	0	0	0	1.0000
39	39	0.114649	0.0	11	18	17	1	2	0	0	0	0	0	0	1.0000
40	40	0.012000	0.0	11	24	24	1	2	0	0	0	0	0	0	1.0000
40	40				20	20									
41	41	-0.012000	0.0	11	22	22	2	2	0	0	0	0	0	0	1.0000
42	42	-0.021000	0.0	11	24	24	2	2	0	0	0	0	0	0	1.0000
43	43	0.004415	60.0	12	17	17	0	0	0	0	0	0	0	0	1.0000

43	43				17 22										
43	43				17 24										
43	43				17 20										
43	43				20 24										
43	43				20 22										
44	44	0.120758	180.0	12	17 17	0	0	0	0	0	0	0	0	1.0000	
44	44				17 22										
44	44				17 24										
44	44				17 20										
44	44				20 24										
44	44				20 22										
45	45	-0.005000	60.0	12	24 24	0	0	0	0	0	0	0	0	1.0000	
45	45				24 22										
46	46	0.127000	180.0	12	24 24	0	0	0	0	0	0	0	0	1.0000	
46	46				24 22										
47	47	0.009000	0.0	13	24 24	0	0	0	0	0	0	0	0	1.0000	
47	47				24 22										
48	48	0.002000	120.0	13	24 24	0	0	0	0	0	0	0	0	1.0000	
48	48				24 22										
49	49	-0.031000	0.0	11	24 27	2	2	0	0	0	0	0	0	1.0000	
49	49				17 26										
49	49				20 27										
49	49				20 26										
50	50	-0.111786	60.0	12	18 25	0	0	0	0	0	0	0	0	1.0000	
50	50				15 25										
50	50				19 25										
51	51	0.003544	180.0	12	18 25	0	0	0	0	0	0	0	0	1.0000	
51	51				15 25										
51	51				19 25										
52	52	-0.113355	60.0	12	22 26	0	0	0	0	0	0	0	0	1.0000	
52	52				24 26										
53	53	0.028418	180.0	12	22 26	0	0	0	0	0	0	0	0	1.0000	
53	53				24 26										
54	54	-0.052000	60.0	12	24 27	0	0	0	0	0	0	0	0	1.0000	
54	54				17 27										
54	54				22 27										
55	55	0.049000	180.0	12	24 27	0	0	0	0	0	0	0	0	1.0000	
55	55				17 27										
55	55				22 27										
56	56	-0.041000	0.0	11	26 26	8	2	0	0	0	0	0	0	1.0000	
57	57	0.011000	60.0	12	27 27	0	0	0	0	0	0	0	0	1.0000	
57	57				25 26										
57	57				27 26										
58	58	-0.011000	180.0	12	27 27	0	0	0	0	0	0	0	0	1.0000	
58	58				25 26										
58	58				27 26										
59	59	0.008793	0.0	4	2 8	0	0	0	0	0	0	0	0	1.0000	
60	60	0.008150	0.0	4	2 2	0	0	0	0	0	0	0	0	1.0000	
61	61	-0.031000	0.0	11	18 26	8	2	0	0	0	0	0	0	1.0000	
61	61				19 26										
62	62	-0.041000	0.0	11	26 27	2	2	0	0	0	0	0	0	1.0000	

KON= 11

CARTESIAN COORD.

	X	Y	Z
1	0.000000	0.000000	0.000000
2	1.410000	0.000000	0.000000
3	1.880000	1.329361	0.000000
4	2.976000	1.329361	0.000000
5	-0.365333	-1.033319	0.000000
6	-0.365333	0.516659	-0.894880
7	-0.365333	0.516659	0.894880
8	1.514667	1.846020	-0.894880
9	1.514667	1.846020	0.894880

FREQUENCIES FOR MOLECULE

1	2993.35
2	2988.86
3	2988.62
4	2988.60
5	2820.12
6	2819.78
7	1473.03
8	1456.12
9	1455.59
10	1453.34
11	1448.79
12	1443.63
13	1243.06
14	1198.31
15	1186.18
16	1135.71
17	1047.92
18	927.97
19	426.40
20	247.62
21	208.60
22	0.00
23	0.00
24	0.00
25	0.00
26	0.00
27	0.00

B.3 Description of Input Format

1. Two lines of problem information :

(REC(I), I=1,18) 18A4

(REC(I), I=1,18) 18A4

2. NMOL, the number of molecules(i.e., different conformations) to be calculated, plus options controlling dihedral angle and output selection :

NMOL, IFS, IFR, IFU, IFL I6, 4I3

IFS=0 ; Only frequencies are calculated.

IFR=0 ; All dihedral angles are determined by the value listed in the CART.

IFU=0 ; No symmetrized G matrix is given in the output.

IFL=2 ; No L matrix is given in the output.

3. NOSPAR, the number of structure parameters that are contained in the next lines :

NOSPAR I3

4. SPAR, the structural parameters used to define the geometry of the input molecules :

(SPAR(I), I=1, NOSPAR) 6F12.6

5. Parameters defining the size of the input molecule :

NOAT, NOBOND, NOOP, NT 4I3

NOAT ; The number of atoms in the molecule.

NOBOND ; The number of bonds in the molecule.

NOOP ; The number of out-of-plane bends defined for the molecule.

NT ; The number of torsional dihedral angles.

6. CART vectors which define the structure of the input molecule :

((NXC(I,L),I=1,NOAT),L=1,8) 8I3

Positions 1-4 ; The atom numbers.

5 ; The index position in the SPAR list that contains the bond distance between #1 and #2.

6 ; The SPAR index for the bond angle formed by atoms #1, #2 and #3.

7 ; The SPAR index for the dihedral angle formed by atoms #1, #2, #3 and #4.

8 ; The SPAR index for the mass of atom #1.

7. Table of atom "kinds" for each in the molecule :

(KIND(I), I=1, NOAT) 24I3

1=H or D

2=C sp3

3=C sp2

8=O(singly bonded)

9=F

16=O(doubly bonded)

8. Definition of bonds :

(NB1(I), NB2(I), I=1,NOBOND) 12(2I3)

9. If NT>0, the torsional coordinates are defined :

(KBON(I),KBTOR(I),KTNUM(I),KARTAU(I),ANGTAU(I),I=1,NT)

4I3, F12.6

KBON ; The bond number for the central bond of the torsion coordinate.

KBTOR ; The designator for the number of bonds used to define the torsional coordinate.

KBTOR=1 ; All 4-atom combinations about the central bond are used to form the torsional coordinate.

APPENDIX C

EXPERIMENTAL SECTION

C.1 Determination of hydroxy number(ASTM D4274)

This is the method to determine hydroxy number by pressure bottle phthalation. Phthalic anhydride is prepared in dry pressure bottles and two of them are reserved for blank test. Hydroxy terminated poly(propylene oxide)(HPPO) then is added to rest of bottles. The bottles are capped and kept at 98 ± 2 °C for 2 hrs. Then they are allowed to cool to room temperature. When the bottles have cooled, they are uncapped carefully to release any pressure. To each bottle, pyridine and phenolphthalein indicator solution are added and the phthalic acid generated from the reaction of HPPO and phthalic anhydride is titrated with standard NaOH solution. Refer to ASTM D4274 for quantitative amount of each reagent. Hydroxyl number is then calculated from equation (C.1) in milligrams of KOH per gram of sample. In this equation, A and B stand for NaOH required for titration of the sample and the blank in milliliter, respectively, and N and W for normality of the NaOH and the sample used in gram.

$$\text{Hydroxyl number, mgr KOH/gr.} = [(B-A)N \times 56.1]/W \qquad (C.1)$$

C.2 Fourier transform Raman spectroscopy[19]

Fourier transform Raman(FT-Raman) spectroscopy were utilized for chain conformational study and analysis of ionic status in the polymer matrix using a Bruker

FRA 106 spectrometer. A Nd:Yag laser with a wavelength of 1064 nm and line band width of 1 cm^{-1} was used as excitation. This spectrometer is equipped with Michelson type interferometer consisting of CaF_2 beam splitter, moving and fixed mirrors.[19] The interferometer was aligned by taking interferogram with tungsten(W) lamp as a light source and germanium(Ge) diode as a detector. The intensity of the centerburst of the interferogram was maximized when best alignment of the optics was achieved by adjusting moving mirror. The centerburst is appeared at the point giving equal distance of fixed mirror and moving mirror to the beam splitter. For alignment of Raman optics (laser source and detector), Raman spectrum of standard sample, sulfur(yellow powder) was taken and compared with the reference spectrum given by Bruker company. The maximum spectral resolution is limited by the line band width of the excitation laser. FT-Raman or infrared spectral resolution is determined by the length of the moving mirror travel of the Michelson interferometer as well. Therefore, because of that limited traveling distance of the moving mirror, the optimum resolution available is 2 cm^{-1}.

All spectra were taken with 500 mW of the laser output power. 1024 scans were loaded to obtain an enhanced signal to noise ratio. The excitation collection geometry was 180^o and spectral resolution maintained at 4 or 2 cm^{-1} depending on the experimental demands. All of linear samples were contained in vials made of glass and having caps. The films were put on a piece of aluminum coated mirror and positioned in the sample holder directly. The sample chamber of FT-Raman was circulated with dry air all the time and drying agent was put in the chamber near the sample during the measurement.

C.3 Impedance spectroscopy[20]

Polymer electrolytes in the electric field can be represented by an equivalent circuit using electrical components, a resistor(**R**) and a capacitor(**C**). Since a resistor can

represent for ionic migration in the polymer matrix and a capacitor for polarization of polymer in the alternating electric field, we can set up the equivalent circuit as shown in Figure C.1 to express our polymer electrolyte system since ionic migration and polymer polarization occur in parallel.

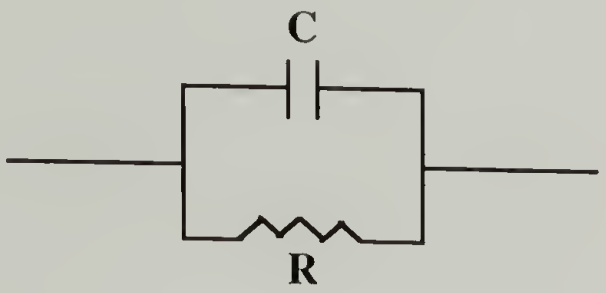

Figure C.1 The equivalent circuit for a combination of resistor,R and capacitor, C in parallel.

A sinusoidal voltage across a resistor is always in phase with the current passing through it, that is, phase difference $\theta = 0$ and the magnitude of the impedance is given by resistance $R = |Z|$. The impedance is independent of frequency. For a capacitor, θ is always $-\pi/2$ and the impedance is now frequency dependent : $|Z| = 1/\omega C$, where C stands for the capacitance. Then the impedance of the parallel combination of **R** and **C** can be given by equation (C.2). In this equation, Z^* is impedance, ω is angular frequency and i is the imaginary number. By arranging equation (C.2), Z^* is expressed by equation (C.3) in terms of real part Z' and imaginary part Z''. Figure C.2 shows the plot of -Z'' versus Z' and it is called the impedance diagram. Semicircle is obtained for the equivalent circuit shown in Figure C.1. At the frequency corresponding to the maximum of the semicircle, ω_{max}, R is equal to $1/\omega C$. The resistance R due to ionic migration is determined at the impedance value which Z'' becomes zero.

$$1/Z^* = 1/R - \omega C/i \qquad (C.2)$$

$$Z^*=R[1/(1+(\omega CR)^2]-iR[\omega RC/(1+(\omega RC)^2] \qquad (C.3)$$

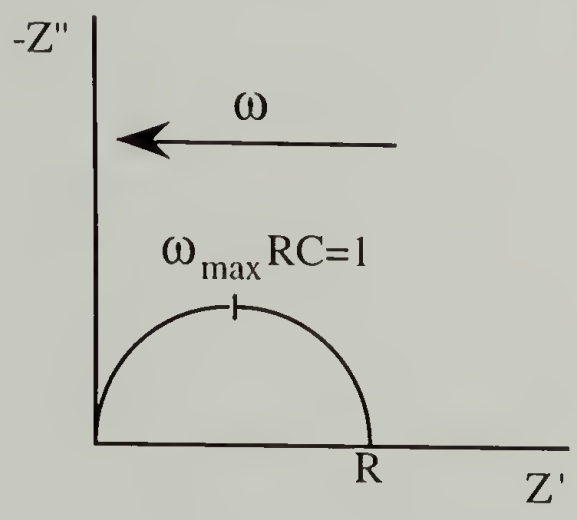

Figure C.2 Impedance diagram for a parallel connection of a resistor, R and a capacitor, C.

The method used to determine the alternating current(AC) impedance can be explained by using simple diagrammatic representation shown in Figure C.3.[20] In this figure, cell represents the cell shown in Figure Figure 4.1. V_V and V_I are AC voltages applied across the cell and standard resistor, **R** in series with the cell, respectively. Current through the **R** is in phase with V_I and same current is through the cell but having phase difference(θ) with V_V. Instrument gives the ratio of V_V to V_I and θ between two, which corresponds to the θ between V_V and current. Absolute value of impedance(|Z|) is given by the result of the multiplication of resistance value of **R** and V_V/V_I. Real and imaginary part of impedance then is calculated from $|Z|\cos\theta$ and $|Z|\sin\theta$, respectively to get impedance diagram.

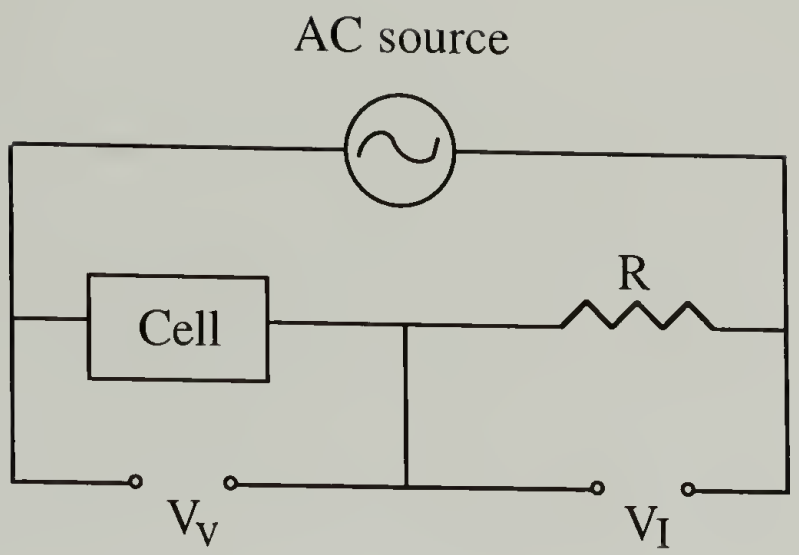

Figure C.3 Diagrammatic representation of impedance analyzer.

References

(1) Tadokoro, H. *J. Chem. Phys.* **1960**, *33*, 1558.

(2) Miyazawa, T.; Ideguchi, Y.; Fukushima, K. *J. Chem. Phys.* **1963**, *38*, 2709.

(3) Zerbi, G. *Applied Spectroscopy Reviews* **1969**, *2*, 193.

(4) Zerbi, G.; Piseri, L.; Cabassi, F. *Molecular Physics* **1971**, *22*, 241.

(5) Snyder, R. G.; Schachtschneider, J. H. *Spectrochim. Acta* **1965**, *21*, 169.

(6) Snyder, R. G. *J. Mol. Spectroscopy* **1960**, *4*, 411.

(7) Snyder, R. G. *J. Mol. Spectroscopy* **1961**, *7*, 116.

(8) Snyder, R. G.; Schachtschneider, J. H. *Spectrochim. Acta* **1963**, *19*, 85.

(9) Schachtschneider, J. H.; Snyder, R. G. *J. Polym. Sci., Part C* **1964**, 99.

(10) Schachtschneider, J. H.; Snyder, R. G. *Spectrochim. Acta* **1963**, *19*, 117.

(11) Scherer, J. R.; Snyder, R. G. *J. Chem. Phys.* **1980**, *72*, 5798.

(12) Snyder, R. G. *J. Chem. Phys.* **1982**, *76*, 3921.

(13) Snyder, R. G.; Wunder, S. L. *Macromolecules* **1986**, *19*, 496.

(14) Snyder, R. G.; Kim, Y. *J. Phys. Chem.* **1991**, *95*, 602.

(15) Hallmark, V. M.; Bohan, S. P.; Strauss, H. L.; Snyder, R. G. *Macromolecules* **1991**, *24*, 4025.

(16) Snyder, R. G. *J. Chem. Soc. Faraday Trans.* **1992**, *88*, 1823.

(17) Flory, P. J. *Statistical Mechanics of Chain Molecules*; John Wiley & Sons: New York, **1969**, pp 55.

(18) Snyder, R. G.; Zerbi, G. *Spectrochim. Acta* **1967**, *23A*, 391.

(19) Griffiths, P. R.; de Haseth, J. A. *Fourier Transform Infrared Spectrometry*; John Wiley & Sons: New York, **1986**.

(20) MacCallum, J. R.; Vincent, C. A., Ed.; *Polymer Electrolyte Reviews* ; Elsevier Applied Science: London, **1987**; Vol. 1.

BIBLIOGRAPHY

Abe, A.; Hirano, T.; Tsuruta, T. *Macromolecules* **1979**, *12*, 1092.

Abe, A.; Tasaki, K. *J. Mol. Struct.* **1986**, *145*, 309.

Aklonis, J. J.; MacKnight, W. J. *Introduction to Polymer Viscoelasticity;* 2nd ed.; John Wiley and Sons: New York, **1983**, pp 77.

Aroney, M. J.; Le Fevre, R. J. W.; Ritchie, G. L. D.; Saxby, J. D. *Aust. J. Chem.* **1967**, *20*, 375.

Bandekar, J.; Kilima, S. *Spectrochim. Acta.* **1992**, *48A*, 1363.

Bandekar, J.; Klima, S. *J. Mol. Struct.* **1991**, *263*, 45.

Barker, J., R. E.; Thomas, C. R. *J. Appl. Phys.* **1964**, *35*, 3203.

Borjesson, L.; Stevens, J. R.; Torell, L. M. *Physica Scripta* **1987**, *35*, 692.

Bruce, P. G.; Evans, J.; Vincent, C. A. *Solid State Ionics* **1988**, *28-30*, 918.

Colthup, N. B.; Daly, L. H.; Wiberley, S. E. *Introduction to Infrared and Raman spectroscopy;* 3rd ed.; Academic press: San Diego, **1990**, pp 327.

Denbigh, K. G. *Faraday Soc. Trans.* **1940**, *36*, 936.

Dickinson, L. C.; Morganelli, P.; Chu, C. W.; Petrovic, Z.; MacKnight, W. J.; Chien, J. C. W. *Macromolecules* **1988**, *21*, 338.

Dupon, R.; Papke, B. L.; Ratner, M. A.; Shriver, D. F. *J. Electrochem. Soc.* **1984**, *131*, 586.

Dupon, R.; Papke, B. L.; Ratner, M. A.; Whitmore, D. H.; Shriver, D. F. *J. Am. Chem. Soc.* **1982**, *104*, 6247.

Faucher, J. A.; Koleske, J. V.; Santee, E. R., Jr.; Stratta, J. J.; Wilson, C. W. *J. Appl. Phys.* **1966**, *37*, 3962.

Ferraro, J. R.; Nakamoto, K. *Introductory Raman Spectroscopy*; Academic Press: San Diego, **1994**.

Flory, P. J. *Statistical Mechanics of Chain Molecules*; John Wiley & Sons: New York, **1969**, pp 55.

Frech, R.; Manning, J.; Black, B. *Polymer* **1989**, *60*, 1785.

Frech, R.; Manning, J.; Teeters, D.; Black, B. E. *Solid State Ionics* **1988**, *28-30*, 954.

Gorecki, W.; Donoso, P.; Berthier, C.; Mali, M.; Roos, J.; Brinkmann, D.; Armand, M. B. *Solid State Ionics* **1988**, *28-30*, 1018.

Gough, K. M. *J. Chem. Phys.* **1989**, *91*, 2424.

Gray, F. M. *Solid State Ionics* **1990**, *40/41*, 637.

Greenbaum, S. G.; Adamic, K. J.; Pak, Y. S.; Wintersgill, M. C.; Fontanella, J. J. *Solid State Ionics* **1988**, *28-30*, 1042.

Griffiths, P. R.; de Haseth, J. A. *Fourier Transform Infrared Spectrometry*; John Wiley & Sons: New York, **1986**.

Hallmark, V. M.; Bohan, S. P.; Strauss, H. L.; Snyder, R. G. *Macromolecules* **1991**, *24*, 4025.

Harris, C. S.; Shriver, D. F.; Ratner, M. A. *Macromolecules* **1986**, *19*, 987.

Hirano, T.; Miyajima, T. *J. Mol. Struct.* **1985**, *126*, 141.

Ichikawa, K.; Dickinson, L. C.; MacKnight, W. J.; Watanabe, M.; Ogata, N. *Polymer* **1992**, *33*, 4699.

Ichikawa, K.; MacKnight, W. J. *Polymer* **1992**, *33*, 4693.

Kakihana, M.; Schantz, S.; Torell, L. M. *J. Chem. Phys.* **1990**, *92*, 6271.

Kawasaki, A.; Furukawa, J.; Tsuruta, T.; Saegusa, T.; Kakogawa, G.; Sakata, R. *Polymer* **1960**, *1*, 315.

Koenig, J. L.; Angood, A. C. *J. Polym. Sci., Part A-2* **1970**, *8*, 1787.

Lee, C. C.; Wright, P. V. *Polymer* **1982**, *23*, 681.

Lin, B.; Halley, J. W. In *The American Physical Society*; San Jose, California, **1995**; pp 50.

MacCallum, J. R.; Tomlin, A. S.; Vincent, C. A. *Eur. Polym. J.* **1986**, *22*, 787.

MacCallum, J. R.; Vincent, C. A., Ed.; *Polymer Electrolyte Reviews* ; Elsevier Applied Science: London, **1987**; Vol. 1.

MacCallum, J. R.; Vincent, C. A., Ed.; *Polymer Electrolyte Reviews* ; Elsevier Applied Science: London, **1989**; Vol. 2.

Manning, J.; Frech, R. *Polymer* **1992**, *33*, 3487.

Manning, J.; Frech, R.; Hwang, E. *Polymer* **1990**, *31*, 2245.

Matsuura, H.; Fukuhara, K. *J. Mol. Struct.* **1985**, *126*, 251.

Maxfield, J.; Shepherd, I. W. *Polymer* **1975**, *16*, 505.

McLin, M. G.; Angell, C. A. *J. Phys. Chem.* **1991**, *95*, 9464.

Miyajima, T.; Hirano, T.; Sato, H. *J. Mol. Struct.* **1984**, *125*, 97.

Miyazawa, T.; Ideguchi, Y.; Fukushima, K. *J. Chem. Phys.* **1963**, *38*, 2709.

Munshi, M. Z. A.; Owens, B. B. *Polym. J.* **1988**, *20*, 577.

Painter, P. C.; Coleman, M. M.; Koenig, J. L. *The theory of vibrational spectroscopy and its application to polymeric materials*; John Wiley & Sons: **1982**.

Papke, B. L.; Ratner, M. A.; Shriver, D. F. *J. Electrochem. Soc.* **1982**, *129*, 1434.

Papke, B. L.; Ratner, M. A.; Shriver, D. F. *J. Phys. Chem. Solids* **1981**, *42*, 493.

Payne, D. R. *Polymer* **1982**, *23*, 690.

Pine, S. H.; Hendrickson, J. B.; Cram, D. J.; Hammond, G. S. *Organic Chemistry;* 4th ed.; McGraw-Hill: New York, **1980**, pp 406.

Price, C. C.; Spector, R.; Tumolo, A. L. *J. Polym. Sci., Part A-1* **1967**, *5*, 407.

Price, C. C.; Tumolo, A. L. *J. Polym. Sci., Part A-1* **1967**, *5*, 175.

Ratner, M. A.; Shriver, D. F. *Chem. Rev.* **1988**, *88*, 109.

Schachtschneider, J. H.; Snyder, R. G. *J. Polym. Sci., Part C* **1964**, 99.

Schachtschneider, J. H.; Snyder, R. G. *Spectrochim. Acta* **1963**, *19*, 117.

Schantz, S.; Torell, L. M.; Stevens, J. R. *J. Appl. Phys.* **1988**, *64*, 2038.

Scherer, J. R.; Snyder, R. G. *J. Chem. Phys.* **1980**, *72*, 5798.

Scrosati, B., Ed.; *Second International Symposium on Polymer Electrolytes*; Elsevier Applied Science: London, **1990**.

Snyder, R. G. *J. Chem. Phys.* **1982**, *76*, 3921.

Snyder, R. G. *J. Chem. Soc. Faraday Trans.* **1992**, *88*, 1823.

Snyder, R. G. *J. Mol. Spectroscopy* **1960**, *4*, 411.

Snyder, R. G. *J. Mol. Spectroscopy* **1961**, *7*, 116.

Snyder, R. G. *Macromolecules* **1990**, *23*, 2081.

Snyder, R. G.; Kim, Y. *J. Phys. Chem.* **1991**, *95*, 602.

Snyder, R. G.; Schachtschneider, J. H. *Spectrochim. Acta* **1963**, *19*, 85.

Snyder, R. G.; Schachtschneider, J. H. *Spectrochim. Acta* **1965**, *21*, 169.

Snyder, R. G.; Strauss, H. L. *J. Chem. Phys.* **1987**, *87*, 3779.

Snyder, R. G.; Wunder, S. L. *Macromolecules* **1986**, *19*, 496.

Snyder, R. G.; Zerbi, G. *Spectrochim. Acta* **1967**, *23A*, 391.

Sperling, L. H. *Introduction to physical polymer science;* 1st ed.; Wiley: New York, **1986**, pp 272.

Strommen, D. P.; Nakamoto, K. *Laboratory Raman Spectroscopy*; John Wiley & Sons: New York, **1984**, pp 21.

Sung, C. S. P.; Schneider, N. S. *Macromolecules* **1975**, *8*, 68.

Tadokoro, H. *J. Chem. Phys.* **1960**, *33*, 1558.

Takahashi, H.; Kyu, T.; Tran-Cong, Q.; Yano, O.; Soen, T. *J. Polym. Sci., Part B* **1991**, *29*, 1419.

Torell, L. M.; Schantz, S. *J. Non-Cryst. Solids* **1991**, *131-133*, 981.

Vachon, C.; Vasco, M.; Perrier, M.; Prud'homme, J. *Macromolecules* **1993**, *26*, 4023.

Watanabe, M.; Ikeda, J.; Shinohara, I. *Polym. J.* **1983**, *15*, 65.

Watanabe, M.; Ikeda, J.; Shinohara, I. *Polym. J.* **1983**, *15*, 175.

Watanabe, M.; Ogata, N. *Brit. Polym. J.* **1988**, *20*, 181.

Watanabe, M.; Oohashi, S. I.; Sanui, K.; Ogata, N.; Kobayashi, T.; Ohtaki, Z. *Macromolecules* **1985**, *18*, 1945.

Watanabe, M.; Rikukawa, M.; Sanui, K.; Ogata, N. *J. Appl. Phys.* **1985**, *58*, 736.

Watanabe, M.; Rikukawa, M.; Sanui, K.; Ogata, N.; Kato, H.; Kobayashi, T.; Ohtaki, Z. *Macromolecules* **1984**, *17*, 2902.

Watanabe, M.; Sanui, K.; Ogata, N.; Kobayashi, T.; Ohtaki, Z. *J. Appl. Phys.* **1985**, *57*, 123.

Watanabe, M.; Togo, M.; Sanui, K.; Ogata, N.; Kobayashi, T.; Ohtaki, Z. *Macromolecules* **1984**, *17*, 2908.

Williams, M. L.; Landel, R. F.; Ferry, J. D. *J. Am. Chem. Soc.* **1955**, *77*, 3701.

Yoon, S.; Ichikawa, K.; MacKnight, W. J.; Hsu, S. L. *Macromolecules* **1995**, *28*, 4278.

Zerbi, G. *Applied Spectroscopy Reviews* **1969**, *2*, 193.

Zerbi, G.; Piseri, L.; Cabassi, F. *Molecular Physics* **1971**, *22*, 241.